

AD-A034 425

RENSELAER POLYTECHNIC INST TROY N Y DEPT OF ELECTRI--ETC F/G 9/1  
INTERFACE STATES IN SCHOTTKY BARRIER DIODES.(U)

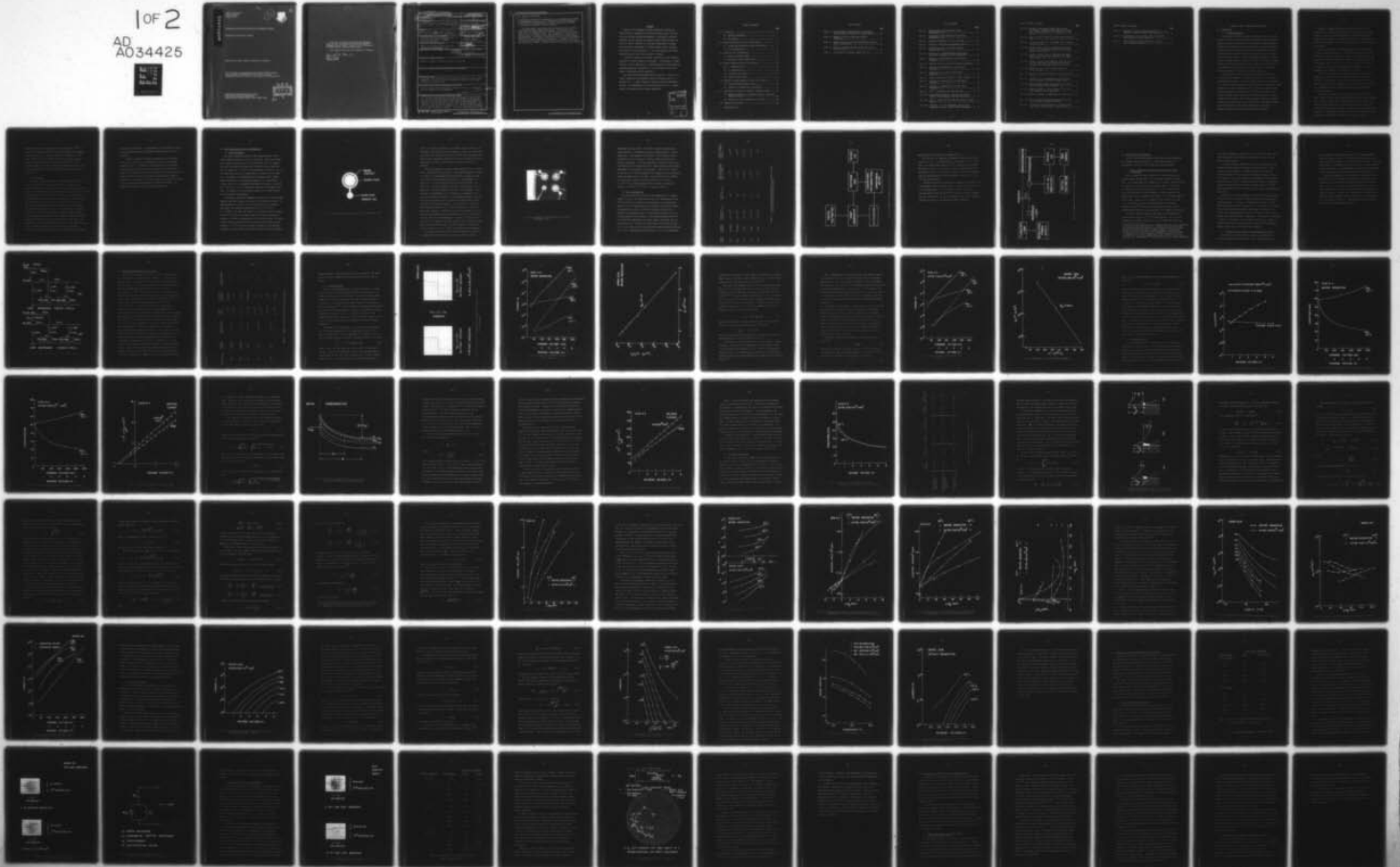
AUG 76 J M BORREGO, R J GUTMANN  
SCIENTIFIC-1

F19628-74-C-0102  
NL

UNCLASSIFIED

RADC-TR-76-266

1 OF 2  
AD 34425



ADA 034425

RADC-TR-76-266  
Interim Report  
August 1976

12



FLG.

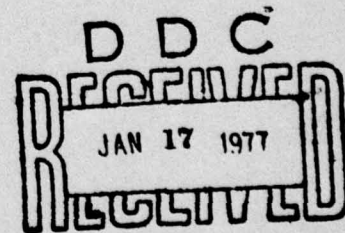
INTERFACE STATES IN SCHOTTKY BARRIER DIODES

Rensselaer Polytechnic Institute

Approved for public release; distribution unlimited

This research was supported by the Defense Nuclear Agency  
under Subtask Z99QAXTB056, Work Unit 52, entitled  
"Radiation Effects on Solid State Microwave Device Structures"

ROME AIR DEVELOPMENT CENTER  
AIR FORCE SYSTEMS COMMAND  
GRIFFISS AIR FORCE BASE, NEW YORK 13441



Q7

This report has been reviewed by the RADC Information Office (OI) and is releasable to the National Technical Information Service (NTIS). At NTIS it will be releasable to the general public, including foreign nations.

This technical report has been reviewed and is approved.

*Donald A. Neamen*

DONALD A. NEAMEN  
Contract Monitor

Unclassified

SECURITY CLASSIFICATION OF THIS PAGE (When Data Entered)

19 REPORT DOCUMENTATION PAGE		READ INSTRUCTIONS BEFORE COMPLETING FORM	
1. REPORT NUMBER RADC-TR-76-266	2. GOVT ACCESSION NO.	3. RECIPIENT'S CATALOG NUMBER 9	
4. TITLE (and Subtitle) INTERFACE STATES IN SCHOTTKY BARRIER DIODES.		5. TYPE OF REPORT & PERIOD COVERED Scientific Interim <i>rept.</i>	
7. AUTHOR(s) Jose M. Borrego <del>and</del> Ronald J. Gutmann		6. PERFORMING ORG. REPORT NUMBER Scientific <del>Report No. - 1</del>	14
		8. CONTRACT OR GRANT NUMBER(s) F 19628-74-C-0102 <i>NEW</i>	15
9. PERFORMING ORGANIZATION NAME AND ADDRESS Electrical and Systems Engineering Dept. Rensselaer Polytechnic Institute Troy, New York 12181		10. PROGRAM ELEMENT, PROJECT, TASK AREA & WORK UNIT NUMBERS 62704H, CDNA0025	
11. CONTROLLING OFFICE NAME AND ADDRESS Deputy for Electronic Technology (RADC) Hanscom AFB, Massachusetts 01731 Monitor/Walter Shedd/ETSD		12. REPORT DATE Aug 1976	11
14. MONITORING AGENCY NAME & ADDRESS (if different from Controlling Office)		13. NUMBER OF PAGES 120	
	12 101p.	15. SECURITY CLASS. (of this report) Unclassified	
16. DISTRIBUTION STATEMENT (of this Report) Approved for public release; distribution unlimited			
17. DISTRIBUTION STATEMENT (of the abstract entered in Block 20, if different from Report)			
18. SUPPLEMENTARY NOTES This research was supported by the Defense Nuclear Agency under Subtask Z990AXTB056, Work Unit 52 entitled "Radiation Effects on Solid State Microwave Device Structures."			
19. KEY WORDS (Continue on reverse side if necessary and identify by block number) Schottky Barrier, Gallium Arsenide, Interface States, Neutron Radiation Effects, Transient Ionizing Radiation <i>(10 to the minus 8th power approx/cm)</i>			
20. ABSTRACT (Continue on reverse side if necessary and identify by block number) The electrical behavior of Schottky barrier junctions before and after neutron irradiation have been explored. Guarded Au/nGaAs diodes were fabricated from bulk and epitaxial material with a preirradiation n factor of 1.03 and saturation current density of $10^{-8}$ amps/cm. After irradiation with low neutron fluences (i.e., carrier removal less than 10%) the reverse current increased by one to two orders of magnitude with only a slight increase in n factor. I-V and C-V measurements from 77°K <i>over</i>			

DD FORM 1 JAN 73 1473

EDITION OF 1 NOV 65 IS OBSOLETE S/N 0102-014-6601

Unclassified 401653 SECURITY CLASSIFICATION OF THIS PAGE (When Data Entered)

20. Abstract (Continued)

to 360<sup>g</sup>K and photoelectric measurements at room temperature were taken in developing an understanding of the effect of neutron irradiation on the electrical characteristics of these Schottky barrier diodes (including with transient ionizing radiation).

The experimental results have been interpreted from an interface state density model as suggested by Levine. The results of this model have been compared to those reported by Levine and Crowell and Roberts with unirradiated diodes. The limitations of interpreting the results using the interface state density model have been delineated experimentally. Calculations indicate that current from field-enhanced emission is present in addition to thermionic emission current from the interface state model. Implications of these results on the use of Schottky junction devices in neutron radiation environments are presented.

FOREWORD

Under Air Force Cambridge Research Laboratories Contract No. F19628-74-C-0102, sponsored by the Defense Nuclear Agency, the Electrical and Systems Engineering Department of Rensselaer Polytechnic Institute has been carrying out research devoted toward studying the effect of neutron irradiation on the metal-semiconductor interface and the resultant performance of Schottky barrier diodes (including with transient ionizing radiation). This report presents the results obtained during the first twelve months of research.

A number of students at Rensselaer contributed to the successful completion of various stages of the program. In particular, J. Narain assisted in device fabrication, M. Kusiak designed and constructed the automated measurement equipment and S. Ashok assisted in the latter stages of measurement and data reduction.

The authors wish to acknowledge the help given by J. Floyd in the neutron irradiations at Brookhaven National Laboratory and by D. E. Lapierre and J. R. Capelli during the transient ionizing irradiations at AFCRL. The suggestions of our contract monitor, Dr. D. A. Neamen, during this program have been deeply appreciated.

ACCESSION for	
NTIS	White Section <input checked="" type="checkbox"/>
DDC	Buff Section <input type="checkbox"/>
UNANNOUNCED	<input type="checkbox"/>
JUSTIFICATION	
BY	
DISTRIBUTION/AVAILABILITY CODES	
Dist.	AVAIL. and/or SPECIAL
A	

## TABLE OF CONTENTS

	<u>Page</u>
1.0 Introduction .....	1
1.1 Technical Background .....	1
1.2 The Program .....	3
2.0 Device Fabrication and Test Instrumentation .....	5
2.1 Au-GaAs Schottky Barrier Junction Fabrication .....	5
2.2 Test Instrumentation .....	9
3.0 Radiation Test Considerations .....	14
3.1 Neutron (Brookhaven BMRR) .....	14
3.2 Transient Ionizing (AFCRL LINAC) .....	15
4.0 Neutron Radiation Results and Discussion .....	18
4.1 I-V Characteristics .....	20
4.2 C-V Characteristics .....	28
4.3 Interface State Density .....	38
4.4 Excess Reverse Current .....	60
5.0 Transient Ionizing Radiation Results and Discussion .....	70
5.1 Au-GaAs Schottky Barrier Junction .....	70
5.2 Evaluation of IMPATT Diode Aftereffects .....	75
6.0 Implications of Results on Radiation Hardening Design .....	82
6.1 Neutron Implications in IMPATT's, MESFET's, and other Microwave Devices .....	82
6.2 Transient Ionizing Implications in IMPATT's .....	85
7.0 Summary and Conclusions .....	87

DISTRIBUTION LIST

LIST OF TABLES

	<u>Page</u>
Table 2.1 Room Temperature Characteristics of Au/nGaAs Schottky Diodes with Different Starting Material .....	10
Table 4.1 Summary of Devices Tested Under Neutron Irradiation .....	19
Table 4.2 Summary of Carrier and Trap Concentrations obtained from C-V Measurements .....	40
Table 5.1 Transient Ionizing Radiation Results for 316 at $8 \times 10^9$ rads/sec .....	71
Table 5.2 Photoresponse of Schottky IMPATT 1B10 (D1) .....	77

LIST OF FIGURES (Continued)

	<u>Page</u>
Fig. 4.13 Schematic Relationship between Barrier Height and Change in Interface State Charge for (a) zero bias (b) reverse bias and (c) forward bias (after Levine <sup>(1)</sup> ).....	42
Fig. 4.14 Surface Electric Field vs. Barrier Height Change for 2E16 .....	50
Fig. 4.15 Log Reverse Current vs. Log Square Root of Reverse Voltage for 2E16 .....	52
Fig. 4.16 Surface Electric Field vs. Barrier Height Change for 2E16 with Image Force Corrections (near zero barrier height change) .....	53
Fig. 4.17 Surface Electric Field vs. Barrier Height Change for 2E16 with Image Force Corrections (for large reverse bias) .....	54
Fig. 4.18 Density of States from Equations (4.40) and (4.41) for 2E16 (data points at far right are obtained independently from linear region of Fig. 4.17) .....	55
Fig. 4.19 Arrhenius Plot of $I_R/T^2$ for 2E16 Before and After Irradiation .....	57
Fig. 4.20 Density of States from Equations (4.40) and (4.41) for 316 .....	58
Fig. 4.21 Comparison of I-V Characteristics of Series 316 After Irradiation at Device and Wafer Levels .....	59
Fig. 4.22 Reverse Current-Voltage Characteristics for 2E16 with Temperature After Irradiation .....	61
Fig. 4.23 Reverse Current vs. (Total Voltage) <sup>-1/2</sup> for 2E16 with Temperature After Irradiation .....	65
Fig. 4.24 Effective Barrier vs. Temperature for 2E16 and 316 ...	67
Fig. 4.25 Reverse Current-Voltage Characteristics for 2E16 with Temperature (Without Irradiation) .....	68
Fig. 5.1 Photographs of Typical Results of Schottky Diode Photocurrent under Transient Ionizing Radiation .....	73

LIST OF FIGURES (Continued)

	<u>Page</u>
Fig. 5.2    Equivalent Circuit for Avalanche Diode with Transient Ionizing Radiation (from Shedd et.al. <sup>(35)</sup> )..	74
Fig. 5.3    Photographs of GaAs Schottky IMPATT Photocurrent under Transient Ionizing Radiation .....	76
Fig. 5.4    IMPATT Diode Bias Circuit Model with Impedance Loci (following Brackett <sup>(37)</sup> ) .....	79

## INTERFACE STATES IN SCHOTTKY BARRIER DIODES

### 1.0 INTRODUCTION

#### 1.1 Technical Background

Schottky barrier diodes are used as rectifying junctions in a wide variety of devices, such as field effect transistors, impact avalanche transit time diodes (IMPATT diodes), RF detectors, and clamping diodes. Although the advantages of using Schottky barriers in these applications are well documented, the Schottky junction has always been less understood than the pn junction. However, recent work by Levine indicated that an interface state model could quantitatively describe the forward and reverse characteristics measured on a variety of different Schottky barriers, such as Cr/Si, Au/GaAs, Ag/ZnS, Au/SrTiO<sub>3</sub>, and ZrSi<sub>2</sub>/n-Si.<sup>(1,2)</sup> This interface state model was used to explain many of the Schottky barrier characteristics previously considered anomalous.

Various transient radiation effects and displacement radiation effects have been measured in Schottky barrier diodes. Yu and Snow<sup>(3)</sup> investigated the behavior of silicon Schottky barriers under low energy (15 to 20 KeV) electron irradiation and fast neutron (greater than 0.1 MeV) irradiation. Planar configurations with a diffused p-n guard ring and a gate controlled structure were used. The principal effects of the neutron radiation were an increase in series resistance due to carrier removal and an increase in both reverse saturation current and forward current due to the decrease in bulk lifetime (for large barrier heights). The principal effect of the ionizing radiation was a decrease in breakdown voltage due to positive space charge in the oxide.

Aukerman<sup>(4)</sup> studied the effect of low energy (0.2 to 0.4 MeV) protons on silicon surface barrier detectors. In particular the damage created in the high field depletion region of the Schottky barrier was compared to that created in comparable bulk material. The main emphasis was on the determination of trap levels, and not on the electrical behavior of the device.

Neamen and Grannemann<sup>(5)</sup> investigated the effect of fast neutrons on GaAsP Schottky barrier diodes. In particular, primary effects such as decrease in carrier concentration, decrease in carrier mobility, and decrease in minority lifetime were evaluated. Epi-layers of GaAsP with concentrations from  $5.7 \times 10^{14}$  to  $3.5 \times 10^{17} \text{ cm}^{-3}$  were grown on GaAs substrates, with chromium metallization used exclusively. Annealing experiments were performed at temperatures up to  $580^\circ\text{C}$ .

Chaffin<sup>(6)</sup> has reported that commercial silicon Schottky barrier diodes did not exhibit an increased leakage current at fluences to  $10^{16} \text{ n/cm}^2$ . However, there is difficulty in reconciling these results with previously reported information (see pages 164 and 165 in reference 6). Considerations such as semiconductor material and metallization type were not explored.

Besides this uncertainty in Schottky junction behavior, devices using Schottky junctions have exhibited anomalous behavior under irradiation. Schottky barrier IMPATT (impact avalanche transit time) diodes exhibit unexpected aftereffects under transient electron exposure,<sup>(7)</sup> while diffused junction devices exhibit characteristics in agreement with theory.<sup>(8,9)</sup> Furthermore, Schottky gate field effect transistors exhibit deterioration under neutron irradiation at fluences an order of

magnitude below that of comparable junction gate devices.<sup>(10,11)</sup> In addition, the saturation current of Ag surface barrier GaAs varactors actually decreased by an order of magnitude after exposure to  $10^{15}$  fast neutrons/cm<sup>2</sup>, while similar diffused GaAs varactors showed an expected increase (attributed to usual bulk effects).<sup>(12)</sup> These anomalous radiations effects in devices with Schottky junctions cannot be explained from the Schottky junction radiation results previously reported.<sup>(3-6)</sup>

#### 1.2 The Program

The purpose of this program was to explore the effect of fast neutron irradiation on the metal-semiconductor interface and the resultant performance of Schottky barrier diodes (including the effect of transient ionizing radiation). Gallium arsenide was selected since it is the semiconductor of greatest interest in a variety of high performance microwave devices (IMPATT's, FET's and mixer diodes). Gold was selected as a metallization since there was a variety of results reported in the literature for comparison purposes (although in the next phase of this program aluminum will be used). The device structure (described in Section 2.1) was selected to eliminate surface leakage and permit electrical measurements giving a clear indication of changes introduced at the metal-semiconductor interface during neutron irradiation. The experimental results are interpreted using the interface state model and, where necessary, an enhanced field emission model. Well-known radiation effects, such as compensation, are included when interpreting

the data with these models. The implications of our findings on the use of Schottky junction devices in radiation hardened systems are also considered.

In Chapter 2 the device structure and fabrication are described (Section 2.1) as well as the instrumentation used in the electrical measurements (2.2). In Chapter 3, the facilities and test apparatus used in neutron and transient ionizing irradiations are described. In Chapter 4, the neutron radiation and discussion are presented, while the transient ionizing results and discussion are presented in Chapter 5. In Chapter 6, the implications of these findings on the design of Schottky junction devices for radiation hardened systems are presented. In Chapter 7, we summarize the conclusions from this work.

## 2.0 DEVICE FABRICATION AND TEST INSTRUMENTATION

### 2.1 Device Fabrication

The device structure designed for this program consists of four Schottky barrier diodes on a 0.100" x 0.100" chip. Three of the diodes have a guard ring and consist of a gold center dot 15 mil in diameter and a gold outer guard ring three mils in width and one mil away from the gold center dot. A sketch of the guarded device is shown in Fig. 2.1. The fourth diode consists of a gold center dot without the outer guard ring. The purpose of the guard ring is to eliminate surface leakage currents flowing out of the center dot during the I-V measurements. On the back surface, 8 mil diameter dots centered with respect to the 15 mil gold center dots on the top surface, are opened on the evaporated metal layer. The purpose of the back-surface openings is to insure reproducible photoelectric measurements.

A fabrication process was developed for obtaining Au-n-GaAs Schottky barrier diodes which conform to the device test structure designed. The starting material is either n type bulk GaAs wafers or  $nn^+$  epitaxial GaAs wafers, with carrier concentrations from  $1.2 \times 10^{15}/\text{cm}^3$  to  $1.0 \times 10^{17}/\text{cm}^3$ . The ohmic back contact to the diodes is made by evaporating 6000 Å of indium on the back surface of the wafer and subsequent alloying in a forming gas atmosphere at  $300^\circ\text{C}$  for two minutes. The nature of this contact was evaluated using bulk material with a doping concentration of  $5 \times 10^{15}/\text{cm}^3$  and it was found to be ohmic in both directions (therefore, the same process is used for both bulk and epitaxial wafers).

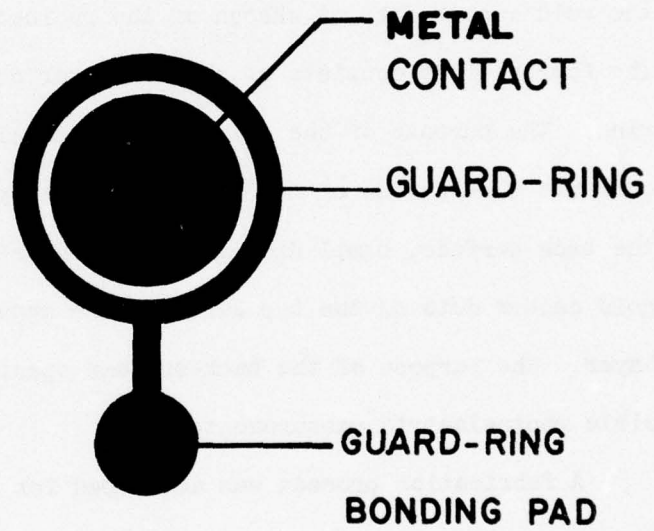


Fig. 2.1 Expanded View of Guarded Diode (Scale: approximately 70:1)

Prior to the alloying operation, 8 mil diameter dots are opened on the evaporated indium layer using photolithographic techniques. These 8 mil holes serve as an optical window for the photoelectric measurements and result in more reproducible photoelectric response measurement since the illumination is always on the same area and edge illumination is prevented.

The Schottky barrier is formed by evaporating  $1000 \text{ \AA}$  of Au over the front (epitaxial) side of the wafer. Just before evaporation the wafer is cleaned with concentrated HCl for a few minutes, rinsed thoroughly with methanol and blown dry with filtered air. The evaporation is carried out in a vacuum system with the wafer heated at  $100^{\circ}\text{C}$ . The device test structure is defined on the gold film with a thin layer of photoresist. The gold thickness of the device test structure is next increased to approximately one or two microns by electroplating gold, using the photoresist as a mask. An IR microscope is used to align the front surface Schottky junction with the back surface optical window described in the previous paragraph. The photoresist is removed by either chemically cleaning or in a plasma oxidation unit. Next, the device test structure is obtained by removing the evaporated gold film from the unwanted areas with an etch consisting of KI and  $\text{I}_2$  dissolved in water, using the electroplated gold as a mask. With this etch a mesa etch is not needed to avoid edge breakdown (as is required if aqua regia is used as the gold etch). The front surface of a chip after dicing is shown in Fig. 2.2, in which the bonding wires are apparent.

After wafer testing and dicing, the chips obtained are mounted in an eight-lead TO-5 header using a silver epoxy, with the curing

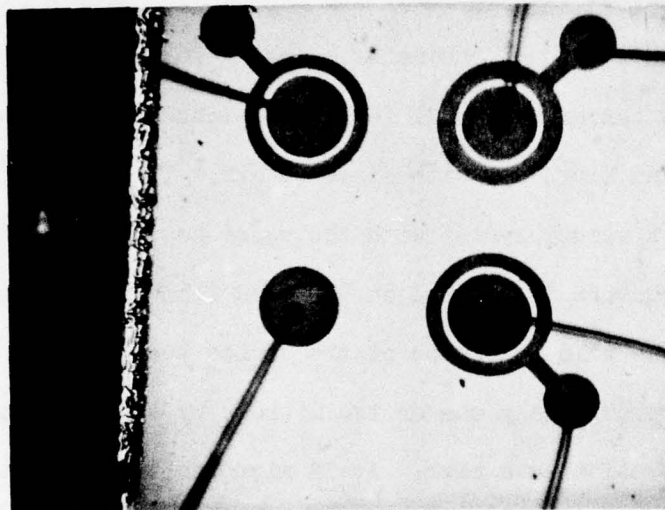


Fig. 2.2 Photograph of Front Surface of Chip (Scale: approximately 30:1)

temperature kept below  $100^{\circ}\text{C}$ . Gold wire is used for connecting the device terminals to the header posts with a bonding machine. The TO-5 header has a 0.085" diameter hole drilled in the bottom which allows illumination of the 4 junctions of the chip structure during photoelectric measurements. With these procedures, Au-nGaAs Schottky diodes were fabricated with forward and reverse current-voltage characteristics comparable to those reported in the literature. That is, the n factor was typically 1.03 (slightly dependent upon forward bias) and the reverse current was approximately  $10^{-9}$  amps. Such good devices were obtained on bulk GaAs with carrier concentrations between  $5 \times 10^{15}$  and  $1 \times 10^{17} \text{ cm}^{-3}$  and epitaxial material having carrier concentrations between  $3 \times 10^{15}$  and  $9 \times 10^{16} \text{ cm}^{-3}$ , as shown in Table 2.1.

## 2.2 Test Instrumentation

Test facilities were developed for the measurement of DC current-voltage (I-V) and 1 MHz capacitance-voltage (C-V) characteristics from  $77^{\circ}\text{K}$  to  $400^{\circ}\text{K}$  and for photoelectric measurements at room temperature. Both the I-V and C-V measurements were automated, using special purpose ramp generators to obtain a linearly increasing voltage and an XY recorder for a permanent record. A block diagram is shown in Fig. 2.3. Two ramp generators were designed - a low voltage, medium current unit for forward bias measurements and a high voltage, low current unit for reverse bias tests. Besides the voltage range, the slope of the ramp (i.e.,  $dv/dt$ ) could also be controlled with the ramp generators developed. The I-V and C-V measurements were recorded on 38 cm x 25 cm graph paper

Device Series	Starting Material	Carrier Concentration ( $\text{cm}^{-3}$ )	n Factor (over $10^{-9}$ - $10^{-7}$ A)	Saturation Current (Amps) (extrapolated from I-V data)	Reverse Current (Amps) at Medium Voltage
228	Epitaxial	$1.2 \times 10^{15}$	1.007	$10^{-12}$	$5 \times 10^{-11}$
2E16	Epitaxial	$3.0 \times 10^{16}$	1.01	$6 \times 10^{-12}$	$4 \times 10^{-11}$
410	Bulk	$6.0 \times 10^{15}$	1.02	$8 \times 10^{-12}$	$6 \times 10^{-9}$
316	Bulk	$8.5 \times 10^{16}$	1.05	$3 \times 10^{-11}$	$2 \times 10^{-9}$
300	Bulk	$1.0 \times 10^{17}$	1.07	$2 \times 10^{-11}$	$10^{-9}$

Table 2.1: Room Temperature Characteristics of Au/nGaAs Schottky Diodes with Different Starting Material

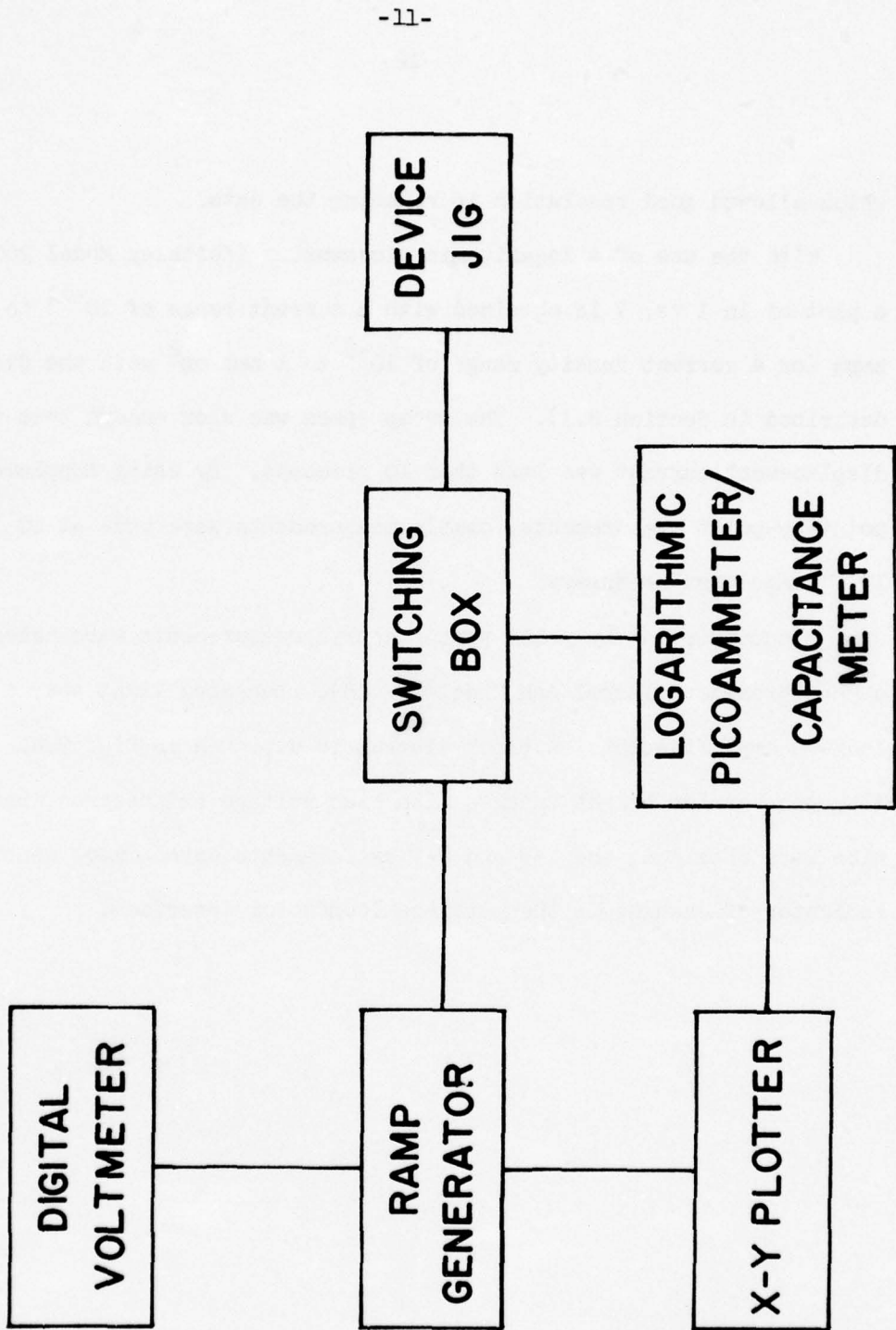


Fig. 2.3 Diagram of Automated I-V and C-V Facility

which allowed good resolution in reducing the data.

With the use of a logarithmic picoammeter (Keithley Model 26000) a plot of  $\ln I$  vs.  $V$  is obtained with a current range of  $10^{-11}$  to  $10^{-3}$  amps (or a current density range of  $10^{-8}$  to  $1 \text{ amp/cm}^2$  with the diodes described in Section 2.1). The sweep speed was slow enough that the displacement current was less than 10 picoamps. By using supplementary point-by-point measurements, stable measurements were made at  $10^{-13}$  to  $10^{-12}$  amps when necessary.

Standard point-by-point photoelectric measurements were taken using a monochromator (Jarrel Ash Model 82-415), a tungsten light source and lock-in amplification. A block diagram is depicted in Fig. 2.4. Although barrier height changes with bias voltage and neutron irradiation were obtained, the I-V and C-V measurements were a more sensitive indicator of changes in the metal-semiconductor interface.

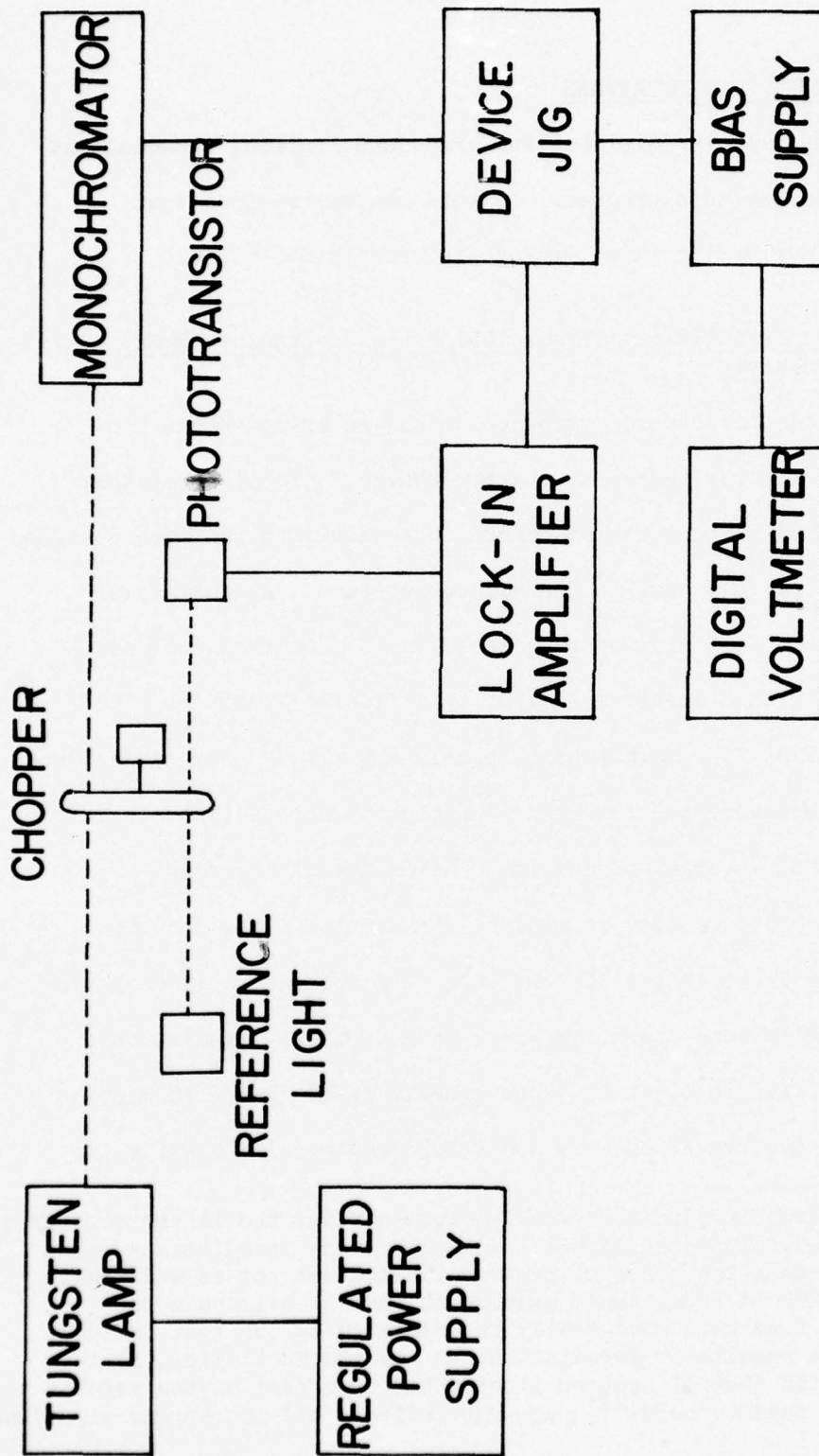


Fig. 2.4 Diagram of Photoelectric Measurement Facility

### 3.0 RADIATION TEST CONSIDERATIONS

Both fast neutron irradiations and transient ionizing irradiations were performed during this program. In this chapter various test considerations involved in this testing are briefly described.

#### 3.1 Neutron Irradiations (Biomedical Research Reactor (BMRR) at Brookhaven

Neutron irradiations were performed on the water-moderated Biomedical Research Reactor (BMRR) at the Brookhaven National Laboratory (BNL). The mounted chips were irradiated in an aluminum fixture designed to support up to 12 TO-5 cans in the allowable space. At full power of 3 megawatts, the fast neutron flux is  $1.7 \times 10^{13}$  neutrons/cm<sup>2</sup>/sec at the core edge with a spectrum similar to a fission spectrum. The thermal neutron flux is somewhat high, namely  $4.5 \times 10^{13}$  neutrons/cm<sup>2</sup>/sec, at full power. However, the low energy of these neutrons (less than 0.5 eV or more than an order of magnitude below the displacement threshold in GaAs<sup>(12)</sup>) results in minimal permanent effects and the radioisotopes produced in the devices were at a tolerable concentration.\*

At the 100 kilowatts operating power used in these irradiations, the fast neutron flux is  $0.6 \times 10^{12}$  neutrons/cm<sup>2</sup>/sec. For a 10 minute irradiation, the neutron fluence is  $3.6 \times 10^{14}$  neutrons/cm<sup>2</sup>, while for

---

\* Preliminary neutron irradiations were performed using the linear accelerator at Rensselaer Polytechnic Institute. Although these irradiations were discontinued because the absolute neutron fluence was not as well calibrated as the BMRR at Brookhaven, cadmium shields to eliminate the thermal neutron flux were more easily incorporated in the test fixture. By comparing the results of irradiations at the two facilities, it is concluded that the thermal neutron fluence had no effect on the results reported, i.e., subthreshold<sup>(13)</sup> radiation effects did not appear significant.

a 60 minute irradiation the fluence is  $2.2 \times 10^{15}$  neutrons/cm<sup>2</sup>. This core edge position at the BMRR was most suitable for these two fast neutron fluences desired.

In order to minimize heating during the neutron irradiations, the support aluminum fixture was designed for minimum weight (25 grams including 12 TO-5 packages). A thermocouple was used during the initial irradiation to verify that the temperature rise was less than 5°C. During all the neutron irradiation the temperature of the devices was maintained below 30°C, so that no annealing occurred. Although not required on this program, fast neutron fluences as high as  $10^{17}$  n/cm<sup>2</sup> could be obtained using these facilities with the device temperature kept below 125°C.

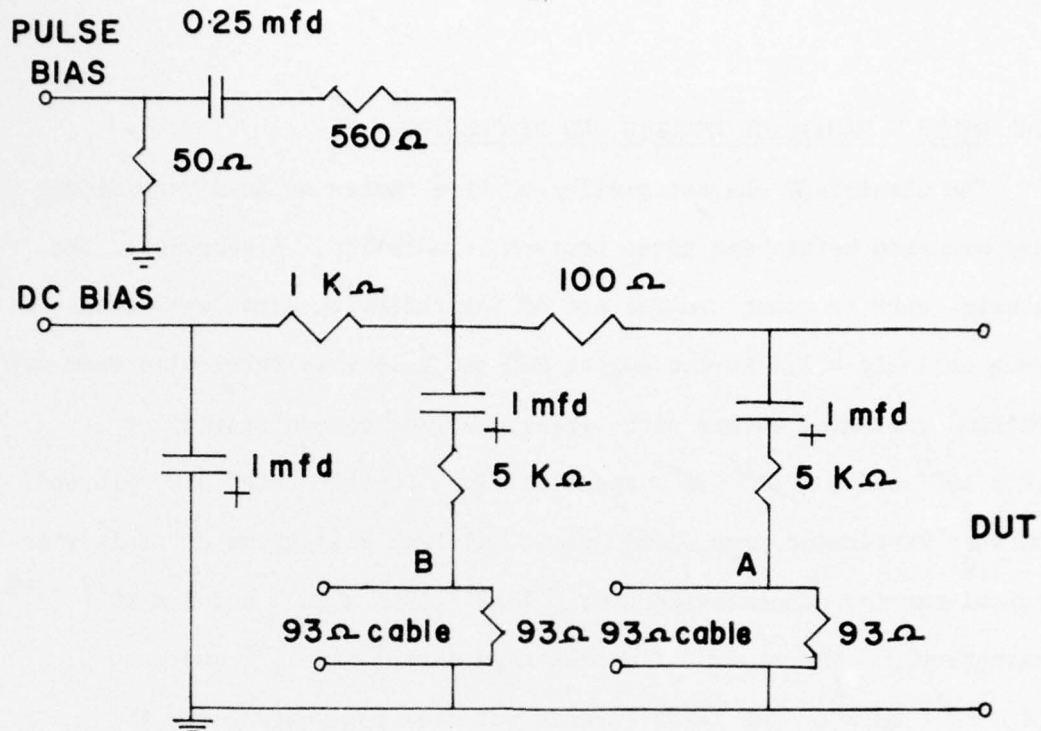
The effect of neutron irradiation on the pin-to-pin package leakage of the TO-5 cans was checked to insure that this parallel current was sufficiently small. In general, the leakage was less than 1 picoamp before and after the neutron irradiations. In some cases, the TO-5 cans with holes drilled for photoelectric measurements (see Section 2.1) showed excess leakage currents as high as  $10^{-10}$  amps (at high voltage) between same pins before neutron irradiation. This leakage was attributed to stresses introduced in the glass during the drilling. However, by careful drilling and TO-5 can pretesting, packages with preirradiation leakage greater than a few picoamps were eliminated.

### 3.2 Transient Ionizing Testing (Linear Accelerator at AFCRL)

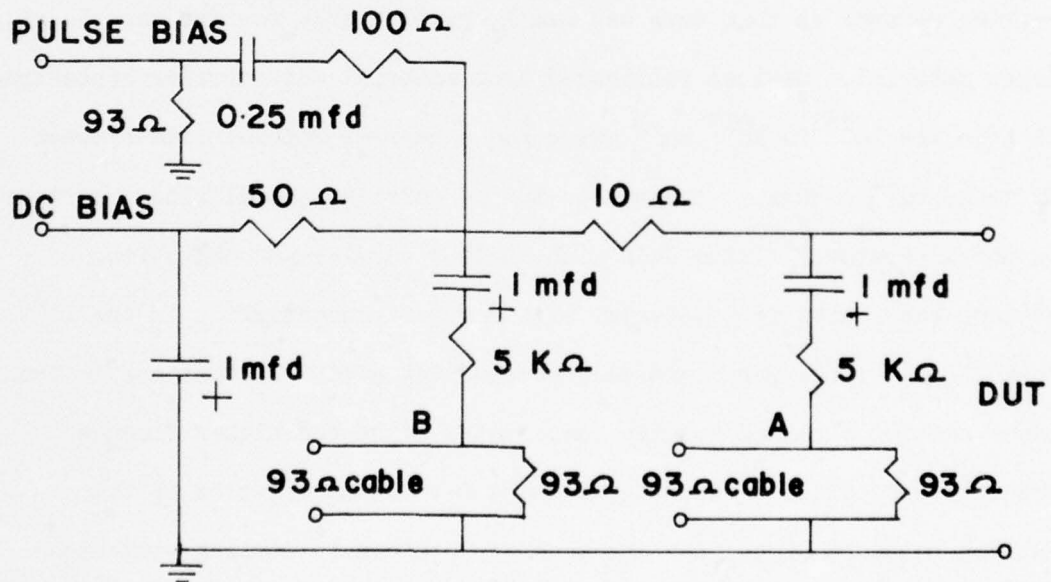
The transient ionizing radiation testing was performed at the linear accelerator (LINAC) facility at AFCRL. The accelerator was

used to generate a 10 MeV electron beam of 100 nanosecond duration. Dose rates between  $10^8$  and  $8 \times 10^9$  rads/sec were achieved with only a small change in beam energy by varying the injector current. The chips were mounted in an evacuation test fixture with the dose rate monitored using TLD dosimetry. The evacuated fixture insured that air ionization effects did not affect the device evaluation during irradiation.

During the irradiation, the photocurrent and photovoltage of the diode under test were measured as a function of bias voltage (below breakdown) or bias current (above breakdown) using the bias circuits shown in Fig. 3.1. Since the Au-n GaAs Schottky diodes in the TO-5 packages are not well heat sunk, pulse biasing was used to obtain the higher bias currents. Typical bias conditions were one-third of the breakdown voltage, breakdown voltage (defined at 0.1 mA and denoted by  $V_B$ ), 40 mA, 100 mA, and 400 mA. Devices were tested using both the 470 ohm and 47 ohm impedance bias circuits.



HIGH IMPEDANCE CIRCUIT (470 Ω)



LOW IMPEDANCE CIRCUIT (47 Ω)

Fig. 3.1 Bias Circuits Used in Transient Ionizing Radiation Testing

#### 4.0 NEUTRON RADIATION RESULTS AND DISCUSSION

The electrical characteristics of five series of Au-n GaAs diodes were measured before and after neutron irradiation. A summary of the material carrier concentration and of the radiation dose level used is given in Table 4.1. Device series 228 and 2E16 were fabricated from n-n<sup>+</sup> VPE(100) epitaxial wafers with typical carrier concentrations of  $1.2 \times 10^{15}$  and  $3 \times 10^{16} \text{ cm}^{-3}$  respectively. Device series 410, 316 and 300 were fabricated from (100) wafers cut from boat grown crystals with typical carrier concentrations of  $6 \times 10^{15}$ ,  $8.5 \times 10^{16}$  and  $1 \times 10^{17} \text{ cm}^{-3}$  respectively. The neutron fluences used were  $3.6 \times 10^{14}$  and  $2.2 \times 10^{15} \text{ n/cm}^2$ . The lower fluence was used for determining the sensitivity of the I-V characteristics to neutron damage as the carrier removal at this dose was small, particularly for the more heavily doped material. Devices fabricated from material with carrier concentration in the  $10^{16}$  to  $10^{17} \text{ cm}^{-3}$  range had a carrier removal rate between 12 to 19  $\text{cm}^{-1}$ . This is comparable to the carrier removal rate reported in the literature<sup>(14)</sup> for GaAs with similar carrier concentration. Devices fabricated from material with carrier concentration in the  $10^{15}$  to  $10^{16} \text{ cm}^{-3}$  range were partially compensated after irradiations to the lower neutron dose and totally compensated after the higher fluence. Nevertheless, evaluation of the I-V and C-V characteristics of these devices helped to interpret the results obtained in devices with higher doping. In what follows we present and discuss in detail the results obtained with devices of the 2E16 series since the epitaxial material used in their fabrication is similar to the one used in GaAs solid state

Device Series	Starting Material	Carrier Concentration ( $\text{cm}^{-3}$ )	Neutron Fluence ( $\text{n/cm}^2$ )	Zero Bias Capacitance Change	Carrier Removal Rate ( $\text{cm}^{-1}$ )
228	Epitaxial	$1.2 \times 10^{15}$	$2.2 \times 10^{15}$	Compensated	----
			$3.6 \times 10^{14}$	-75%	
2E16	Epitaxial	$3 \times 10^{16}$	$3.6 \times 10^{14}$	-10%	12
410	Bulk	$6 \times 10^{15}$	$2.2 \times 10^{15}$	Compensated	----
			$3.6 \times 10^{14}$	-2%	
316	Bulk	$8.5 \times 10^{16}$	$2.2 \times 10^{15}$	-15%	19
			$2 \times 10^{15}$	-20%	
300	Bulk	$1 \times 10^{17}$	$2.2 \times 10^{15}$	-20%	16

TABLE 4.1 Summary of Devices Tested Under Neutron Irradiation

microwave devices. Although similar results were obtained in the other series of devices, complete results are not included for the sake of brevity.

#### 4.1 I-V Characteristics

Figure 4.1 shows photographs of the forward and reverse I-V characteristics before and after irradiation taken with a curve tracer. The forward characteristics show an increase in the series resistance after irradiation. The reverse characteristics show a breakdown voltage of 30 volts at 0.5 mA in agreement with values reported in the literature for GaAs pn junctions.<sup>(15)</sup> After irradiation the breakdown characteristics are softer than before irradiation. Detailed I-V characteristics before irradiation are shown in Fig. 4.2. The ideality factor "n" of the forward characteristics changes from 1.01 at low forward voltages to 1.03 at 300 mV. These values are also in agreement with values previously reported.<sup>(16)</sup>

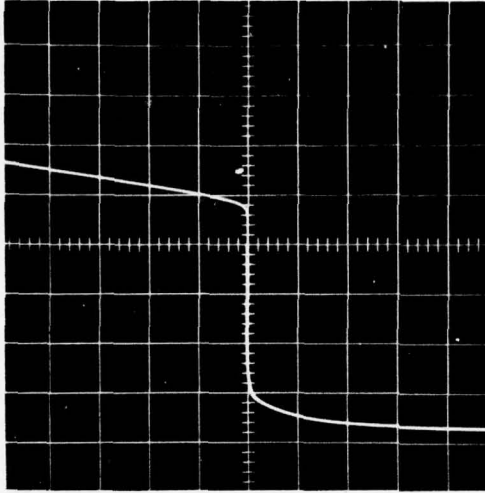
The saturation or leakage current  $I_s$  was obtained by extrapolating the I-V forward characteristics (for voltages higher than  $4 kT/q$ ) to the zero voltage axis. A plot of  $\ln(I_s/T^2)$  vs.  $1/T$  is shown in Fig. 4.3. Since the leakage current in the case of thermionic emission is given by:

$$I_s/A = A^* T^2 \exp[-\phi_B(0)/kT] \quad (4.1)$$

where A is the cross sectional area of the device,  $A^*$  the Richardson constant, T the absolute temperature and  $\phi_B(0)$  the metal-semiconductor barrier height at zero volt bias, the data of Fig. 4.3 gives a barrier height of 0.9 eV. It should be pointed out that the barrier height

SERIES 2E16

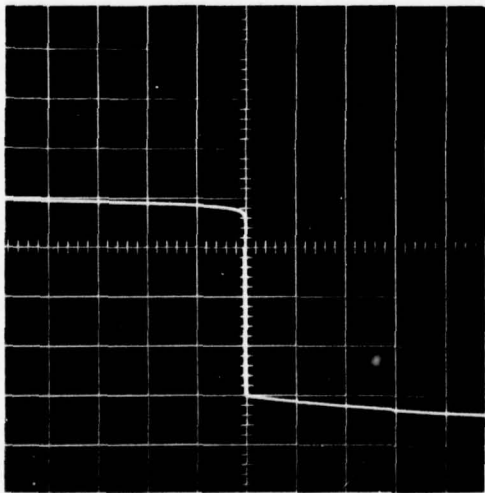
-21-



$I_F \leftarrow \rightarrow I_R$   
(0.5mA/DIV)

$V_R \leftarrow \rightarrow V_F$   
(10 V/DIV) (0.5 V/DIV)

**A. WITHOUT IRRADIATION**



$V_R \leftarrow \rightarrow V_F$   
(10 V/DIV) (0.5V/DIV)

**B. WITH  $0.36 \times 10^{15} \text{ n/cm}^2$**

Fig. 4.1 Overview of I-V Characteristics of 2E16 with and without Irradiation at Room Temperature

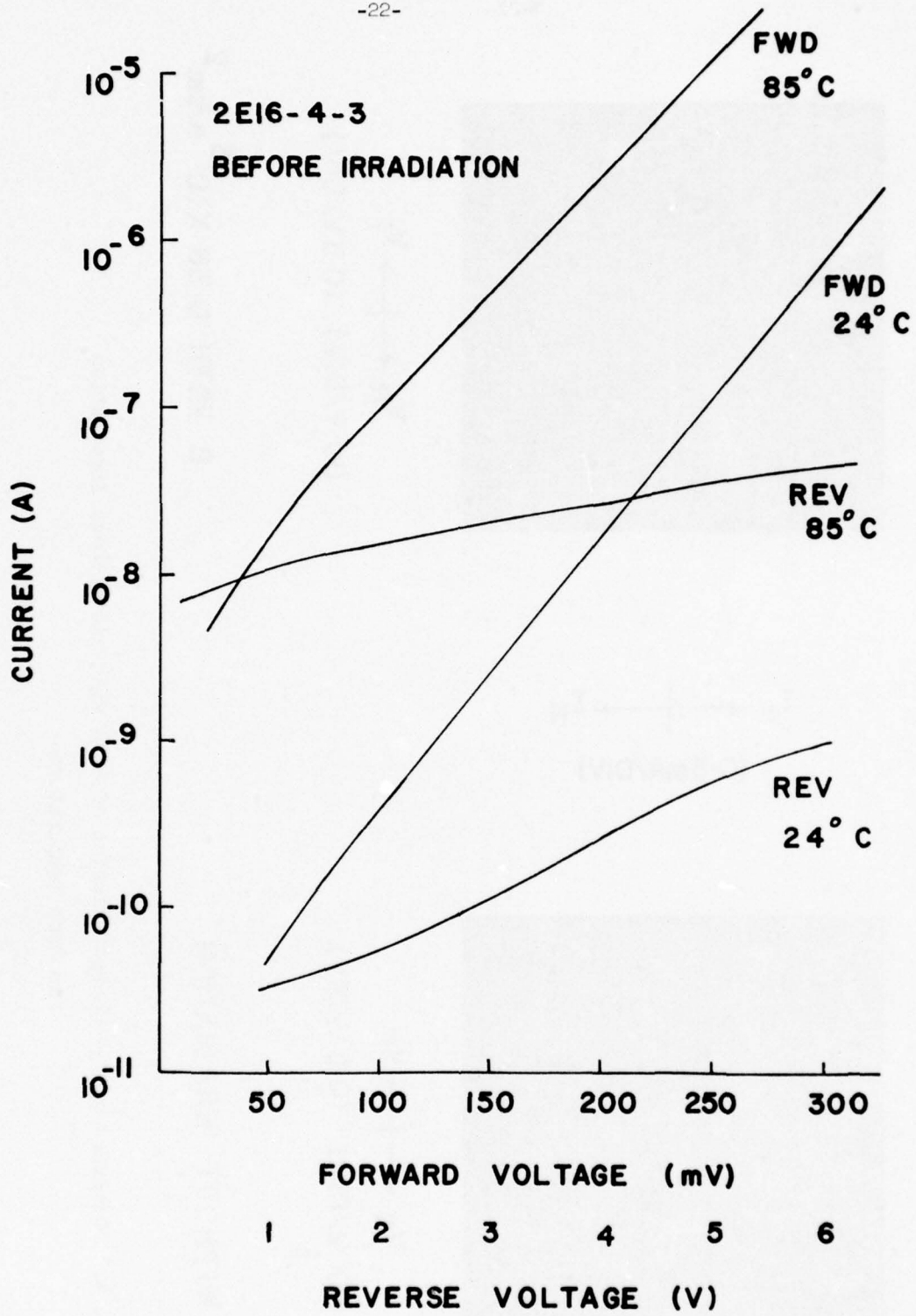


Fig. 4.2 Detailed I-V Characteristics of 2E16  
Before Irradiation

SERIES 2E16  
BEFORE IRRADIATION

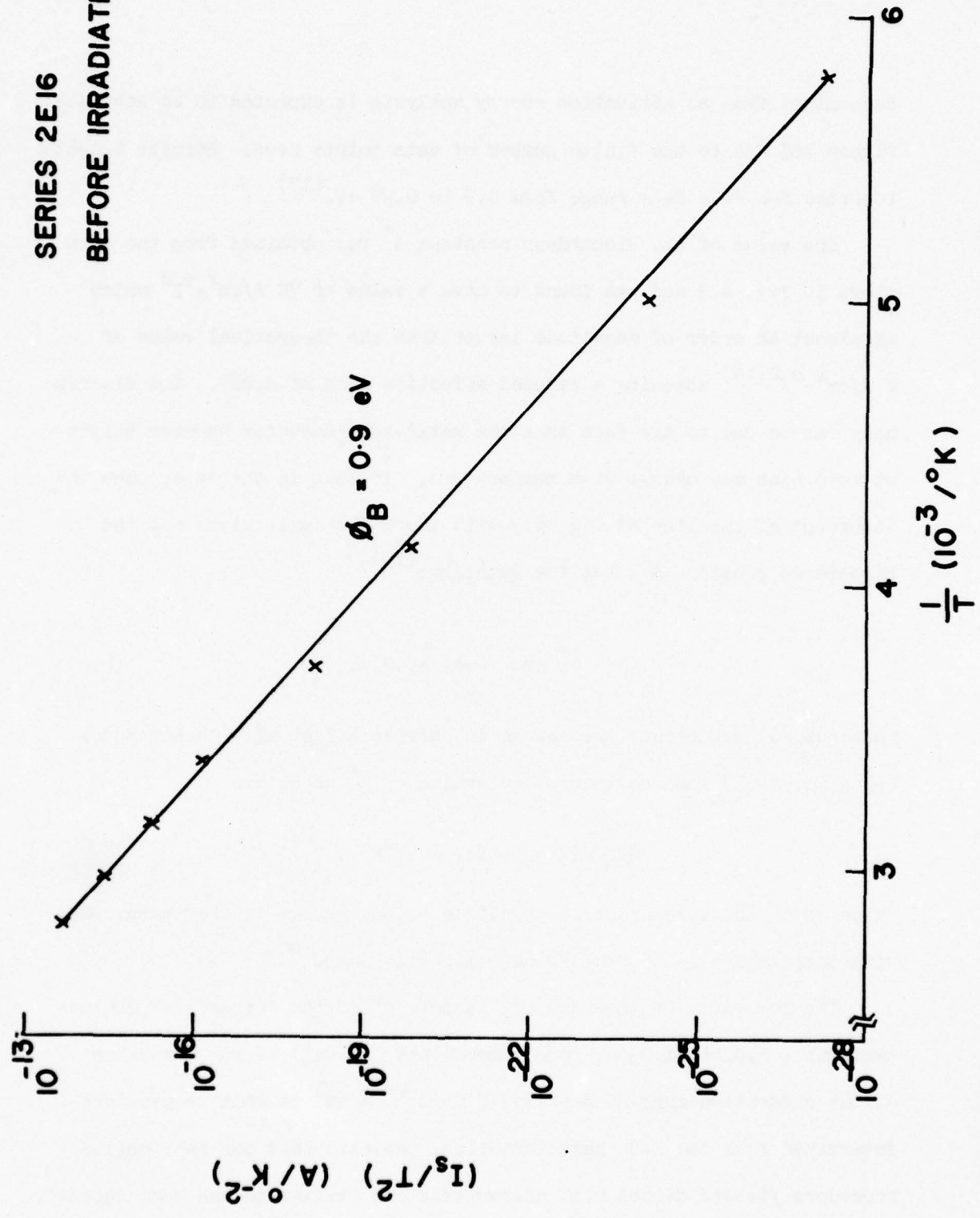


Fig. 4.3 Arrhenius Plot of  $I_s/T^2$  for 2E16 Before Irradiation

determined from an activation energy analysis is expected to be accurate within 10% due to the finite number of data points used. Barrier heights reported for Au-n GaAs range from 0.9 to 0.95 eV. (17)

The value of the Richardson constant  $A^*$  was obtained from the data shown in Fig. 4.3 and was found to have a value of  $70 \text{ A/cm}^2 \cdot \text{K}^2$  which is almost an order of magnitude larger than the theoretical value of  $8 \text{ A/cm}^2 \cdot \text{K}^2$  (18) assuming a reduced effective mass of 0.067. The discrepancy can be due to the fact that the metal-semiconductor barrier height at zero bias may change with temperature. If that is the case, then the intercept of the line of Fig. 4.3 with the  $T = \infty$  axis gives not the Richardson constant  $A^*$ , but the quantity: (19)

$$A^* \exp \left\{ 1/k(d\phi_B/dT) \right\} \quad (4.2)$$

where  $d\phi_B/dT$  represents the change in barrier height with temperature. Using Eq. (4.2) and the theoretical value of  $A^*$  we obtain

$$d\phi_B/dT = -0.17 \text{ meV/}^\circ\text{K}$$

which is of the same order of magnitude as the change of the energy gap with temperature ( $-0.5 \text{ meV/}^\circ\text{K}$ ) determined in GaAs. (20)

The low value of the ideality factor "n" of the forward I-V characteristics, 1.01 to 1.03 at room temperature, as well as the low value of the saturation current density,  $7 \times 10^{-9} \text{ A/cm}^2$  at room temperature determined from the I-V characteristics, indicate that our fabrication procedure yielded diodes with characteristics similar to the best recently reported. (16)

The I-V characteristics for the same device after neutron irradiation are shown in Fig. 4.4. A slight change was found in the forward characteristics. The ideality factor increased to 1.07 at low forward bias voltage and to 1.1 at 300 meV. An activation energy plot of  $I_S/T^2$  vs.  $1/T$  for the irradiated device is shown in Fig. 4.5. The values of the barrier heights determined from the data of Figs. 4.3 and 4.5, 0.9 and 0.91 eV respectively, are each within the limits of experimental error and it can be concluded that the barrier height did not change with neutron irradiation.

In contrast with the forward I-V characteristics, Figs. 4.2 and 4.4 show that, at room temperature and 6 volt reverse bias, the leakage current changed by more than an order of magnitude after irradiation. At higher temperatures the increase is less but appreciable. In silicon devices, it has been found that the increase in reverse current of a neutron irradiated pn junction is due to an increase in the generation rate in the depletion layer caused by neutron displacement damage.<sup>(21)</sup> In order to determine if that is the case in the devices tested, we carried out the following analysis.

The reverse current due to generation in the depletion layer is given by<sup>(22)</sup>

$$I_R = q A W n_i / \tau \quad (4.3)$$

where W is the width of the depletion layer,  $n_i$  the intrinsic carrier concentration and  $1/\tau$  the generation rate due to a deep level. Since the reverse bias depletion layer capacitance  $C_R$  is given by:

$$C_R = \epsilon A / W \quad (4.4)$$

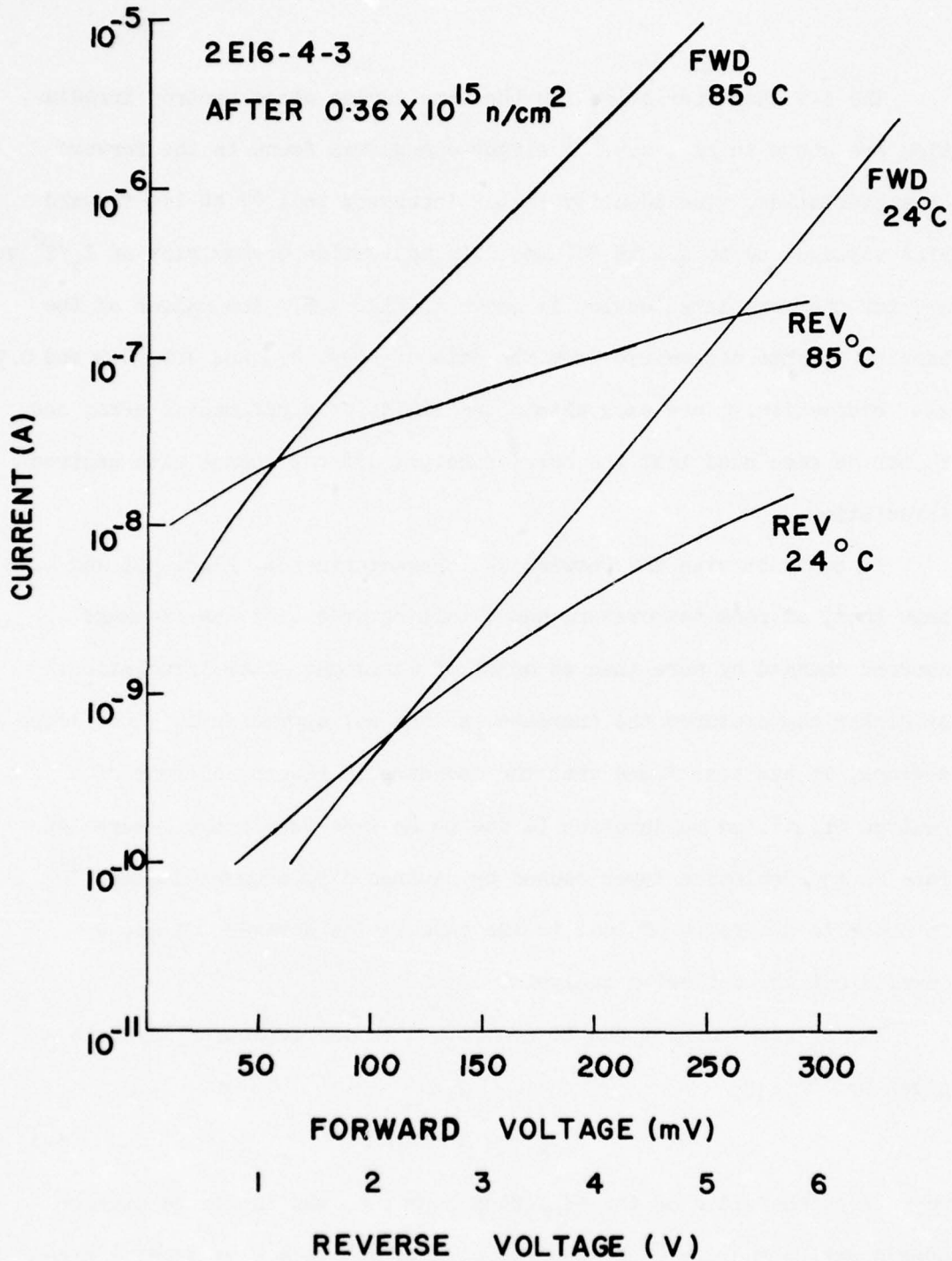


Fig. 4.4 Detailed I-V Characteristics of 2E16 After Irradiation

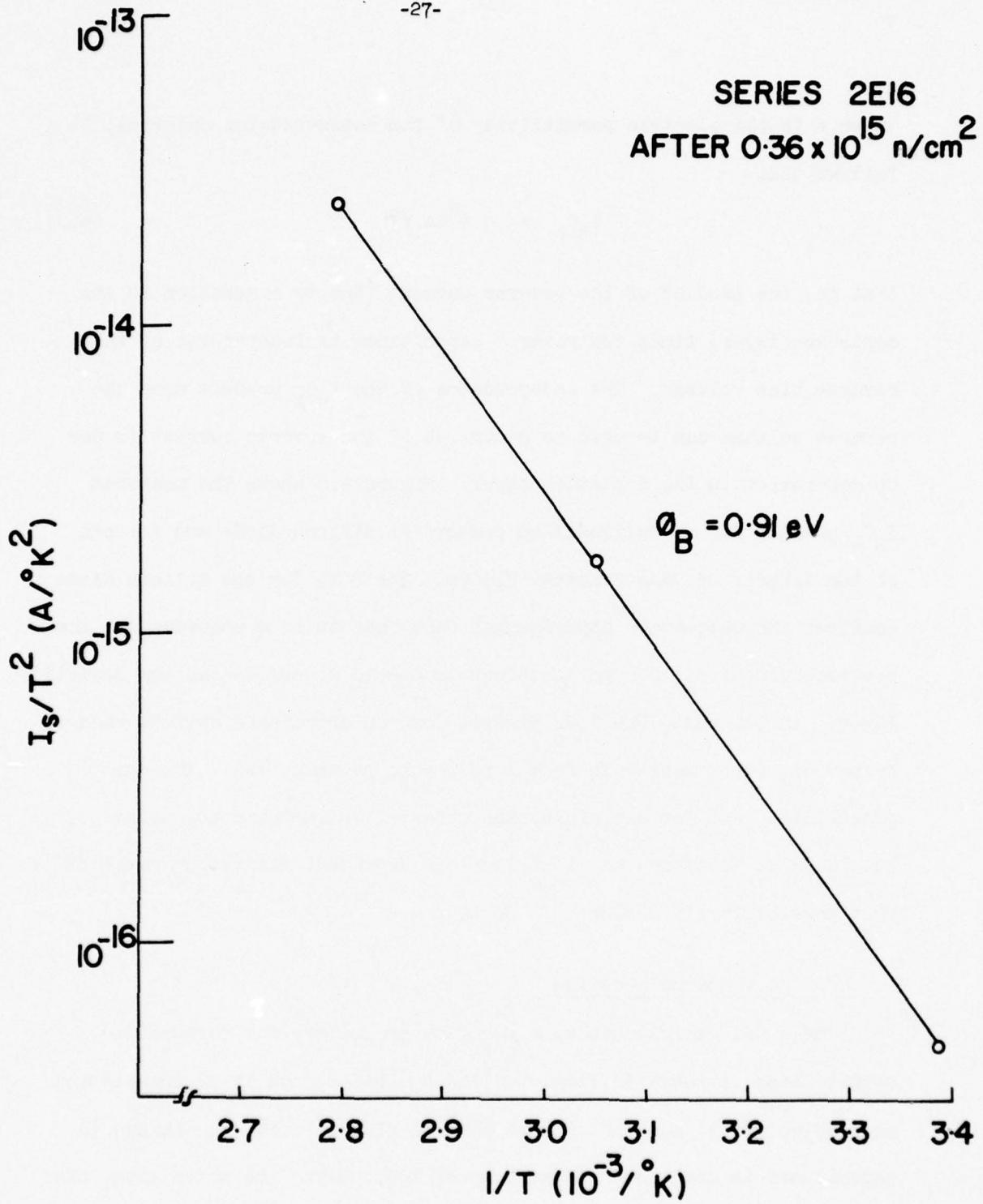


Fig. 4.5 Arrhenius Plot of  $I_s/T^2$  for 2E16 After Irradiation

where  $\epsilon$  is the electric permittivity of the semiconductor material, it follows that

$$I_{RR}C_R = q A^2 \epsilon n_i / \tau \quad (4.5)$$

that is, the product of the reverse current (due to generation in the depletion layer) times the reverse capacitance is independent of the reverse bias voltage. The independence of the  $I_{RR}C_R$  product upon the reverse voltage can be used to determine if the reverse current is due to generation in the depletion layer. Figure 4.6 shows the measured  $I_{RR}C_R$  product for an unirradiated commercial silicon diode and for one of the irradiated GaAs Schottky diodes. The data for the silicon diode confirms the well-known experimental fact that at room temperature, the reverse current silicon pn junctions is due to generation in the depletion layer. In contrast, the  $I_{RR}C_R$  product for the irradiated devices changes by two orders of magnitude from 1 to 6 volt reverse bias. The only possibility left for explaining the observed characteristics using Eq. (4.5) is to assume an electric field dependent generation rate  $1/\tau$ . This possibility is explored in Section 4.4.

#### 4.2 C-V Characteristics

The 1 MHz capacitance as a function of voltage for forward and reverse bias is shown in Figs. 4.7 and 4.8 before and after irradiation respectively. Because of the low neutron fluence used, the change in capacitance is small and of the order of 10%. Using the above data, the quantity  $1/C^2$  was plotted as a function of reverse bias voltage and the results are shown in Fig. 4.9. In order to analyze the data of Fig. 4.9,

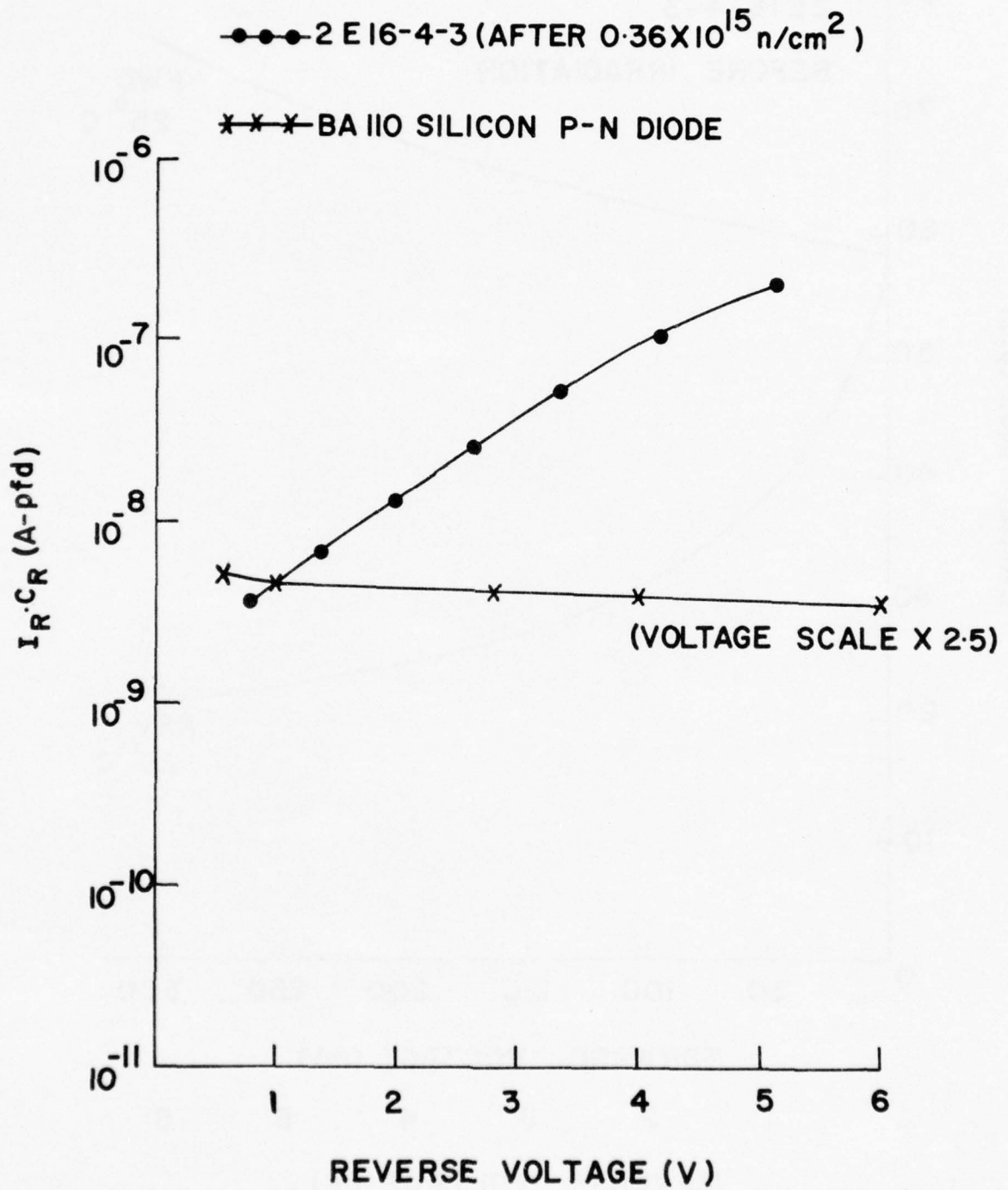


Fig. 4.6 Current Capacitance Product vs. Reverse Voltage

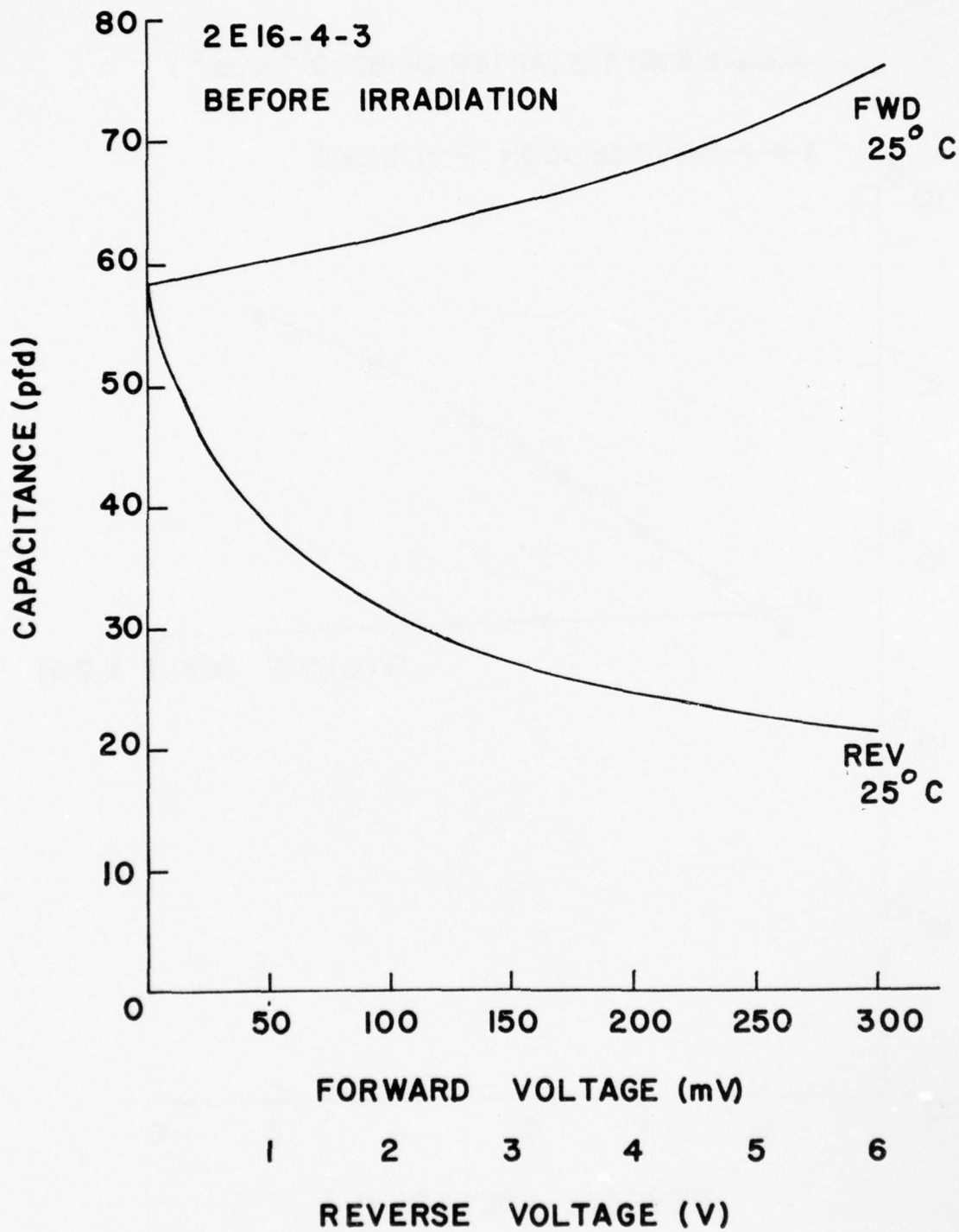


Fig. 4.7 Detailed C-V Characteristics of 2E16 Before Irradiation

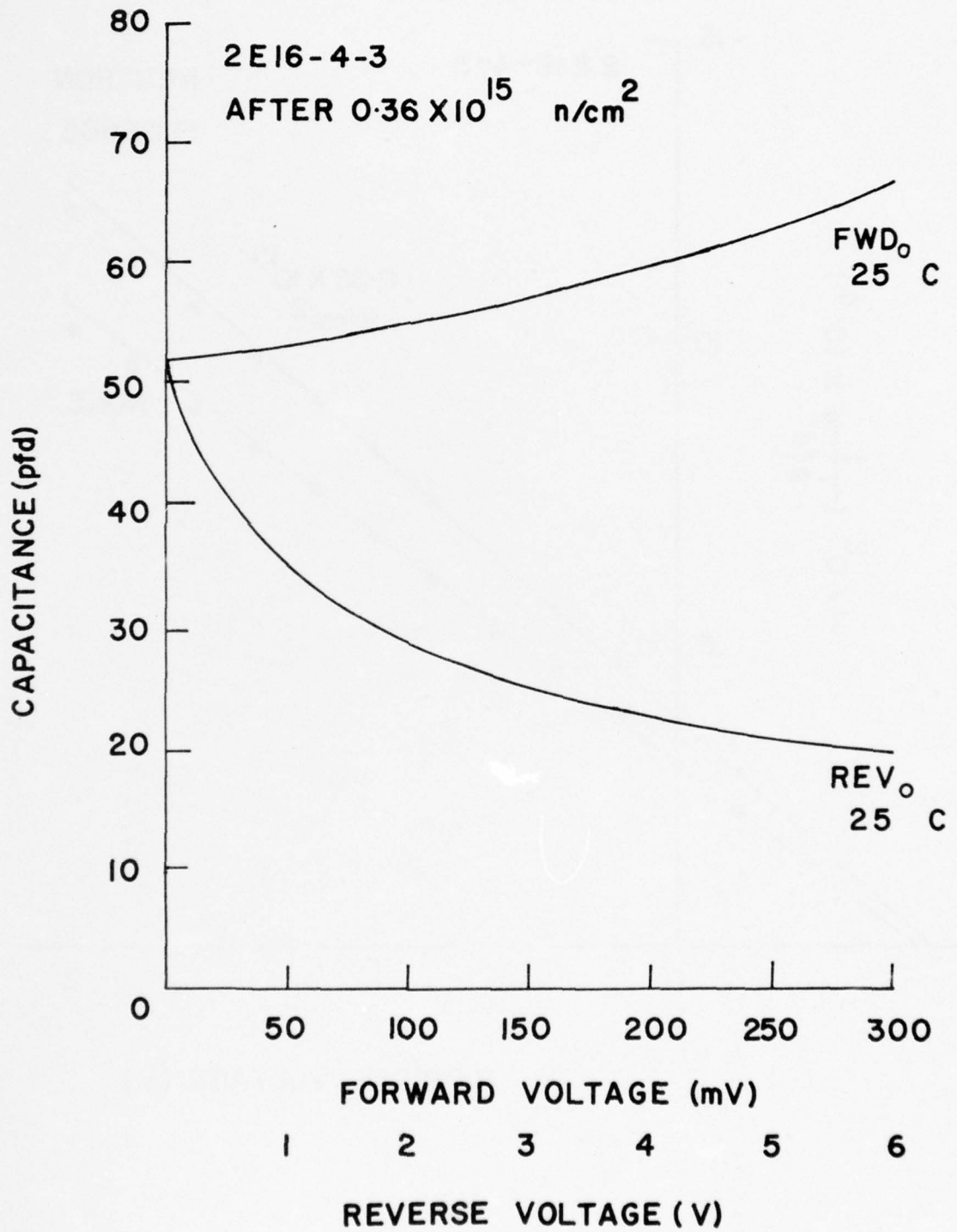


Fig. 4.8 Detailed C-V Characteristics of 2E16 After Irradiation

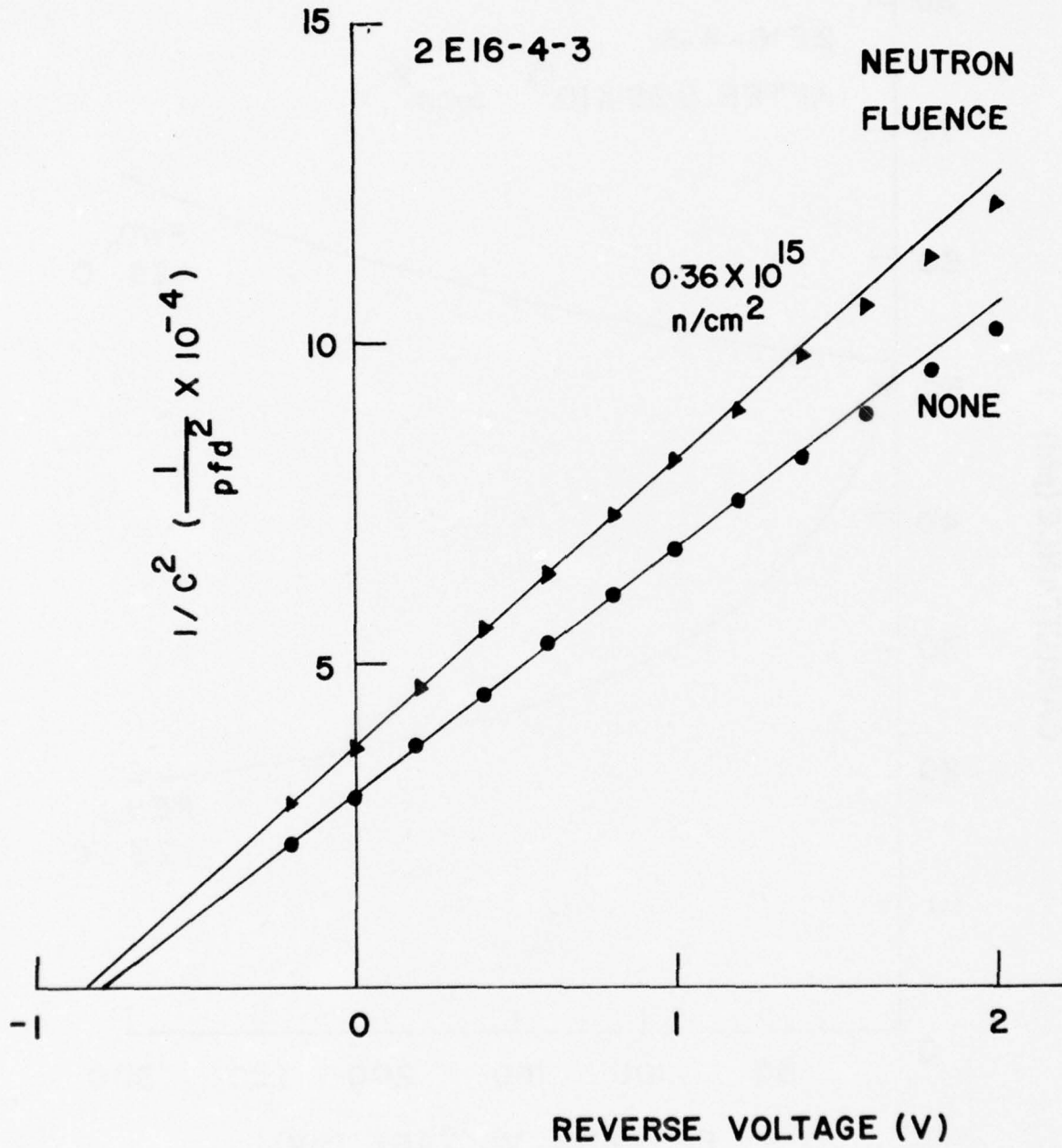


Fig. 4.9  $1/c^2$  vs. Voltage for 2E16 Near Zero Bias

it is necessary to consider the charge distribution in the depletion layer. Figure 4.10 shows the energy band diagram in a reverse biased Schottky diode.<sup>(23)</sup>  $E_{Fn}$  represents the quasi-Fermi level for electrons,  $E_D$  the energy level of shallow donor assumed to be completely ionized,  $E_t$  a trap level,  $W$  the width of the depletion layer and  $y_t$  the distance at which the trap level crosses the electron quasi-Fermi level.

If the capacitance is measured at high enough frequency such that only the free charge at  $W$  follows the small signal voltage variations, then the small signal capacitance is given by:<sup>(24)</sup>

$$C = \epsilon A/W \quad (4.6)$$

Assuming that the trap level is an acceptor then the relationship between  $W$  and the applied voltage  $-V$  is given by:<sup>(24)</sup>

$$W = \frac{N_t}{N_D} \sqrt{\frac{2\epsilon V_t}{q(N_D - N_t)}} + \sqrt{\frac{2\epsilon}{qN_D} (V_D - V - V_t N_t / N_D)} \quad (4.7)$$

where  $N_D$  is the donor density,  $N_t$  the trap density,  $V_D$  the contact potential and  $qV_t$  is the energy difference between the trap level and the Fermi level in the bulk, that is:

$$V_t = \frac{E_F - E_t}{q} \quad (4.8)$$

If the trap level is a donor instead of an acceptor, it is easily shown that:

$$W = \frac{N_t}{N_D + N_t} \sqrt{\frac{2\epsilon V_t}{qN_D}} + \sqrt{\frac{2\epsilon}{q(N_D + N_t)} (V_D - V - V_t N_t / (N_t + N_D))} \quad (4.9)$$

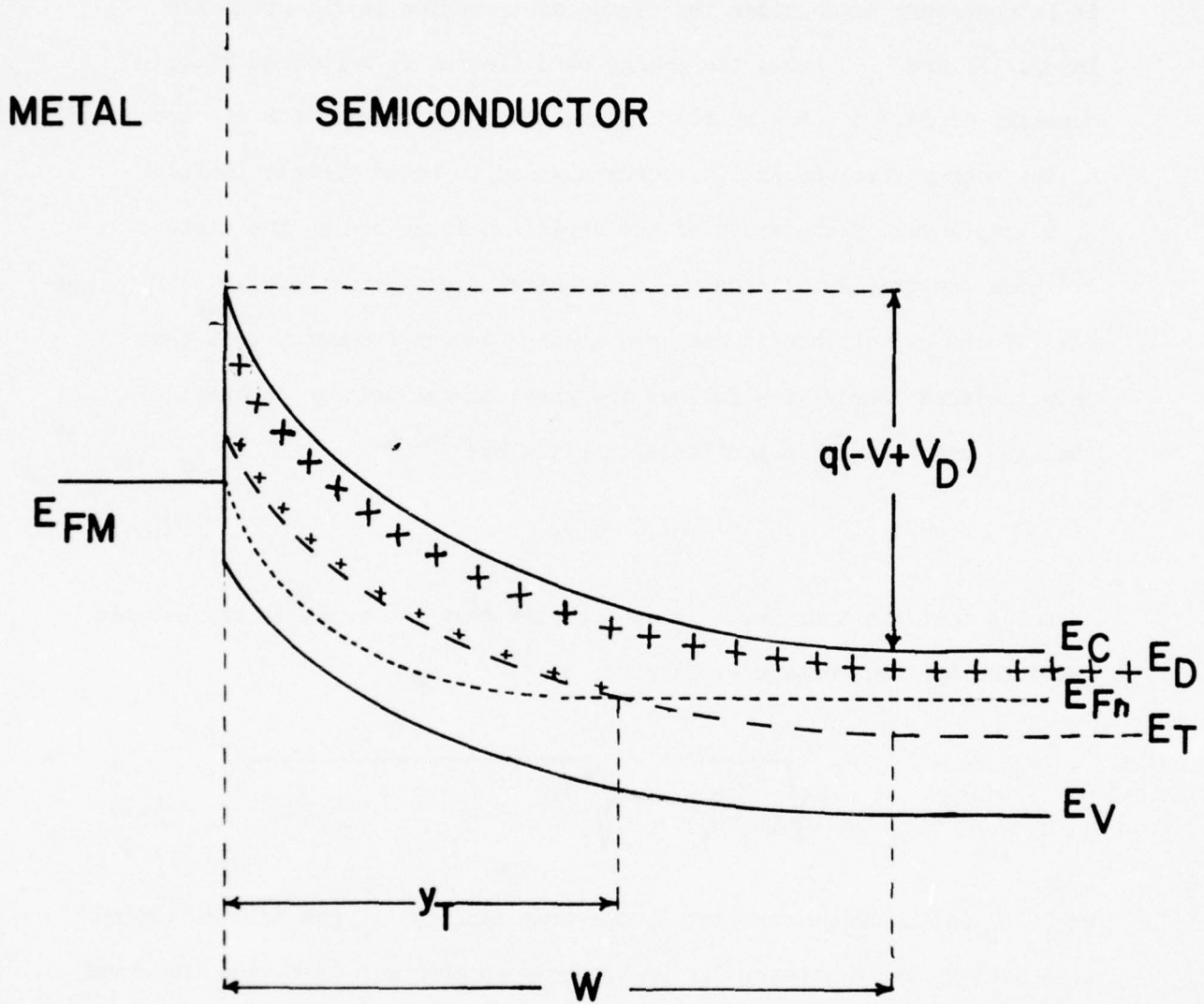


Fig. 4.10 Energy Band Diagram for a Reverse Bias Schottky Junction with a Shallow Donor and a Deep Trap

Equations (4.7) and (4.9) show that, as long as  $N_t$  is of the same order of magnitude as  $N_D$ ,  $W^2$ , i.e.,  $1/c^2$ , is a non-linear function of the bias voltage. The data of Fig. 4.9 shows that  $1/c^2$  is linear with voltage in the range of 0.2 to -1.0 volts for both the unirradiated and the irradiated device. This means that either  $N_t \ll N_D$  or that in the above voltage range the charge state of the trap level does not change within the depletion region. This last condition implies that  $y_t = 0$  in Fig. 4.10 and that  $V_t$  has to be larger than the diffusion or contact potential  $V_D$  but less than the band gap. From Fig. 4.9 the contact potential for the unirradiated device is 0.8 V.

The above analysis has shown that between +0.2 and -1.0 volts, Eqs. (4.7) and (4.9) simplify to:

$$W^2 = \frac{2\epsilon}{qN_D} (V_D - V) \quad (4.10)$$

that is:

$$1/c^2 = \frac{2(V_D - V)}{qeA^2 N_D} \quad (4.11)$$

Using the above equation, the data of Fig. 4.9 gives  $N_D = 2.2 \times 10^{16} \text{ cm}^{-3}$  before irradiation and  $N_D = 1.9 \times 10^{16} \text{ cm}^{-3}$  after a neutron fluence of  $3.6 \times 10^{14} \text{ n/cm}^2$ . That is, after irradiation, the net positive charge concentration in the depletion layer has decreased. This implies that neutron irradiation has transformed some of the original shallow donors into non-ionized deep donors or that very shallow acceptors have been introduced. This is the only way in which the difference in slopes of

$1/c^2$  vs.  $V$  shown in Fig. 4.9 before and after irradiation can be explained.<sup>(25)</sup> Results similar to the ones shown in Fig. 4.9 were consistently observed in all the devices tested. Although it is not possible to decide which of the two alternatives is the real one, deep donors or shallow acceptors, there is no doubt that neutron damage in the depletion layer of Schottky diodes consists of levels occupied by electrons and which because of their energy level being in close proximity to the valence band must be in equilibrium with it.

The data in Fig. 4.9 shows that  $1/c^2$  starts to deviate from a straight line for reverse voltages larger than 1 volt. Figure 4.11 shows  $1/c^2$  vs.  $V$  for a larger voltage range. For voltages larger than 2.5 volts the data falls on a straight line. The carrier concentrations determined from the slope of the above curves are  $2.9 \times 10^{16} \text{ cm}^{-3}$  and  $2.5 \times 10^{16} \text{ cm}^{-3}$  for the unirradiated and irradiated devices respectively. The bending of the data of Fig. 4.11 that takes place between 1 and 2.5 volts can be due to either a non-uniform doping concentration or to the uncovering of a trapping level. This last condition seems to be more reasonable since the slope of the  $1/c^2$  plot remains constant for voltages larger than 2.5 volts. If the doping were nonuniform one should expect a changing slope at higher voltages as well.

If the trap density in the depletion layer is completely ionized at large reverse bias, then its density is the difference between the concentration at large reverse bias and the concentration at low reverse bias. This difference is between  $6 \times 10^{15}$  and  $7 \times 10^{15} \text{ cm}^{-3}$  for both the irradiated and unirradiated devices.

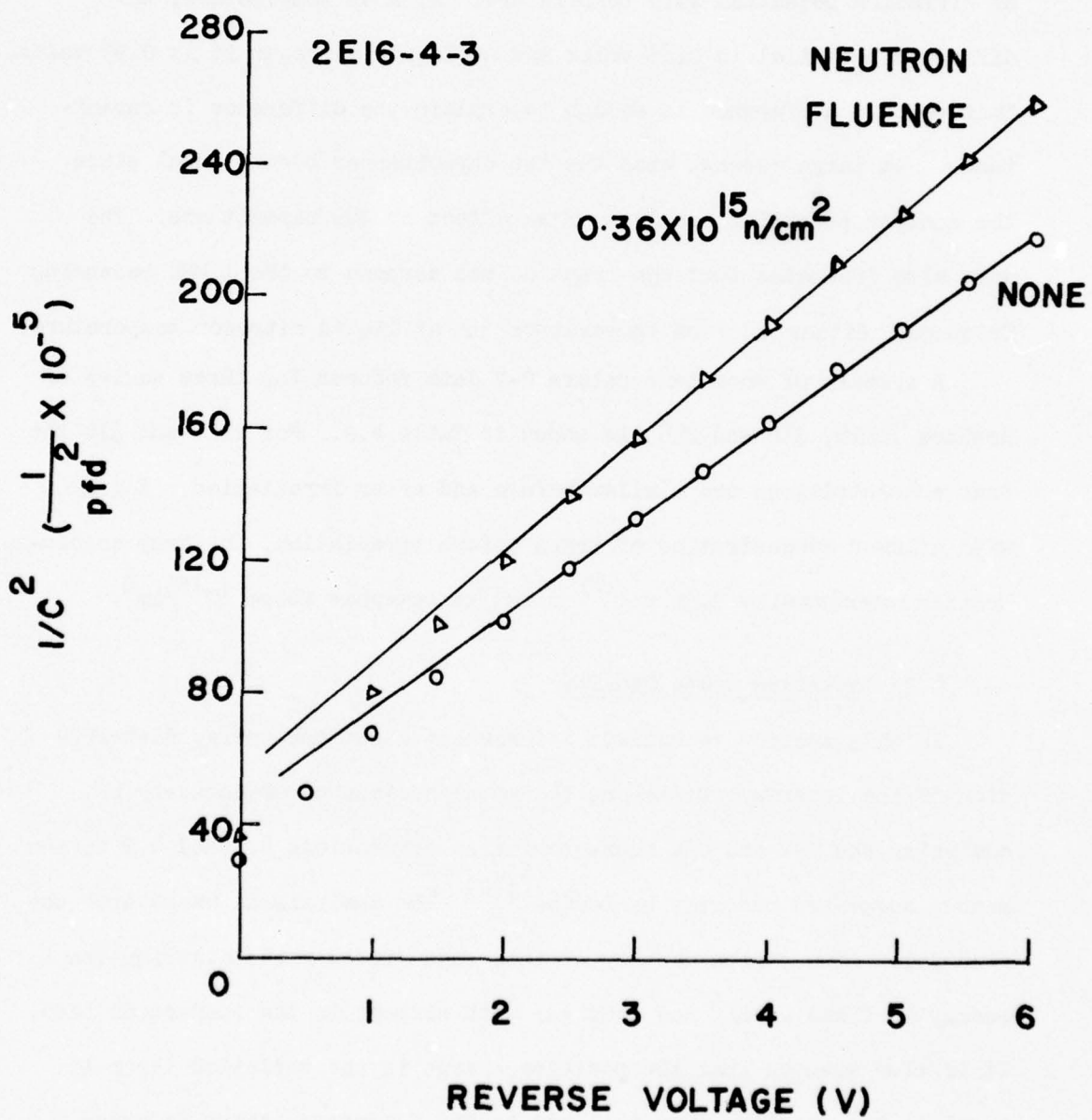


Fig. 4.11  $1/C^2$  vs. Voltage for 2E16 Over Wide Range of Reverse Voltage

Figure 4.12 shows the reverse bias capacitance of an irradiated device at room temperature and close to liquid nitrogen temperatures. The difference in capacitance at zero bias can be explained by the change of diffusion potential with temperature. At room temperature, the diffusion potential is 0.85 volts and at liquid nitrogen it is 0.95 volts. That voltage difference is enough to explain the difference in capacitance. At large reverse bias the two capacitances become equal since the contact potential has less of an effect on the capacitance. The data also indicates that the traps do not respond to the 1 MHz measuring frequency either at room temperature or at liquid nitrogen temperature.

A summary of room temperature C-V data reduced for three series of devices (2E16, 316 and 228) is shown in Table 4.2. For 2E16 and 316 the trap concentrations are similar before and after irradiation. For 228, with a lower concentration of traps before irradiation, the trap concentration introduced by  $0.36 \times 10^{15} \text{ n/cm}^2$  is somewhat above  $10^{15}/\text{cm}^3$ .

#### 4.3 Interface State Density

In this section we extract information about the energy distribution of the interface states at the metal-semiconductor boundary by analyzing the I-V and C-V characteristics of Sections 4.1 and 4.2 in the manner suggested recently by Levine.<sup>(1,2)</sup> The analysis is based upon the assumption of a finite density of interface states whose distribution in energy is fixed within the band gap with respect to the conduction band. It is also assumed that the positive charge in the depletion layer is equal to the negative charge stored in the interface states in order to

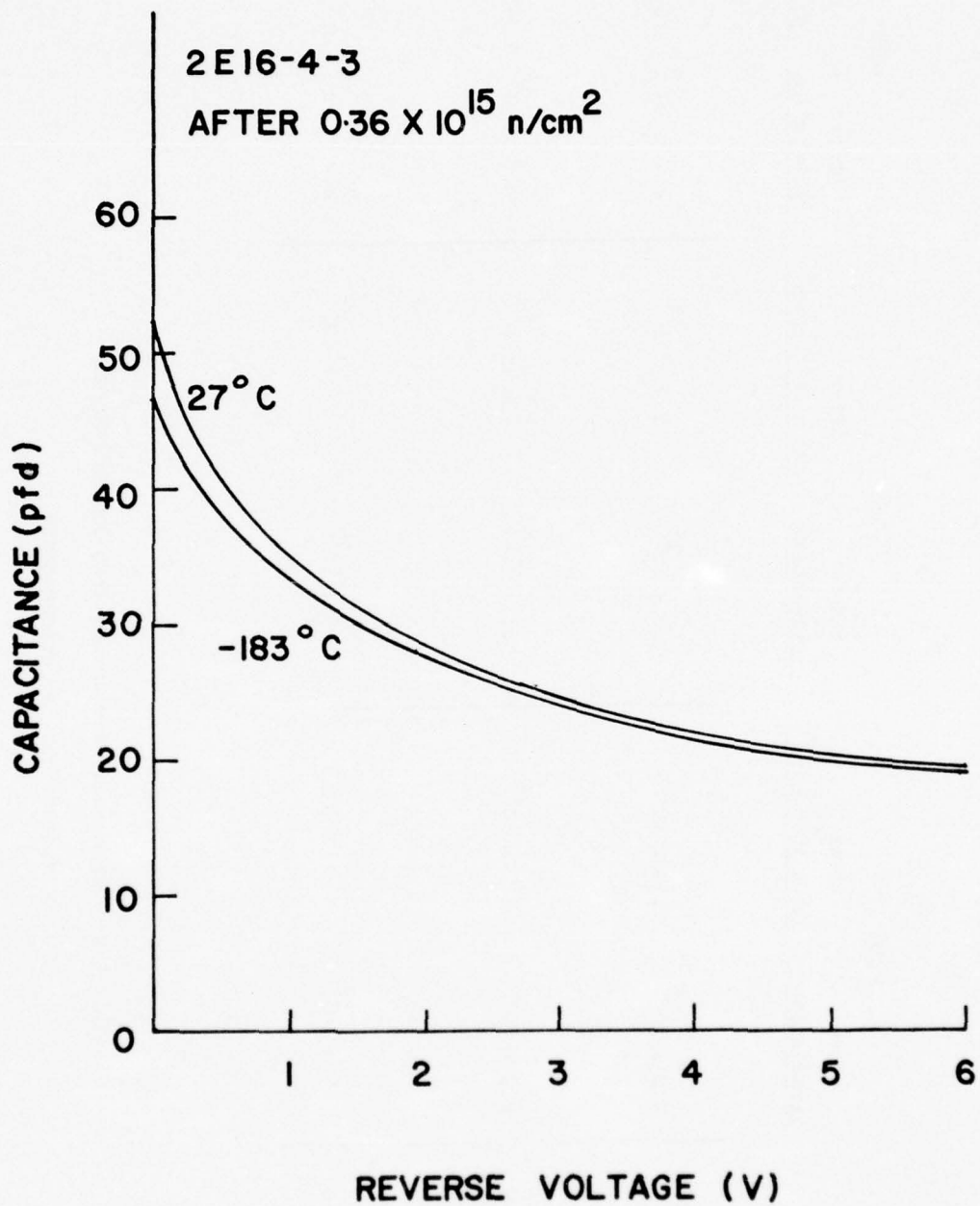


Fig. 4.12 Detailed C-V for Irradiated 2E16 at Room Temperature and Near Liquid Nitrogen Temperature

	2E16	316	228
	Before Irradiation	Before Irradiation	Before Irradiation
	After	After	After
	$.36 \times 10^{15} \text{ n/cm}^2$	$.36 \times 10^{15} \text{ n/cm}^2$	$.36 \times 10^{15} \text{ n/cm}^2$
Actual Carrier Concentration (from C-V near zero bias)	$2.2 \times 10^{16}$	$7.8 \times 10^{16}$	$2.4 \times 10^{15}$
Apparent Carrier Concentration (from C-V at high reverse voltage)	$1.9 \times 10^{16}$	$6.9 \times 10^{16}$	$\approx 0.5 \times 10^{15}$
Trap Concentration (difference in above)	$2.9 \times 10^{16}$	$7.8 \times 10^{16}$	$4.8 \times 10^{15}$
	$7 \times 10^{15}$	$9 \times 10^{15}$	$2.4 \times 10^{15}$

Table 4.2: Summary of Carrier and Trap Concentrations

Obtained from C-V Measurements

guarantee charge neutrality. It follows from the above two assumptions that the metal-semiconductor barrier height is controlled by the energy distribution of the interface states and by the external applied bias.

The energy band diagrams for an n-type Schottky barrier using the above model are shown in Fig. 4.13 for three cases: (a) zero bias, (b) reverse bias and (c) forward bias. The barrier height is  $\phi_B$ , the applied voltage is  $V$  and the difference between the conduction band edge and the Fermi level is  $\psi$ . The quantity  $\phi^*$  represents the barrier height under flat band conditions, i.e., zero charge in the interface states. The quantity of negative charge for each bias is shown as the black areas and depends upon the difference  $\phi^* - \phi_B$ . It follows from the assumptions of the model that the barrier height increases for forward bias and decreases for reverse bias. The way in which interface state density information can be obtained from the I-V and C-V characteristics is shown by the following analysis.

The relationship between the negative charge density  $Q_{ss}$  stored in the interface states and the density of interface states  $N_{ss}$  is given by:

$$Q_{ss} = q \int_{-\infty}^{+\infty} N_{ss}(\phi) f(\phi) d\phi \quad (4.12)$$

where  $f(\phi)$  is the probability that a surface state of energy  $\phi$  is occupied. It is assumed that the electrons in the interface states are in equilibrium with the metal and the function  $f(\phi)$  is the Fermi-Dirac distribution given by:

$$f(\phi) = [1 + \exp(\phi - \phi_f)/kT]^{-1} \quad (4.13)$$

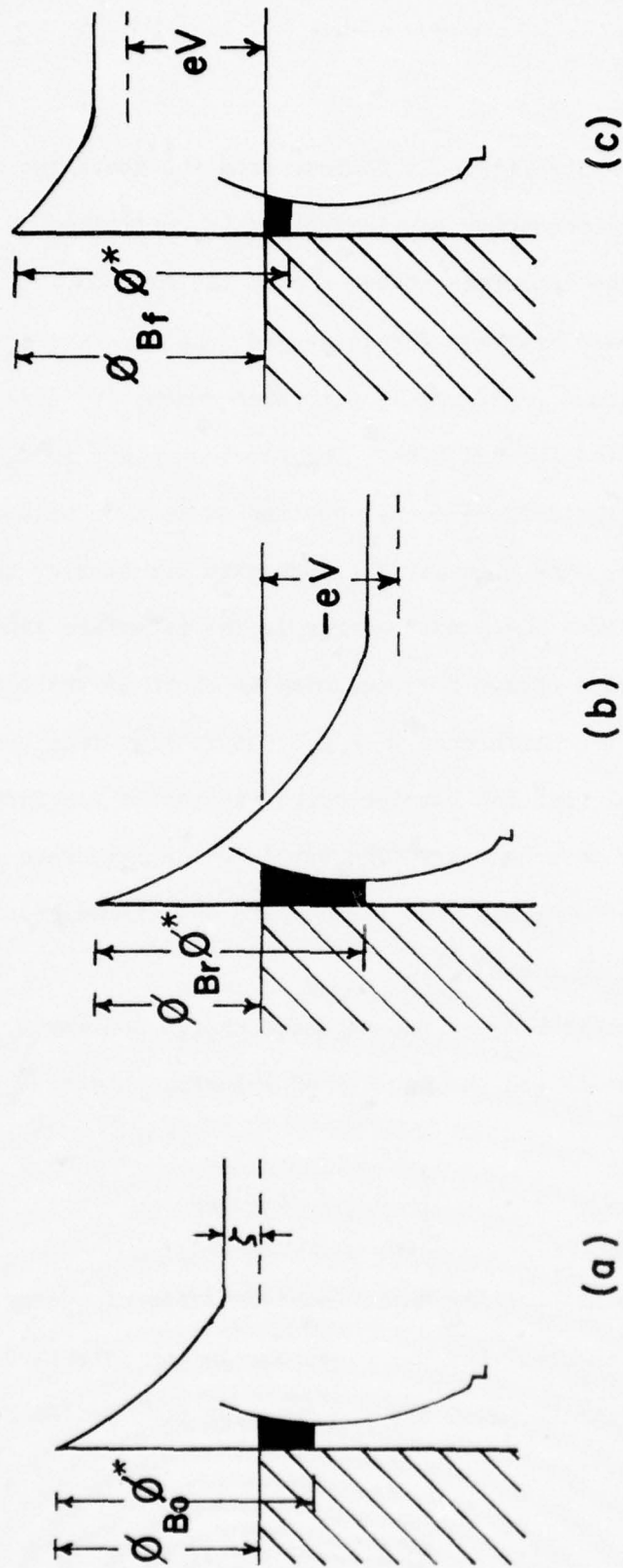


Fig. 4.13 Schematic Relationship between Barrier Height and Change in Interface State Charge for (a) zero bias (1), (b) reverse bias and (c) forward bias (after Levine (1))

where  $\phi_f$  is the metal Fermi level. In the zero temperature approximation  $f(\phi)$  is unity for  $\phi < \phi_f$  and zero for  $\phi > \phi_f$ . Then

$$dQ_{ss}/d\phi_f = qN_{ss}(\phi_f) \quad (4.14)$$

For a temperature  $T > 0$ , it is shown that<sup>(25)</sup>

$$\frac{dQ_{ss}}{d\phi_f} = qN_{ss} + \frac{q\pi^2}{12} (kT)^2 \frac{d^2N_{ss}}{d\phi^2} \Big|_{\phi_f} + \dots \quad (4.15)$$

As long as the curvature of the  $N_{ss}$  vs.  $\phi$  relationship, evaluated at  $\phi = \phi_f$ , is small compared to  $N_{ss}/(kT)^2$  the zero temperature approximation is valid. We will assume the zero temperature approximation which, as will be shown later, turns out to be valid in our case. Since  $\phi_B + \phi_f$  is a constant, it follows that the left-hand side of Eqs. (4.14) and (4.15) can be written as:

$$dQ_{ss}/d\phi_f = - (dQ_{ss}/d\phi_B) \quad (4.16)$$

Equations (4.14) or (4.15) and (4.16) indicate that in order to determine  $N_{ss}$  it is necessary to know  $Q_{ss}$  as a function of  $\phi_B$ . The charge density in the interface states  $Q_{ss}$  can be determined from the C-V characteristics and the barrier height  $\phi_B$ , or barrier height change, from either the I-V characteristics or from measurement of the barrier height by photoelectric measurements. We used the I-V characteristics for determining the barrier height change because of the greater accuracy and rapidity with which we can carry out those measurements in our laboratory.

The charge density  $Q_{ss}$  is related to the electric field by the equation:

$$Q_{ss} = \epsilon E_s \quad (4.17)$$

where  $\epsilon$  is the static electric permittivity and  $E_s$  is the electric field at the metal-semiconductor interface. The relationship between this electric field and the high frequency capacitance is considered next, taking into account the presence of deep donor traps. In reference to Fig. 4.10 an increase  $\Delta V_r$  in reverse bias uncovers a charge  $qN_t \Delta y_t$  at  $y_t$  and charge  $qN_D \Delta W$  at  $W$ . The increase in electric field  $\Delta E_s$  and the increase in voltage  $\Delta V_r$  are given by:

$$\Delta E_s = \frac{qN_t}{\epsilon} \Delta y_t + q \frac{N_D}{\epsilon} \Delta W \quad (4.18)$$

$$\Delta V_r = \frac{q N_t y_t}{\epsilon} \Delta y_t + q \frac{N_D W}{\epsilon} \Delta W \quad (4.19)$$

Since

$$W - y_t = \sqrt{\frac{2\epsilon V_t}{qN_D}} \quad (4.20)$$

and the high frequency capacitance  $C$  is given by

$$C = \frac{\epsilon A}{W} \quad (4.21)$$

it follows from Eqs. (4.18), (4.19), (4.20) and (4.21) that:

$$E_s(V_r) - E_s(0) = 1/\epsilon A \int_0^{V_r} C dV + \frac{qN_t}{\epsilon} \sqrt{\frac{2\epsilon V_t}{qN_D}} \ln \frac{C(0)}{C(V_r)} \quad (4.22)$$

where  $E_s(V_r)$  is the electric field at a reverse bias voltage  $V_r$ . The electric field at zero bias is calculated from the contact potential  $V_D$  and the doping density from the equation:

$$E_s(0) = \sqrt{\frac{2qN_D}{\epsilon} V_D} \quad (4.23)$$

The second term on the right-hand side of Eq. (4.22) represents the contribution to the electric field by charge which is uncovered within the depletion layer. According to the data presented in Section 4.2, the traps start to be uncovered at reverse voltages larger than 1 volt and up to that voltage the increase in electric field is given by the integral term in Eq. (4.22). For reverse voltages larger than 1 volt, the last term has to be taken into account except that  $C(V_r = 1)$  should be used instead of  $C(0)$  in the logarithm term because the traps start to be uncovered at that voltage. Using the values of  $N_t = 7 \times 10^{15} \text{ cm}^{-3}$ ,  $N_D = 2.2 \times 10^{16} \text{ cm}^{-3}$  and  $V_t \approx 1 \text{ V}$  obtained from the data presented in Section 4.2, the value of the constant in front of the logarithm term is  $2.5 \times 10^4 \text{ V/cm}$ . In carrying out the calculations for  $E_s(V_r)$  it was found that the contribution to the electric field due to traps was lower than 10% of the total electric field in device series 2E16 and 316.

The barrier height  $\phi_B$  is determined from the I-V characteristics. Assuming that the current in the Schottky barrier is due to thermionic emission, the relationship between the current I and the voltage V is given by: (27)

$$I/A = A^* T^2 \exp - \frac{\phi_B}{kT} \left( \exp \frac{qV}{kT} - 1 \right) \quad (4.24)$$

If image force lowering of the barrier is taken into account, the above equation changes to:

$$I/A = A^* T^2 \exp - \frac{\phi_B - q\beta \sqrt{E_s}}{kT} \left( \exp \frac{qV}{kT} - 1 \right) \quad (4.25)$$

where  $\beta$  is the image force lowering constant given by: <sup>(27)</sup>

$$\beta = (q/4\pi\epsilon_d)^{1/2} \quad (4.26)$$

and where  $\epsilon_d$  is the high frequency electric permittivity.

For forward bias voltages  $V_f \gg 4kT/q$ , Eq. (4.25) can be approximated by:

$$I_f/A = A^* T^2 \exp - \frac{\phi_B(V_f) - \beta \sqrt{E_s(V_f)}}{kT} \exp \frac{qV_f}{kT} \quad (4.27)$$

where it has been shown explicitly that  $\phi_B$  and  $E_s$  are functions of the voltage  $V_f$ . The above equation shows that the leakage current  $I_s$  obtained by extrapolation of the curve of  $\ln I_f$  vs.  $V_f$  to  $V_f = 0$  is given by:

$$I_s/A = A^* T^2 \exp - \frac{\phi_B(0) - \beta \sqrt{E_s(0)}}{kT} \quad (4.28)$$

Therefore, the leakage current  $I_s$  at a temperature  $T$  can be obtained from the extrapolation of the forward characteristics measured at that temperature. The change in barrier height at a voltage  $V$  can be obtained from Eqs. (4.25) and (4.28) and it is given by:

$$\Delta\phi_B = q\beta \Delta\sqrt{E_s} - kT \ln \frac{I}{I_s \left( \exp \frac{qV}{kT} - 1 \right)} \quad (4.29)$$

where

$$\Delta \phi_B = \phi_B(V) - \phi_B(0) \quad (4.30)$$

$$\Delta \sqrt{E_s} = \sqrt{E_s(V)} - \sqrt{E_s(0)} \quad (4.31)$$

With the help of Eqs. (4.17), (4.22) and (4.29), it is possible to determine  $Q_{ss}$  as a function of  $\Delta \phi_B$  from the I-V and C-V characteristics of the Schottky diode. Once that  $Q_{ss}$  is known as a function of  $\Delta \phi_B$ ,  $N_{ss}$  is determined from Eqs. (4.14) or (4.15).

Another way to obtain  $dQ_{ss}/d\phi_B$  without the necessity of finding  $I_s$  is as follows. Since  $Q_{ss}$  and  $\phi_B$  are functions of the bias voltage  $V$  at a given temperature, it follows that:

$$dQ_{ss}/d\phi_B = (\partial Q_{ss}/\partial V)/(\partial \phi_B/\partial V) \quad (4.32)$$

Neglecting the term due to traps in Eq. (4.22) it follows that:

$$(\partial Q_{ss}/\partial V_f) = -(C/A) ; (\partial Q_{ss}/\partial V_r) = C/A \quad (4.33)$$

The change in barrier height with voltage can be obtained by taking the derivative of the left-hand side of Eq. (4.29) with respect to voltage:

$$\frac{1}{q} \frac{\partial \phi_B}{\partial V_f} = -\frac{kT}{q} \frac{\partial \ln I_f}{\partial V_f} + \beta \frac{\partial \sqrt{E_s}}{\partial V_f} + \frac{1}{1 - \exp(-qV_f/kT)} \quad (4.35)$$

$$\frac{1}{q} \frac{\partial \phi_B}{\partial V_r} = -\frac{kT}{q} \frac{\partial \ln I_r}{\partial V_r} + \beta \frac{\partial \sqrt{E_s}}{\partial V_r} + \frac{1}{\exp(qV_r/kT) - 1} \quad (4.36)$$

Introducing the ideality factor  $n$  defined by the equation:

$$1/n = (kT/q) \frac{\partial \ln I_{f,r}}{\partial V_{f,r}} \quad (4.37)$$

Eqs. (4.35) and (4.36) reduce to:

$$\frac{\partial \phi_B}{\partial V_f} = - (1/n) + \beta \frac{\partial \sqrt{E_s}}{\partial V_f} + \frac{1}{1 - \exp - \frac{qV_f}{kT}} \quad (4.38)$$

$$\frac{\partial \phi_B}{\partial V_r} = - (1/n) + \beta \frac{\partial \sqrt{E_s}}{\partial V_r} + \frac{1}{\exp \frac{qV_r}{kT} - 1} \quad (4.39)$$

Substitution of Eqs. (4.33), (4.38) and (4.39) in (4.32) gives

$dQ_{ss}/d\phi_B$ . In the zero temperature approximation, the expression for the density of states  $N_{ss}$  (Eq. 4.14) reduces to a very simple expression in terms of the capacitance  $C$  and ideality factor  $n$ . For bias voltages larger than  $4 kT/q$ ,  $N_{ss}$  is given by: \*

$$N_{ss} = \frac{C}{qA(1 - \frac{1}{n} + \beta \frac{\partial \sqrt{E_s}}{\partial V_f})} \quad (4.40)$$

for forward bias voltages and by:

$$N_{ss} = \frac{C}{qA(\frac{1}{n} - \beta \frac{\partial \sqrt{E_s}}{\partial V_r})} \quad (4.41)$$

for reverse bias voltages.

\* For a more detailed derivation of the surface-state model see "Interface State Density in Au-nGaAs Schottky Diodes", by J. M. Borrego, R. J. Gutmann and S. Ashok in Solid State Electronics (1976).

Using the equations developed in the preceding analysis we have extracted interface state information from the I-V and C-V characteristics presented in Sections 4.1 and 4.2. Figure 4.14 shows a semilog plot of the surface electric field  $E_s$  as a function of barrier height change  $-\Delta\phi_B$  in the reverse direction, without taking into account image force barrier height lowering. The data is for a device of series 2E16 at two different temperatures, 24°C and 85°C, before and after neutron irradiation. For low barrier height changes, the data shows that  $\ln E_s$  is linear with  $-\Delta\phi_B$ . This indicates that  $Q_{ss}$  is an exponential function of the barrier height  $\phi_B$ , that is:

$$Q_{ss} = Q_c \exp - \phi_B/\phi_o \quad (4.42)$$

where  $Q_c$  and  $\phi_o$  are constants of the distribution.

From the data of Fig. 4.14, the value of  $\phi_o$  at 85°C is 0.045 eV before irradiation and 0.074 eV after irradiation. The value of 0.045 eV agrees with the value of 0.040 eV obtained by Levine<sup>(1)</sup> for the Au-n GaAs diode reported by Padovani.<sup>(28)</sup> For lower temperatures and for higher reverse voltages (larger  $-\Delta\phi_B$ ) the data of Fig. 4.14 shows that Eq. (4.42) does not hold. This is better shown in Fig. 4.15 which is a log-log plot of the reverse current as a function of  $\sqrt{V_R + V_D}$ . Levine<sup>(2)</sup> has shown that the reverse current has a dependence upon the total junction voltage given by:

$$I_r \propto (\sqrt{V_R + V_D})^2 \phi_o/kT \quad (4.43)$$

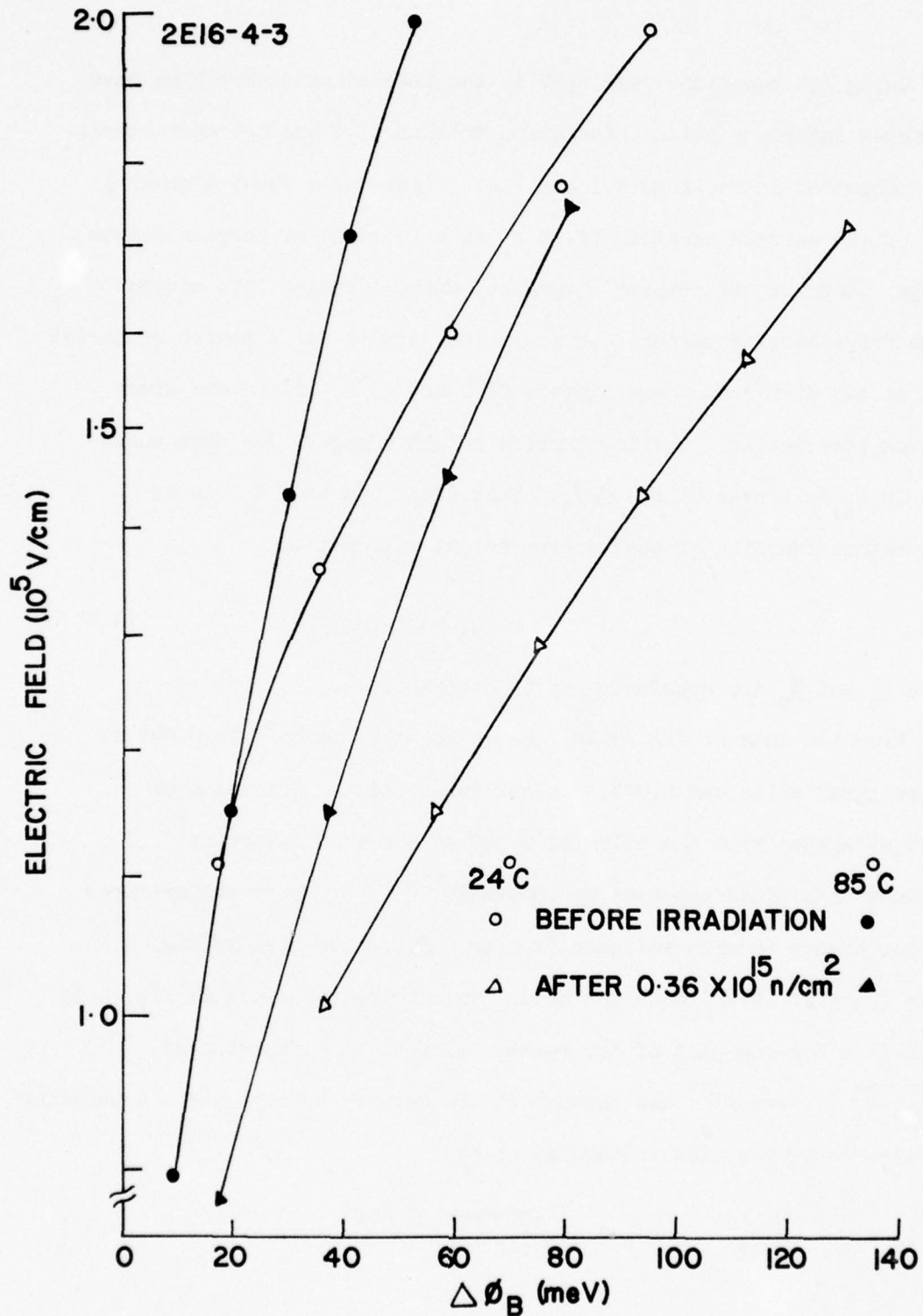


Fig. 4.14 Surface Electric Field vs. Barrier Height Change for 2E16

if Eq. (4.42) is satisfied. The data of Fig. 4.15 shows that Eq. (4.43), and also Eq. (4.42), are not valid for low temperatures and for high reverse voltages. We conclude then, that exponential distribution of  $Q_{SS}$  with  $\phi_B$  found by Levine<sup>(2)</sup> is either valid only in a limited temperature and voltage range or that an additional excess current is present at low temperatures and high voltages. Furthermore, the distribution of  $Q_{SS}$  with  $\phi_B$  found by Levine does not take into account the effect of image force upon barrier height lowering.

Using Eqs. (4.22) and (4.29), we have obtained the electric field at the interface  $E_s$ , i.e.,  $Q_{SS}$ , as a function of barrier height change  $-\Delta\phi_B$  taking into account image force effects. The results are shown in Figs. 4.16 and 4.17. In the low temperature approximation, the slope of the curves of Figs. 4.16 and 4.17 is proportional to  $N_{SS}$ . The data of Fig. 4.16 shows then, that before irradiation  $N_{SS}$  peaks at a value close to  $\Delta\phi_B \approx 0$  (i.e., at the Fermi-level at zero bias) and that after irradiation  $N_{SS}$  is approximately constant and of lower value.

As mentioned in the analysis, another way to determine  $N_{SS}$  is by means of Eqs. (4.40) and (4.41). Figure 4.18 shows  $N_{SS}$  for the same device using the above two equations. The value of  $N_{SS}$  determined from the slope of the curves of Fig. 4.17 for large values of  $-\Delta\phi_B$  are shown on the right of Fig. 4.18 and agree very well with the values determined from Eq. (4.41). The data of Fig. 4.18 shows that  $N_{SS}$  peaks at the Fermi-level at zero bias and that  $N_{SS}$  is less peaked and its value reduced by a factor of approximately 4 after irradiation. Before irradiation and at 85°C, the  $N_{SS}$  has approximately an exponential dependence upon barrier

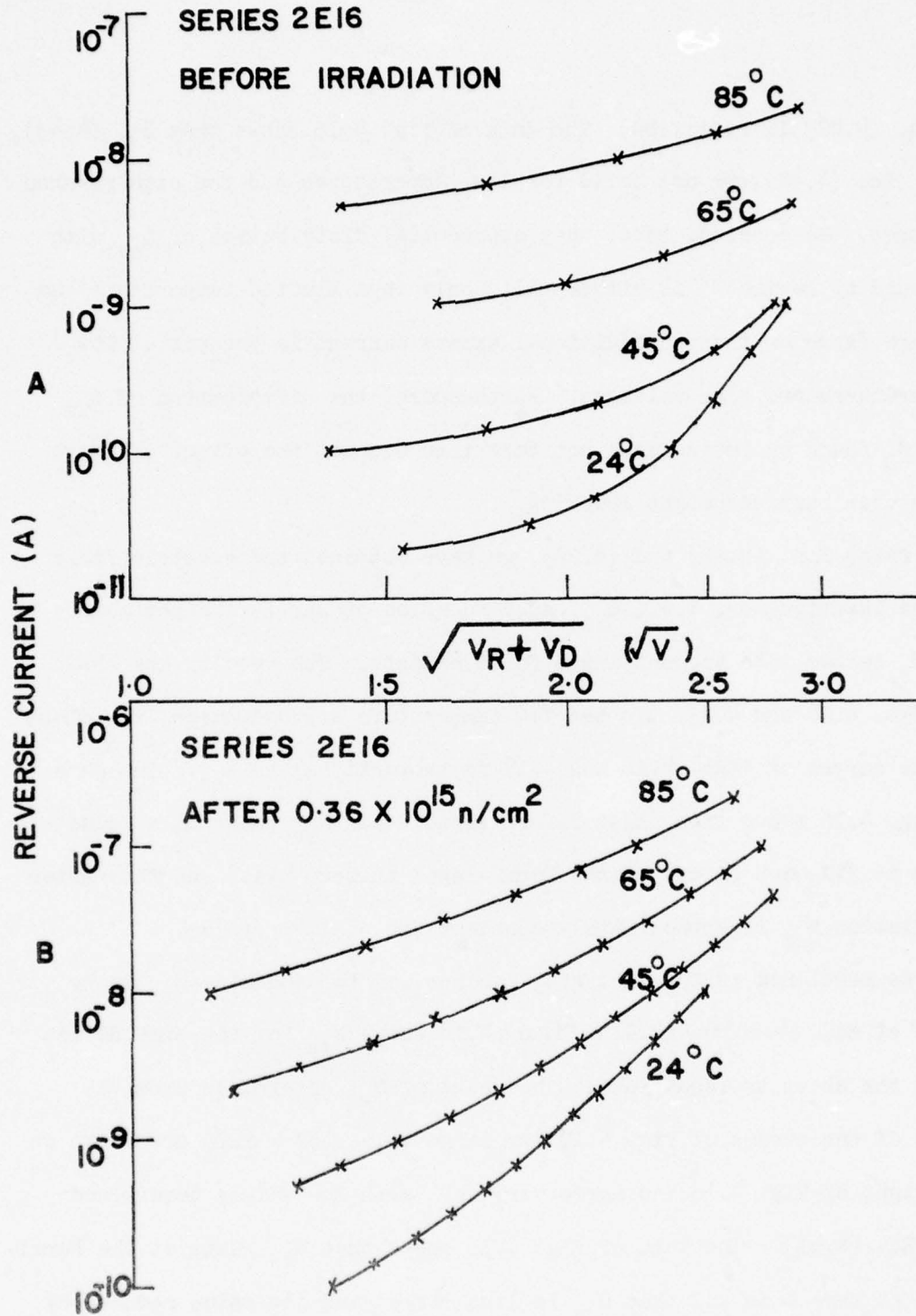


Fig. 4.15 Log Reverse Current vs. Log Square Root of Reverse Voltage for 2E16

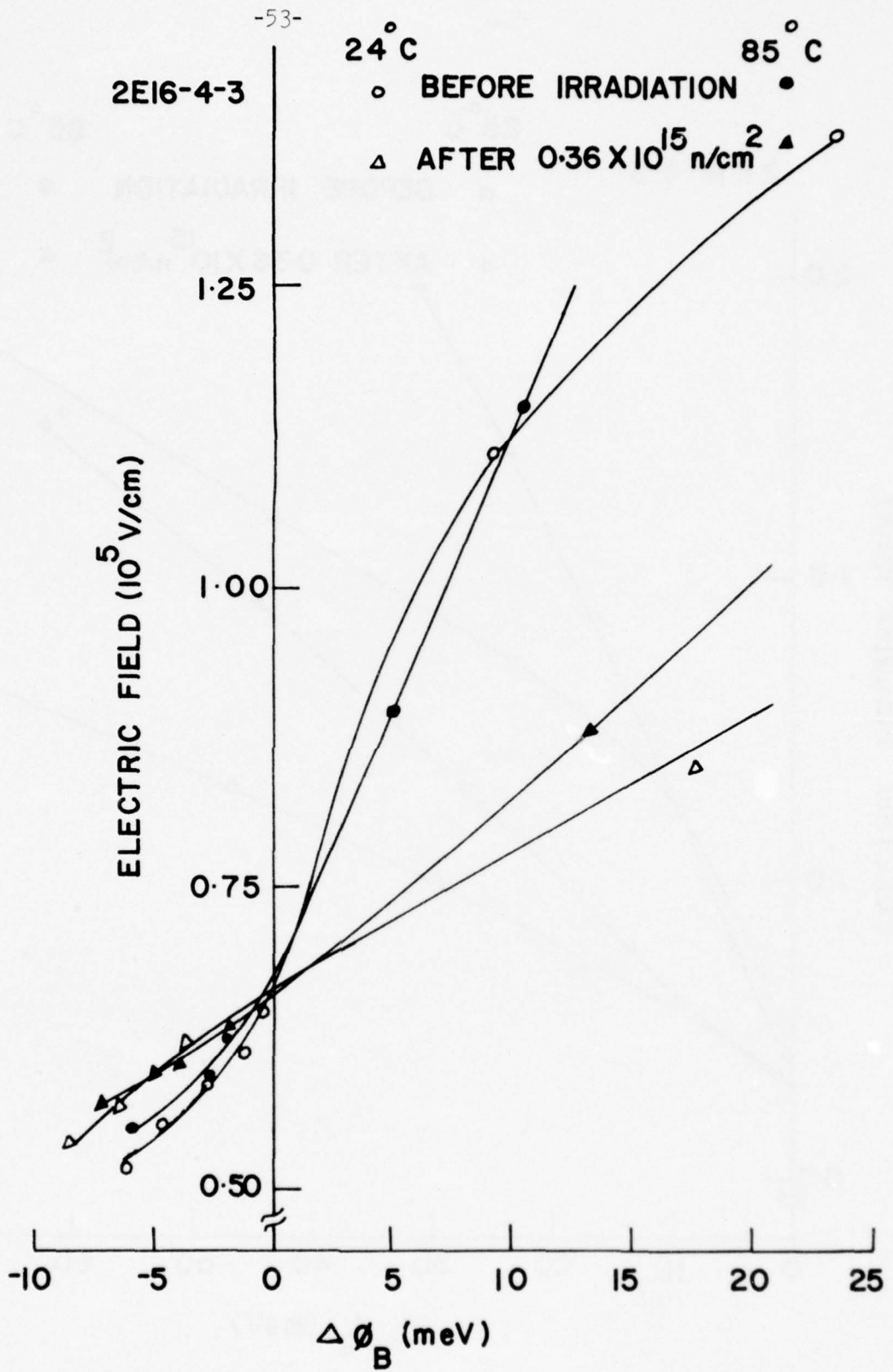


Fig. 4.16 Surface Electric Field vs. Barrier Height Change for 2E16 with Image Force Corrections (near zero barrier height change)

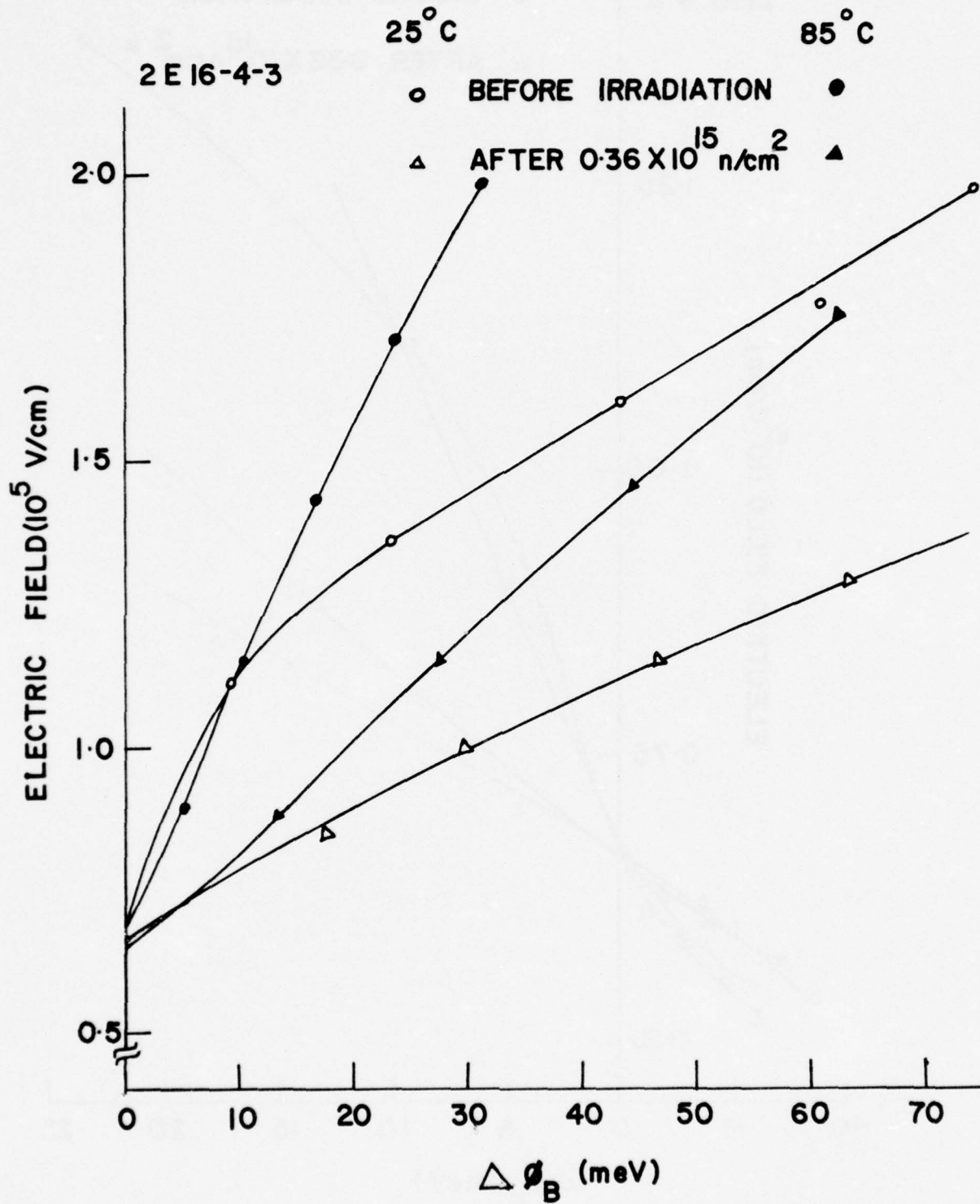


Fig. 4.17 Surface Electric Field vs. Barrier Height Change for 2E16 with Image Force Corrections (for large reverse bias)



height, Eq. (4.42), for  $-\Delta\phi_B > 0$  with a value of  $\phi_0 \approx 0.040$  eV similar to the one found by Levine.<sup>(1)</sup> For  $\Delta\phi_B < 0$ ,  $N_{ss}$  decreases very fast with  $\phi_B$  and shows a behavior similar to the one found by Crowell and Roberts in Au-Si Schottky barrier diodes.<sup>(26)</sup>

A question that arises in determining  $N_{ss}$  from either Eqs. (4.22) and (4.29) or from Eqs. (4.40) and (4.41) is how valid is the assumption, especially at reverse bias, that the current in the Schottky diode is due to thermionic emission, i.e., given by Eq. (4.25). Figure 4.19 shows  $I_R/T^2$  vs.  $1/T$  for several reverse bias voltages before and after irradiation. It shows that the current flow has the characteristics of thermionic emission current up to 1 volt reverse bias at room temperature and up to 5 volts reverse bias at  $85^\circ\text{C}$  for the unirradiated devices. The corresponding limits for the irradiated devices are 1 and 2 volts. This means that the  $N_{ss}$  plots of Fig. 4.18 are valid up to  $-\Delta\phi_B \approx 0.020$  eV at room temperature and up to  $-\Delta\phi_B \approx 0.040$  eV at  $85^\circ\text{C}$ . For higher reverse bias voltages, i.e., higher  $-\Delta\phi_B$ , there is an additional reverse current which does not conform to thermionic emission characteristics. This will be further discussed in Section 4.4.

Using Eq. (4.41) we determined  $N_{ss}$  for devices of series 316 and its plot is shown in Fig. 4.20. We estimate the curves to be valid up to  $-\Delta\phi_B \approx 0.120$  eV for the reasons discussed previously. The  $N_{ss}$  distribution shows similar changes after irradiation as the ones shown in Fig. 4.18.

In order to determine if the changes in  $N_{ss}$  with irradiation were due to possible neutron damage in the metal close to the metal-semiconductor interface, a wafer of device series 316 was irradiated before the

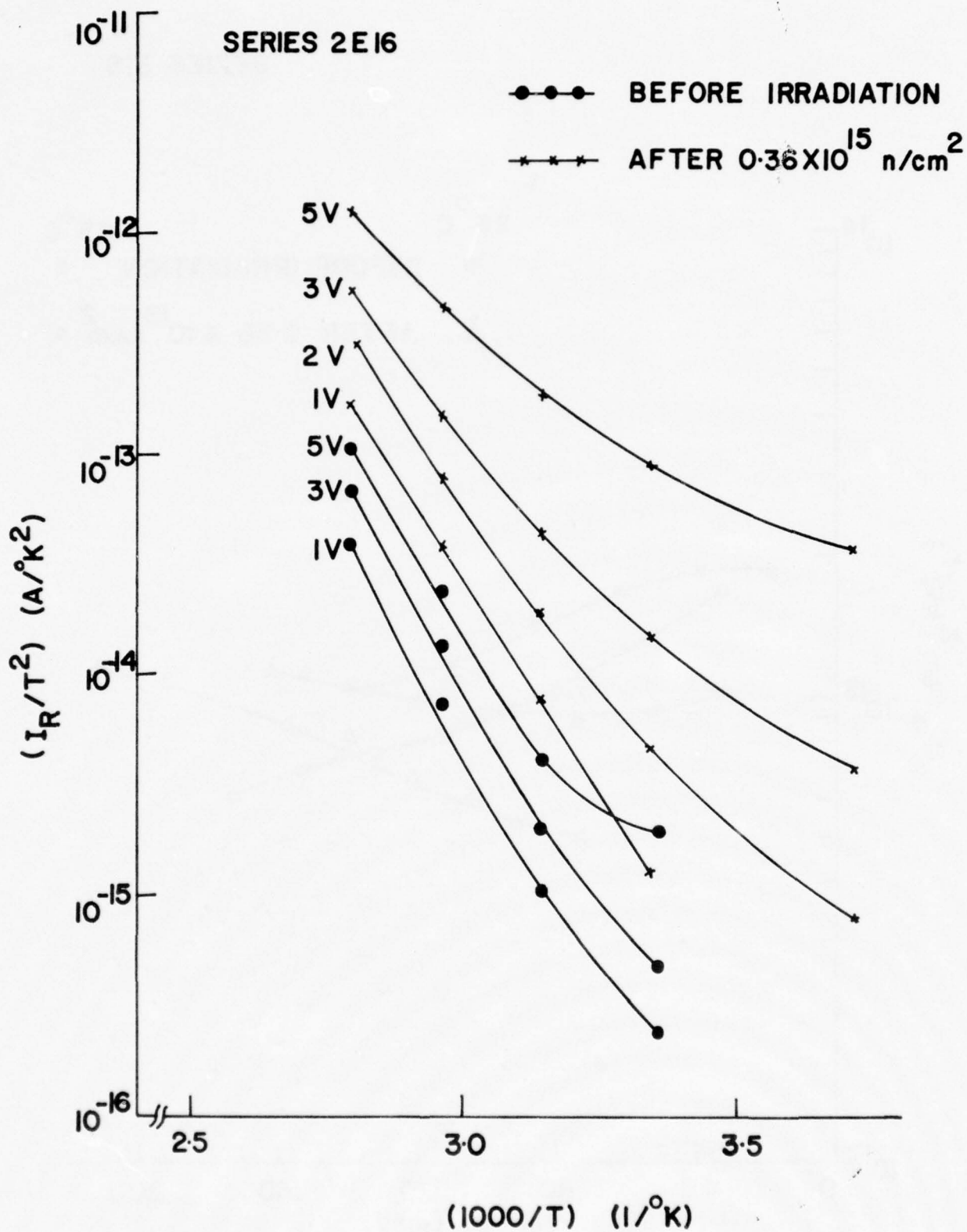


Fig. 4.19 Arrhenius Plot of  $I_R/T^2$  for 2E16 Before and After Irradiation

SERIES 316

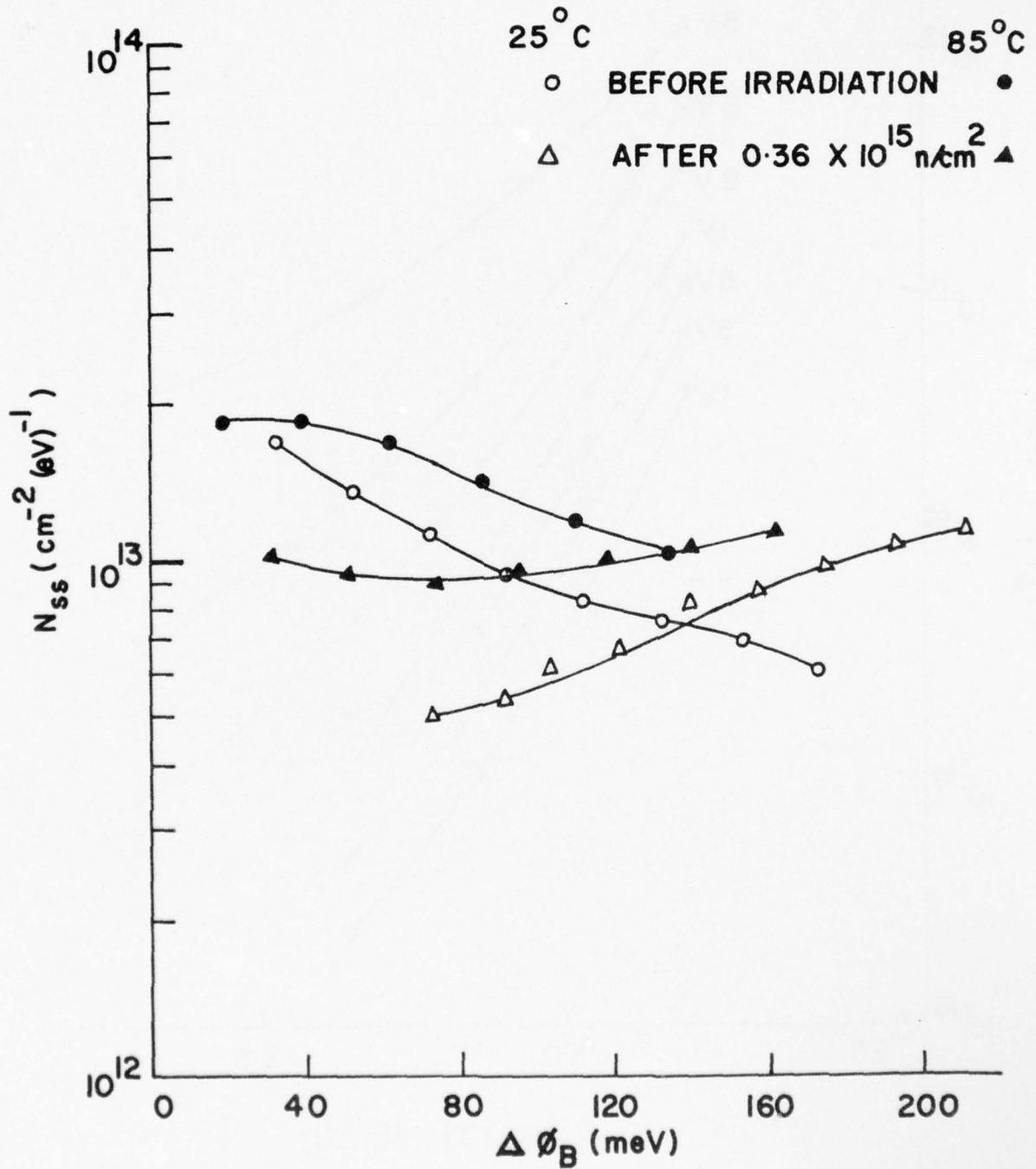


Fig. 4.20 Density of States from Equations (4.40) and (4.41) for 316

SERIES 316

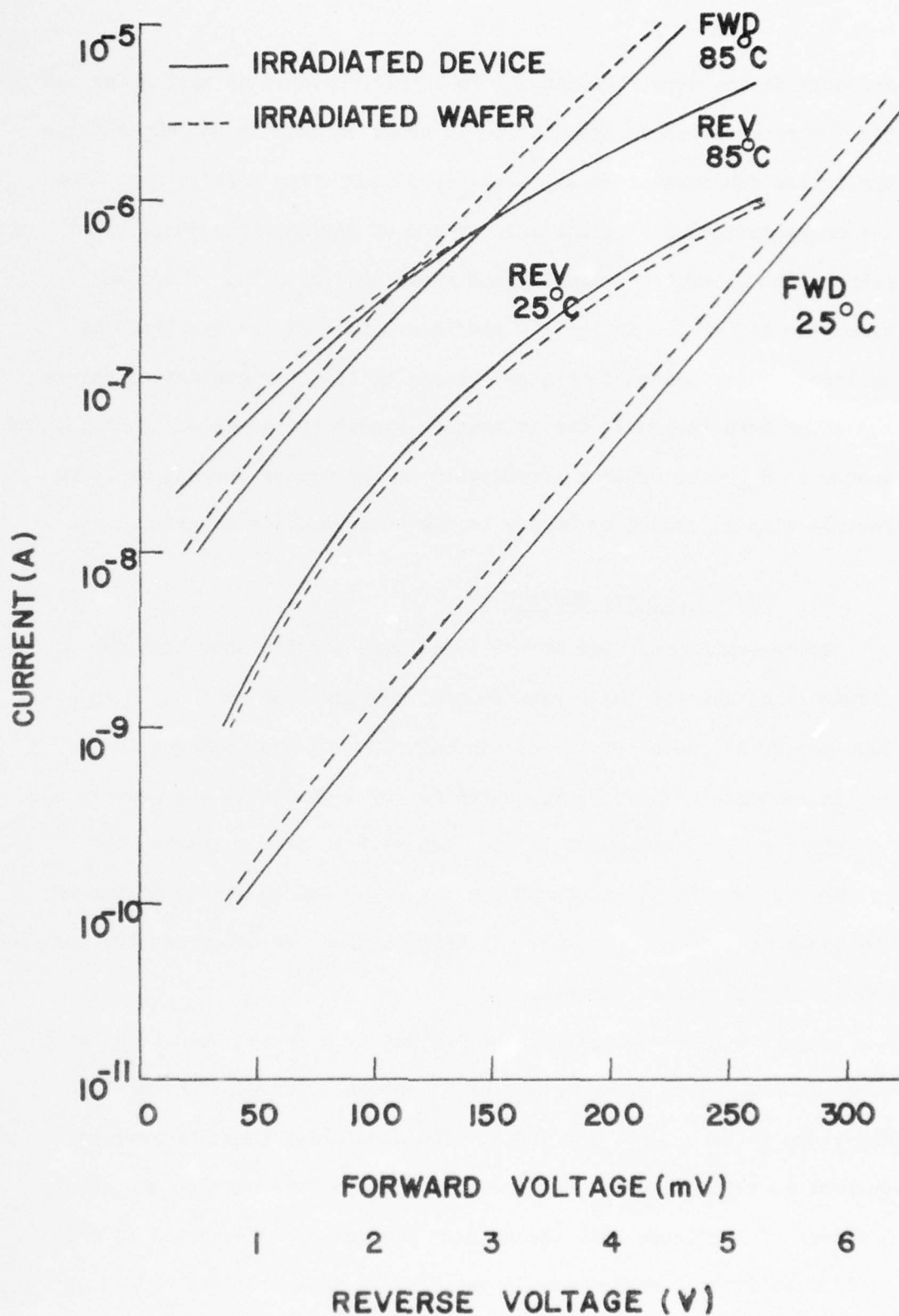


Fig. 4.21 Comparison of I-V Characteristics of Series 316 After Irradiation at Device and Wafer Levels

Schottky diodes were fabricated. The ohmic contacts on that wafer had been fabricated before irradiation in order to avoid high temperatures during the fabrication of the Schottky diodes after irradiation. The I-V characteristics of those devices and of devices irradiated after fabrication on similar material are shown in Fig. 4.21. There was almost no difference in the I-V characteristics of the two types of devices. This indicates that any change in the characteristics before and after irradiation is due to neutron damage in the GaAs. That is, the change in  $N_{ss}$  with neutron irradiation or the excess current at large reverse bias is caused by damage in the semiconductor material.

#### 4.4 Excess Reverse Current

The results presented in the preceding section show that for forward bias and for small reverse bias voltages the current in Au-n GaAs diodes is caused by thermionic emission and that changes in the I-V characteristics can be accounted for by a change in the density of interface states. At moderate and high reverse bias voltages, the reverse current is in excess of the one which can be accounted for by thermionic emission processes. In this section, we determine the possible nature of that excess current.

Figure 4.22 shows the reverse current of a series 2E16 irradiated diode as a function of reverse bias at several different temperatures in the range between  $300^{\circ}\text{K}$  and  $100^{\circ}\text{K}$ . The data shows that the reverse current is strongly dependent upon the voltage (the current changes by 3 orders of magnitude when the voltage changes by a factor of 6) and it is relatively temperature independent (a change of two orders of

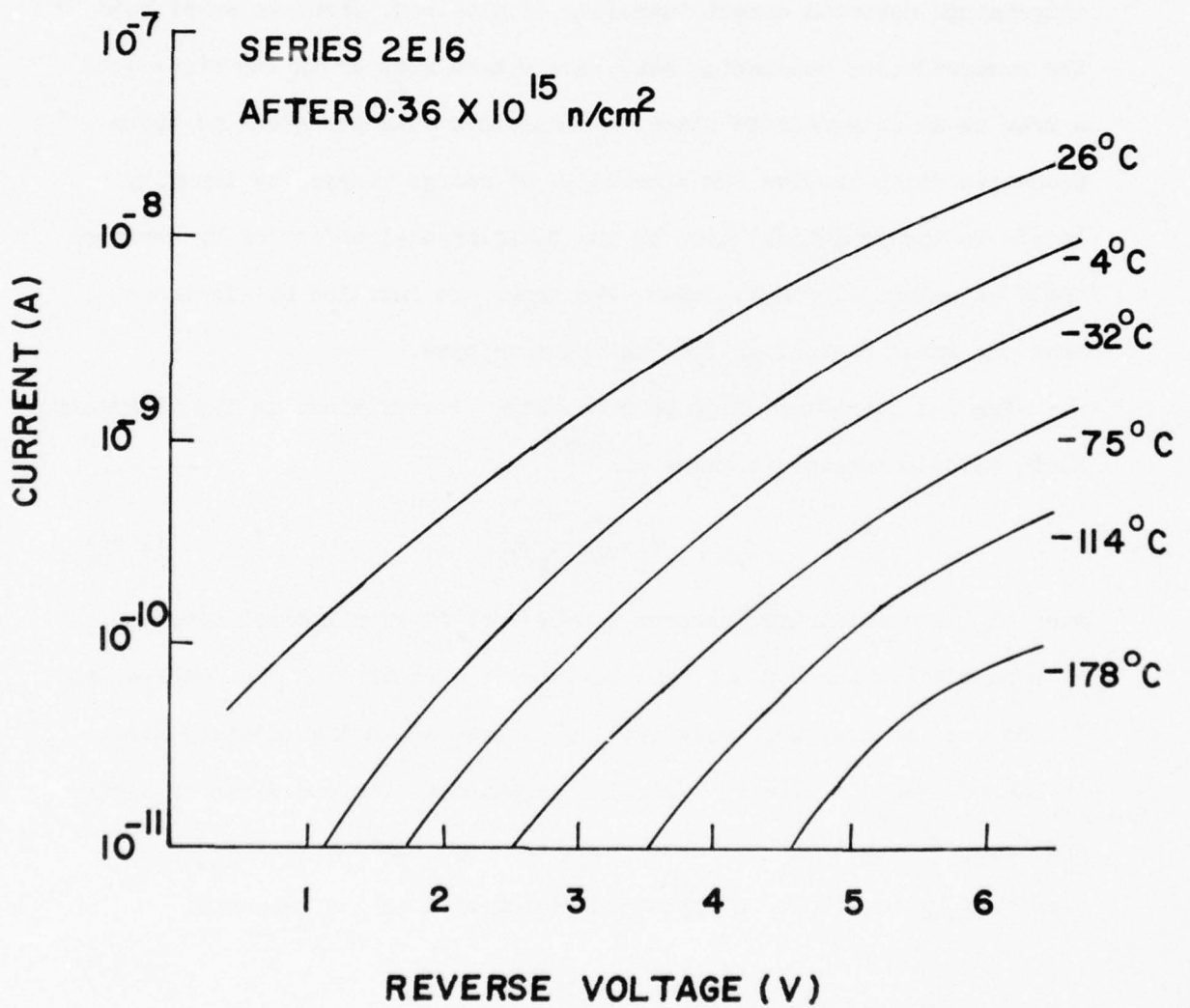


Fig. 4.22 Reverse Current-Voltage Characteristics for 2E16 with Temperature After Irradiation

magnitude in current for a change in temperature by a factor of 3). These characteristics strongly suggest that the reverse current must be caused by a high field effect process. For the purpose of this discussion we will classify the possible rate-limiting mechanism as barrier limited or bulk limited. By barrier limited we mean mechanisms such as temperature assisted direct tunneling of electrons from the metal into the semiconductor conduction band in a single step or in two steps with a trap as an intermediate state. We consider bulk processes as those processes which involve the liberation of charge trapped by impurity levels in the depletion layer by the Poole-Frenkel effect or by enhanced field emission. In these cases, the traps are refilled by electrons from the metal contact or from the valence band.

The I-V characteristics of a Schottky barrier diode in the thermionic field emission regime is given by:<sup>(29)</sup>

$$I_r = I_s \exp V_r/V_0 \quad (4.42)$$

where  $I_s$  is a saturation current slowly varying with applied bias and  $V_0$  a constant which depends upon the donor concentration and temperature. In the case of two step tunneling with a trap as an intermediate step, it can be shown, following a similar argument as the one given by Parker and Mead,<sup>(30)</sup> that the I-V characteristics are similar to the one expressed by Eq. (4.42) except for a factor of 2 in the exponent:

$$I_r \propto \exp V_r/2V_0 \quad (4.43)$$

Equations (4.42) and (4.43) indicate that  $\ln I_r$  is proportional to the reverse bias voltage  $V_r$ . The data of Fig. 4.22 does not follow either

of the above two equations and it is concluded that the excess reverse current is not due to direct one-step or two-step tunneling.

In a depletion region in which the emission process dominates over the capture process, the current due to the liberation of charge from a level is given by:

$$I = q N_t f_t e_n \quad (4.44)$$

where  $N_t$  is the total number of levels in the depletion layer,  $f_t$  the probability of those levels being occupied by electrons and  $e_n$  the electron emission rate. The fraction  $f_t$  can be expressed in terms of the emission rates  $e_p$  and  $e_n$  of holes and electrons:

$$f_t = e_p / (e_p + e_n) \quad (4.45)$$

Therefore, the expression for the current becomes:

$$I = q N_t (e_p e_n) / (e_p + e_n) \quad (4.46)$$

If one of the emission processes dominates over the other, the current is determined by the slowest emission rate. In that case, we will write Eq. (4.46) as:

$$I = q N_t / \tau \quad (4.47)$$

where  $1/\tau$  is the smallest of  $e_n$  and  $e_p$ .

In the case of the Poole-Frenkel effect, i.e., lowering of the energy barrier by an electric field, the expression for  $1/\tau$  is: <sup>(31)</sup>

$$1/\tau \propto \exp -(\phi_t - \frac{q\beta}{2} \sqrt{E})/kT \quad (4.48)$$

where  $\beta$  is the constant used in the Schottky effect and  $\phi_t$  is the energy required for emission of a free carrier from the trap. Equations (4.47) and (4.48) indicate that in the case of the Poole-Frenkel effect, the  $\ln I$  is given by:

$$\ln I = (\phi_t - \frac{q\beta}{2} \sqrt{E})/kT + \text{constant} \quad (4.49)$$

We attempted to fit the data of Fig. 4.22 to Eq. (4.49) without success.

The last mechanism considered is field emission from a trap. Franz<sup>(32)</sup> has derived an expression for the emission by tunneling of carriers trapped in a spherical well and gives:

$$1/\tau = \frac{qE}{2(m^* \phi_t)^{1/2}} \exp - 4/3 \frac{\sqrt{2m^*} \phi_t^{3/2}}{q \hbar E} \quad (4.50)$$

Substitution of Eq. (4.50) into Eq. (4.47) gives:

$$\ln I = -4/3 \frac{\sqrt{2m^*} \phi_t^{3/2}}{q \hbar E} + \text{constant} \quad (4.51)$$

where we have neglected the  $\ln E$  term. Using the data of Fig. 4.22, we have plotted  $\ln I$  vs. the inverse of the peak electric field at the barrier and the results are shown in Fig. 4.23. At high electric fields and low temperatures, the current follows Eq. (4.51). At low electric fields and high temperature the current is in excess of the one expected from Eq. (4.51) and is due to thermionic emission through the metal-semiconductor barrier. From the slope of the straight lines of Fig. 4.23,

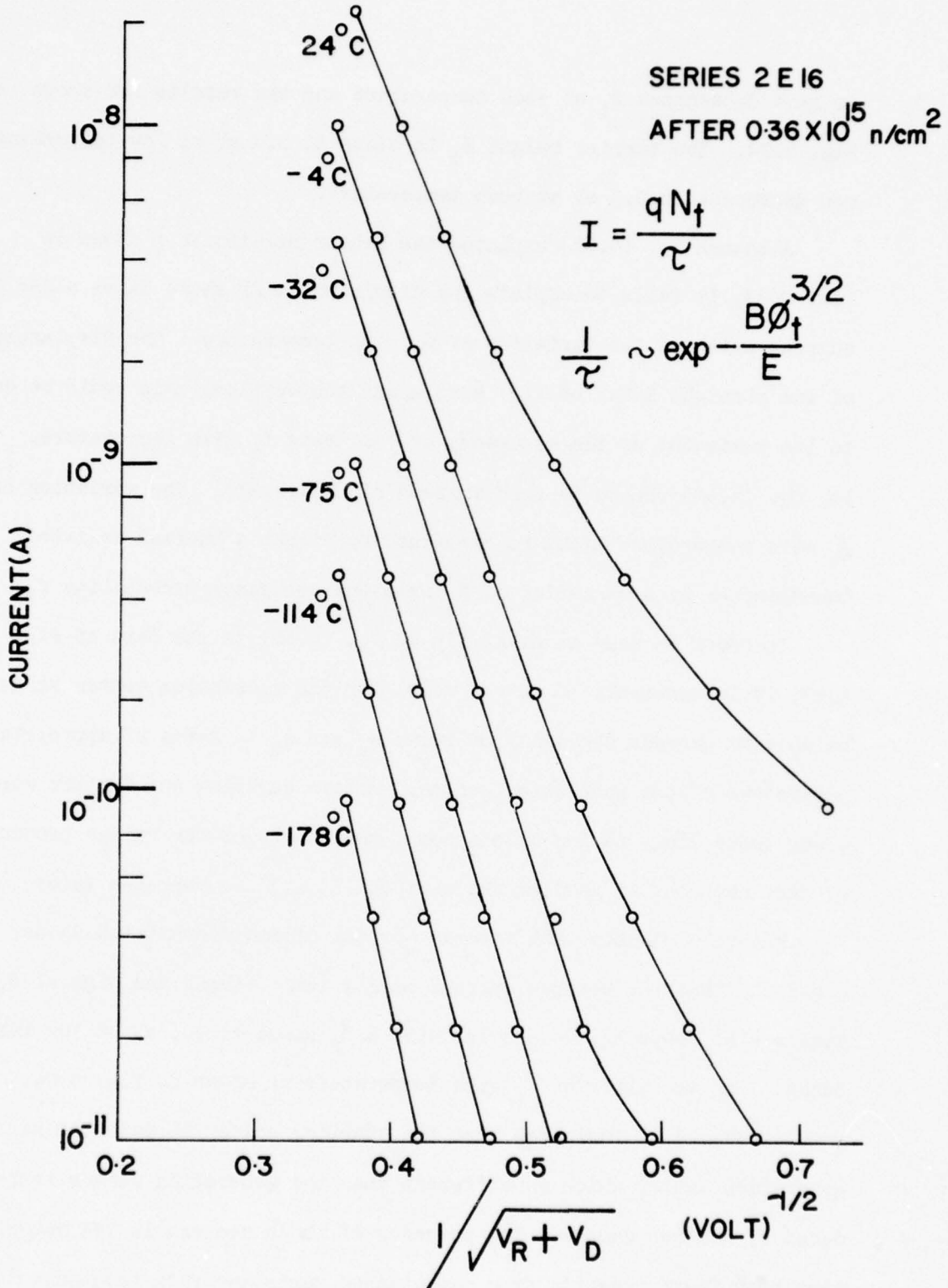


Fig. 4.23 Reverse Current vs. (Total Voltage)<sup>-1/2</sup> for 2E16 with Temperature After Irradiation

we have determined  $\phi_t$  at each temperature and the results are shown in Fig. 4.24. The barrier height  $\phi_t$  is close to 0.4 eV at low temperatures and decreases to 0.3 eV at room temperature.

Although Eq. (4.51) explains the linear relationship shown in Fig. 4.23, it fails to explain the displacement of those lines along the current axis and the variation of  $\phi_t$  with temperature. The displacement of the straight lines of Fig. 4.23 along the vertical axis could be due to the variation of the occupancy of the traps  $f_t$  with temperature. That is, Eq. (4.46) should be used instead of Eq. (4.47). The variation of  $\phi_t$  with temperature might be explained by either a thermal assisted tunneling or by a variation of  $\phi_t$  with the occupancy probability  $f_t$ .

In order to make an exact fit of Eq. (4.46) to the data of Fig. 4.23, it is necessary to have a model for the generation center so as to be able to express the emission rates  $e_p$  and  $e_n$  in terms of appropriate parameters of the generation center. We are carrying out further work along these lines taking into account the nature of the damage produced by fast neutrons in gallium arsenide and it will be reported later.

Figure 4.25 shows the reverse current of an unirradiated diode. It was found that the reverse current at low temperatures and high electric fields also obeys Eq. (4.51) but with a  $\phi_t$  close to 0.5 eV at low temperatures. The variation of  $\phi_t$  with temperature is shown in Fig. 4.24. The data of Fig. 4.24 indicates that the starting epitaxial material has a generation center which is different than the generation center introduced by neutron damage. The presence of those centers in VPE material have been found recently from capacitance variation with frequency.<sup>(33)</sup> The trap energy reported for one of the centers agrees with the one of 0.5 eV that we found by a completely different technique.

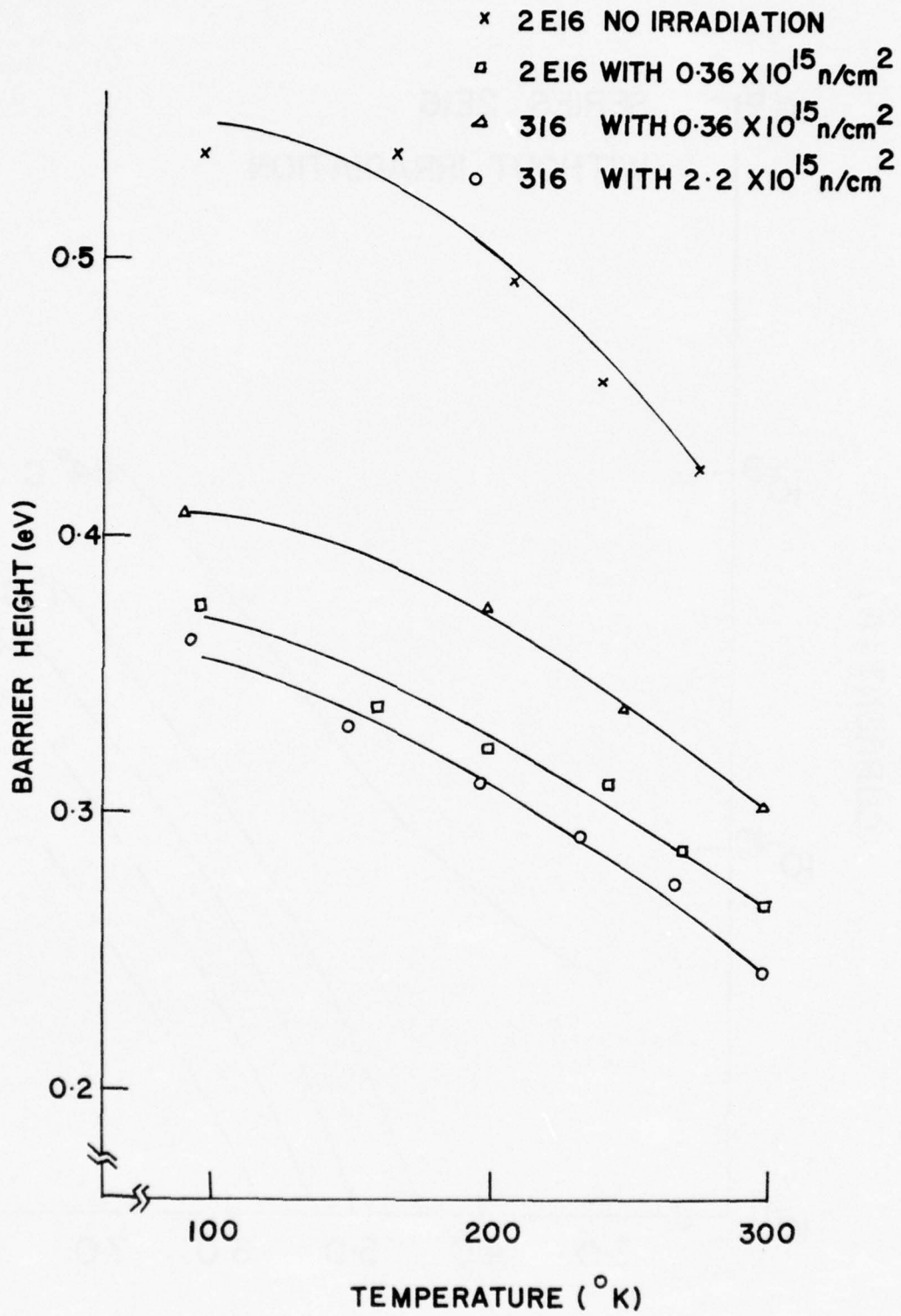


Fig. 4.24 Effective Barrier vs. Temperature for 2E16 and 316

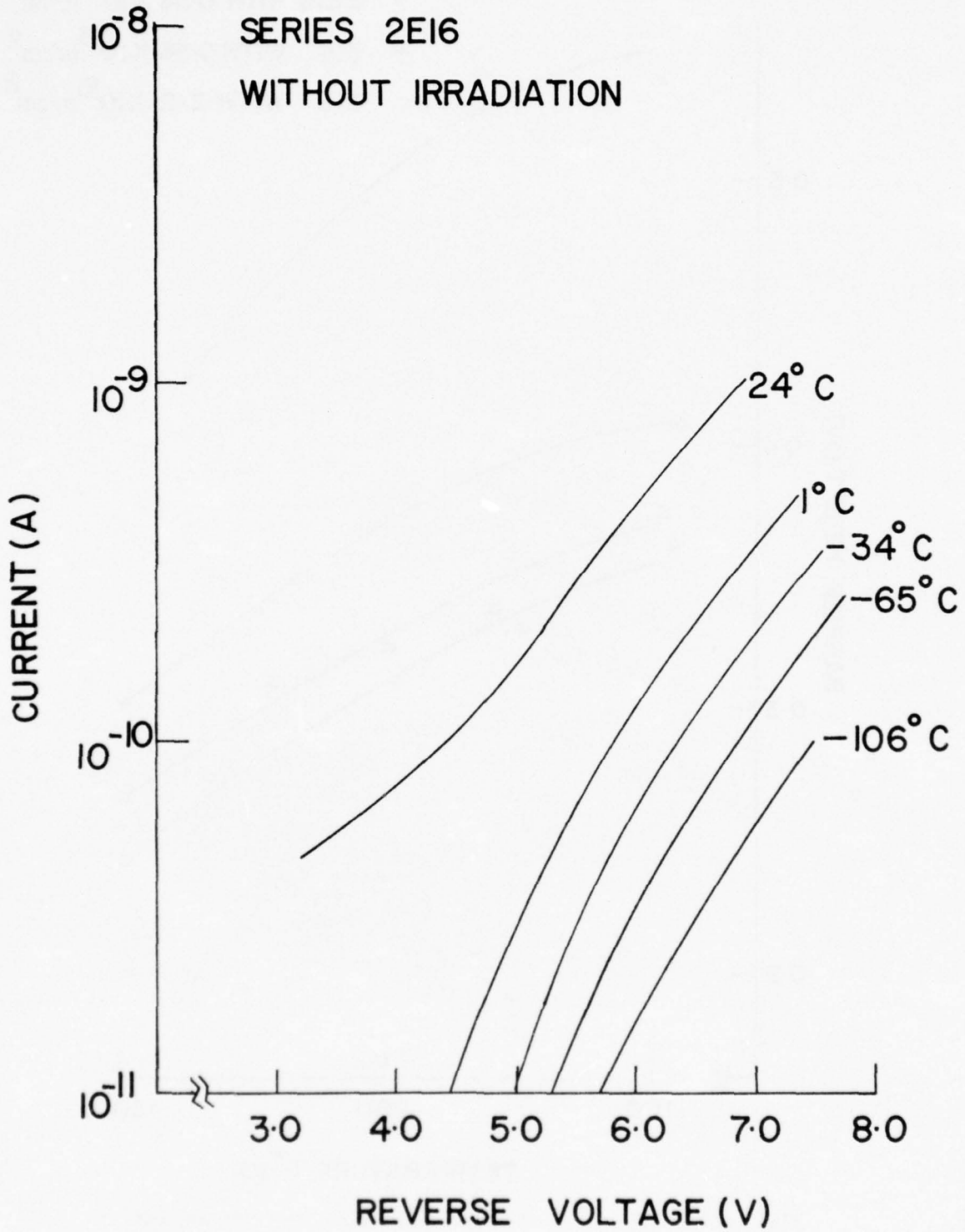


Fig. 4.25 Reverse Current-Voltage Characteristics for 2E16 with Temperature (Without Irradiation)

It should be pointed out that Eq. (4.46) implies emission of both electrons and holes. The emission of electrons is from the trap center to the conduction band. The emission of holes is from the trap center into either the semiconductor valence band or into the metal. These two possibilities are very important since it implies that the reverse characteristics of neutron irradiated diffused GaAs and Schottky GaAs junctions can be similar or completely different depending upon the hole emission process. If hole emission is from the valence band then both types of devices should show similar behavior, but if the hole emission is from the metal because the trap is physically close to the metal semiconductor interface, then the two devices will have different reverse I-V characteristics. We are carrying out further analysis of the data in order to determine which of the two hole emission processes is taking place.

## 5.0 TRANSIENT IONIZING RADIATION RESULTS AND DISCUSSION

Besides the direct effect of neutron irradiation on the characteristics of Schottky barrier junctions, the electrical characteristics during the transient ionizing radiation were also explored using the facilities described in Section 3.2. These results are described in Section 5.1. Data was also taken with commercial X-band Schottky IMPATT diodes in an attempt to uncover the cause of the anomalous aftereffects in these devices.<sup>(34)</sup> This data and discussion are presented in Section 5.2.

The purpose of this testing was to monitor any changes in characteristics of Schottky junctions under transient ionizing radiation with neutron exposure and to explain the IMPATT aftereffects.<sup>(34)</sup> The electrical characteristics of Zener diodes under transient ionizing radiation biased near or in avalanche has been reported previously,<sup>(35)</sup> and the model described will be similarly useful for Schottky diodes.

### 5.1 Au-GaAs Schottky Barrier Junctions

Of the diodes that had been neutron irradiated, series 316 and 300 were measured under transient ionizing radiation at dose rates between  $3 \times 10^8$  and  $8 \times 10^9$  rads/sec. All chips were evaluated under vacuum with either 47 ohm or 470 ohm bias circuit impedances as described in Section 3.2. Measured results at  $8 \times 10^9$  rads/sec are shown for Series 316 in Table 5.1.

At bias conditions below and at breakdown, the increase in junction voltage (photovoltage) is given. At bias currents well into avalanche, the increase in current (photocurrent) flowing through the external

<u>Bias Conditions</u>	<u>Prior Neutron Irradiation</u>	
	<u>None</u>	<u><math>2.2 \times 10^{15} \text{ n/cm}^2</math></u>
470 ohm impedance		
$\frac{V_B}{3}$	1.6 V	1.5 V
$V_B$	2.4 V	2.3 V
40 mA	2 mA	4 mA
100 mA	5 mA	5 mA
47 ohm impedance		
$\frac{V_B}{3}$	.3 V	.3 V
$V_B$	.4 V	.45 V
100 mA	10 mA	20 mA
400 mA	20 mA	20 mA

TABLE 5.1 Transient Ionizing Radiation Results for Series 316  
at a Dose Rate of  $8 \times 10^9$  rads/sec.

$V_B$  - diode breakdown voltage (0.1 mA reverse current)

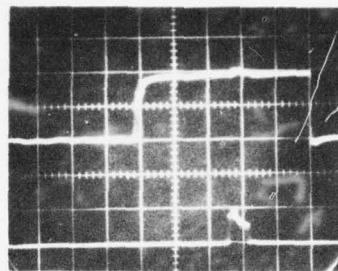
terminals of the diode is given. In all test conditions the voltage and current decreased to the preirradiation condition within 20 nanoseconds after removal of the radiation pulse. Typical photographs indicating the current increase during the radiation pulse are depicted in Fig. 5.1, where the diode is pulse-biased into avalanche with approximately 40 mA, and the increase in current during the  $8 \times 10^9$  rads/sec radiation pulse is less than 5 mA.

The data is in substantial agreement with the diode model for avalanche diodes under transient ionizing radiation developed by Shedd et al,<sup>(35)</sup> and shown in Fig. 5.2. The Series 316 junctions were fabricated on bulk material and have a series resistance ( $R_s$ ) of approximately 50 ohms. From the photovoltage measurements at one-third of the breakdown voltage, a photocurrent ( $I_p$ ) of 3 milliamps is obtained, in substantial agreement with that calculated using the depletion layer dimensions. As the bias is increased, the multiplication factor ( $M$ ) increases and the incremental junction resistance ( $R_o$ ) decreases. As shown by Shedd et al,<sup>(35)</sup> the external photovoltage peaks when  $R_o - R_s$  is approximately equal to the load resistance. Although numerous data points were not taken on each device, this model is in qualitative agreement with our data.

It is concluded that the neutron irradiations had little effect on the transient ionizing radiation characteristics. Although the junctions irradiated at  $2.2 \times 10^{15}$  neutrons/cm<sup>2</sup> had twice the photocurrent response at medium bias currents (see Table 5.1 and Fig. 5.1) slight changes in multiplication factor and dynamic space charge resistance could account

SERIES 316

470Ω BIAS



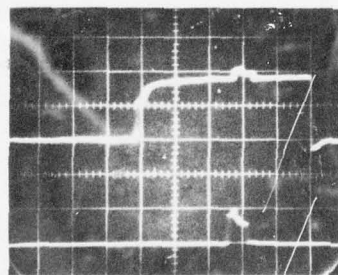
↑ 20 mA/DIV

↑ 10<sup>10</sup> RADS/SEC/DIV



100 nSEC/DIV

A. NO NEUTRON IRRADIATION



↑ 20 mA/DIV

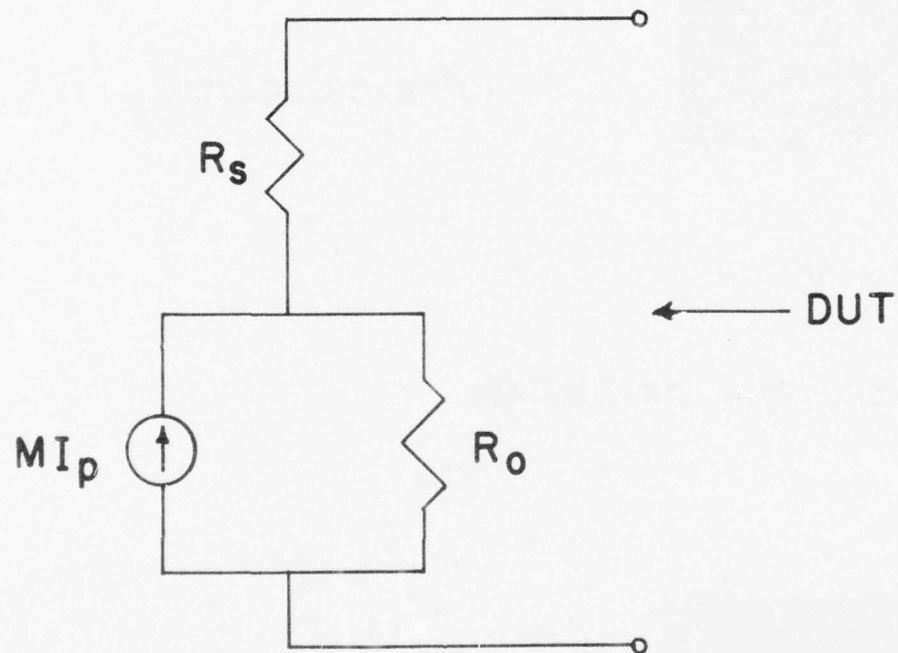
↑ 10<sup>10</sup> RADS/SEC/DIV



100 nSEC/DIV

B. WITH  $2.2 \times 10^{15}$  n/cm<sup>2</sup>

Fig. 5.1 Photographs of Typical Results of Schottky Diode Photocurrent under Transient Ionizing Radiation



$R_s$  - SERIES RESISTANCE

$R_o$  - INCREMENTAL JUNCTION RESISTANCE

$I_p$  - PHOTOCURRENT

$M$  - MULTIPLICATION FACTOR

Fig. 5.2 Equivalent Circuit for Avalanche Diode with Transient Ionizing Radiation (from Shedd et.al. (35))

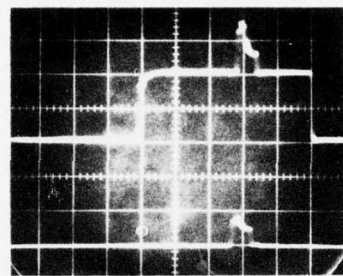
for the difference. More data would be needed to verify whether the difference indicated is real, but the effort was not warranted for this program.

### 5.2 Evaluation of IMPATT Diode Aftereffects

GaAs Schottky IMPATT diodes, including 1B10 (D1) that had previously exhibited aftereffects during RF testing,<sup>(34)</sup> were tested under similar conditions to the Au-GaAs Schottky junctions. The results are given in Table 5.2. There were no indications of aftereffects<sup>(34)</sup> or charge storage<sup>(36)</sup> in these IMPATT diodes in any of the test conditions. That is, the diode voltage and current (which was increased during the radiation pulse) decreased to preirradiation conditions immediately (within 20 nanoseconds) after the radiation pulse at all test conditions. Typical photographs are depicted in Fig. 5.3, where the increase in current during the radiation pulse is shown to be dependent upon the bias impedance.

The most significant information in Table 5.2 is the large step in current during the radiation pulse when the diode is biased well into breakdown, and the dependence of the magnitude on the bias circuit impedance. In particular, at a dose rate of  $7.5 \times 10^9$  rads/sec and a bias current of 100 mA, the magnitude of the current step was 40 mA and 150 mA with a bias circuit impedance of 470 ohms and 47 ohms respectively. In the RF test setup used previously, the test conditions where aftereffects commenced were: dose rate of  $2 \times 10^9$  rads/sec, bias current of 80 mA and bias circuit impedance of 325 ohms. Interpolating these experimental results to the actual RF test conditions, an increase in current

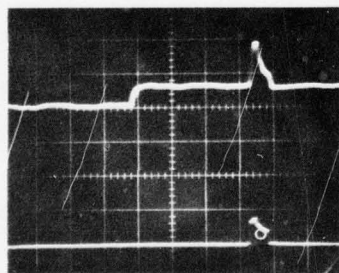
IBIO  
SCHOTTKY  
IMPATT



↑ 50 mA/DIV  
↑  $10^{10}$  RADS/SEC/DIV

→  
100 nSEC/DIV

A. 470 OHM BIAS IMPEDANCE



↑ 200 mA/DIV  
↑  $10^{10}$  RADS/SEC/DIV

→  
100 nSEC/DIV

B. 47 OHM BIAS IMPEDANCE

Fig. 5.3 Photographs of GaAs Schottky IMPATT Photocurrent under Transient Ionizing Radiation

<u>Dose Rate (rads/sec)</u>	<u>Bias Conditions</u>	<u>Bias Circuit Impedance</u>	
		<u>47 ohms</u>	<u>470 ohms</u>
$1.2 \times 10^9$	$.8 V_B$	.2 V	1.4 V
	$V_B$	.6 V	3.0 V
	40 mA	---	5 mA
	100 mA	5 mA	5 mA
	200 mA	10 mA	---
$3.7 \times 10^9$	$.8 V_B$	1.5 V	7 V
	$V_B$	4.0 V	13 V
	40 mA	---	20 mA
	100 mA	40 mA	20 mA
	200 mA	40 mA	---
$7.5 \times 10^9$	$.8 V_B$	7.5 V	16 V
	$V_B$	9.0 V	23 V
	40 mA	---	40 mA
	100 mA	150 mA	40 mA
	200 mA	150 mA	---

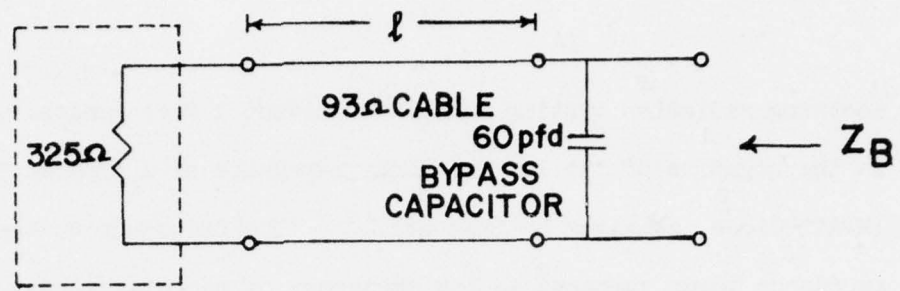
TABLE 5.2 Photoresponse of Schottky IMPATT 1B10(D1)  
 (with RF aftereffects<sup>(34)</sup>)

during the radiation pulse of 15 mA is obtained. Although this current change is significant, the magnitude is not large enough to cause the observed RF aftereffects directly.

Besides the RF circuit considerations previously described, <sup>(34)</sup> we now believe that the bias circuit impedance to be a key factor in controlling the aftereffects. Since the RF aftereffects were originally observed with the GaAs Schottky IMPATT's, Brackett <sup>(37)</sup> treated the tuning-induced failure and bias circuit oscillation problem in IMPATT diodes in some depth. In particular, Brackett showed that GaAs devices are more sensitive to these problems than Si diodes, since the net low frequency negative resistance is larger in GaAs due to inherent material parameters.

It should be emphasized that the bias impedance with frequency from DC to 50 MHz is important in evaluating the bias circuit instability. The 325 ohm bias circuit given previously <sup>(34)</sup> must be modified as shown in Fig. 5.4A to include the length of 93 ohm cable between the bias circuit and diode and the 60 Pf bypass capacitance located at the diode. In order to conveniently shield the bias circuit with the evacuated cavity, four feet of cable was used during the radiation testing. This cable length is over 0.1 wavelengths in length at 20 MHz, and its impedance-transforming properties may be a cause of bias circuit instability.

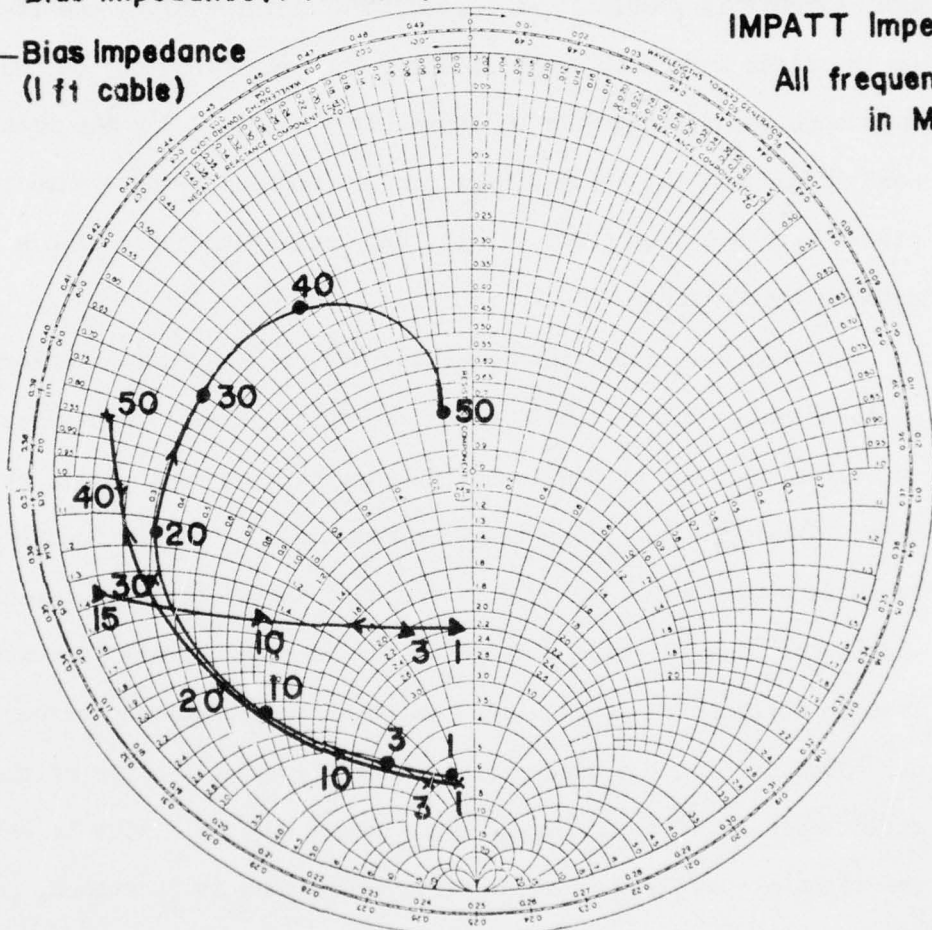
Referring to the Smith Chart in Fig. 5.4B, the bias circuit impedance (normalized to 50 ohms) is plotted with frequency for two cable lengths -- the four foot length actually used in the RF transient



BIAS NETWORK

A. BIAS EQUIVALENT CIRCUIT

- — Bias Impedance (4 ft cable)
  - x — Bias Impedance (1 ft cable)
  - ▲ — Brackett GaAs IMPATT Impedance
- All frequencies in MHz



B.  $Z_B$  WITH FREQUENCY AND CABLE LENGTH AS A PARAMETER (Brackett GaAs IMPATT superimposed)

Fig. 5.4 IMPATT Diode Bias Circuit Model with Impedance Loci (following Brackett<sup>(37)</sup>)

ionizing radiation testing and a more modest 1 foot length. Superimposed is the negative of the low frequency impedance of a typical 5 GHz GaAs IMPATT diode, as given by Brackett.<sup>(37)</sup> The frequency on the diode impedance locus compared to the frequency on the circuit impedance locus at the point of intersection is important. As shown by Brackett, the bias circuit is stable if at the point of intersection, the frequency on the diode impedance locus is lower than the frequency on the bias impedance locus; otherwise an instability exists. For the Brackett GaAs IMPATT and the assumed bias circuit model, the bias circuit is stable with a 1 foot cable length, but becomes unstable with a cable greater than 4 feet.

It should be noted that Brackett has not considered leakage current as a parameter in his IMPATT model, so that a direct comparison of diode impedance loci as a function of leakage current does not exist. However, Misawa<sup>(38)</sup> has shown that the magnitude of the DC induced negative resistance of a Read IMPATT does increase as the leakage current is increased. The DC voltage drops as the leakage current increases because less multiplication is required. Misawa's calculations further confirm our hypothesis of the bias circuit instability as a cause of the after-effects since the diode impedance locus shown in Fig. 5.4 is shifted to the right as the DC induced negative resistance is increased, and a bias instability is more likely.

FOR THE EQUIVALENT CIRCUIT ASSUMED AND THE LOW FREQUENCY GaAs IMPATT IMPEDANCE FROM BRACKETT, THE BIAS CIRCUIT IS NEARLY UNSTABLE WITH THE LONG CABLE NEEDED WHEN SHIELDING THE BIAS CIRCUIT DURING THE

RADIATION TESTING. THIS HAS NOT BEEN DEMONSTRATED EXPERIMENTALLY AND IT WOULD BE PREMATURE TO ASSUME THAT THE AFTEREFFECTS<sup>(34)</sup> HAVE BEEN FULLY EXPLAINED.

In particular, RF testing with controlled bias circuit impedances are necessary. Furthermore, with Brackett's models, there is no difference between diffused and Schottky contacts. From the RF measurements made previously,<sup>(34)</sup> there is a correlation between type of avalanching junction and occurrence of aftereffects. The transverse instability of Van Iperen<sup>(39)</sup> and other two dimensional effects are different for diffused and Schottky contacts and could be a contributing source of the aftereffects. However, from the considerations described in this Section, the bias circuit instability appears to be a possible principal contributor.

## 6.0 IMPLICATIONS OF RESULTS ON RADIATION HARDENING DESIGN

The emphasis of this program was to experimentally evaluate the effect of neutron and transient ionizing irradiation on the electrical characteristics of GaAs Schottky junctions and to understand the basic mechanisms responsible for these electrical characteristics. Although more work is continuing to verify and extend the concepts described in Sections 4 and 5, we have projected the implications of our results on the use of GaAs microwave devices with Schottky junctions in radiation hardened systems.

IT MUST BE EMPHASIZED THAT THESE IMPLICATIONS HAVE NOT BEEN VERIFIED BY CONTROLLED TESTING ON ACTUAL DEVICES. THEY ARE OBTAINED BY USING OUR EXPERIMENTAL DATA AND OUR INTERPRETATION OF THIS DATA TO PREDICT WHAT COULD OCCUR IN HIGH PERFORMANCE GaAs SCHOTTKY JUNCTION DEVICES IN MICROWAVE SYSTEMS EXPOSED TO RADIATION ENVIRONMENTS. ALTHOUGH THESE IMPLICATIONS HAVE NOT BEEN PROVEN, THEY SUGGEST THAT MORE WORK IS NECESSARY BEFORE GaAs SCHOTTKY JUNCTION DEVICES ARE UTILIZED IN RADIATION HARDENED APPLICATIONS.

### 6.1 Neutron Implications in IMPATT's, MESFET's, and Other Microwave Devices

Neutron radiation effects in IMPATT diodes have been studied by many authors, with these results recently reviewed.<sup>(40,41)</sup> However, all devices tested were silicon, flat-profile, diffused junction IMPATT's. In high performance microwave systems, the Read or clump profile, GaAs Schottky-junction IMPATT diodes will be utilized, as these recently developed devices have higher output power with higher efficiencies.<sup>(42,43)</sup>

These improved IMPATT's have a more confined avalanche region with a resultant increase in peak electric field at the junction. Chive et al.<sup>(44)</sup> have described the harmful effect of tunneling on these devices, which is especially critical in Read profile diodes. With neutron irradiation we have shown that tunneling currents (field assisted thermionic emission similar to that described by Chive et al.) increase in neutron irradiated Schottky junctions at fluences where carrier removal effects are small and trapping effects on the drifting charge pulse is also expected to be small.<sup>(45,46)</sup> These two effects have been shown to dominate the RF power reduction in silicon flat-profile, diffused junction IMPATT diodes. The field-assisted thermionic emission is expected to be even more prevalent in neutron-irradiated high efficiency diodes due to the enhanced electric field near the junction.

In addition to this effect on the charge carriers injected into the drift region, the enhanced leakage current of the Schottky junction can reduce the output power directly.<sup>(47)</sup> Although the magnitude of the static leakage current would not be expected to significantly degrade the device operation, increases in dynamic leakage current from the modified surface state density and/or from enhanced field emission could be significant. It should be noted that the transient ionizing results indicate the traps' response times are indeed short, although not necessarily as short as would be necessary to effect the dynamic leakage current. This dynamic leakage current enhancement would have to be considered in detail further.

At this time the direct effect of enhanced field emission on the injected carrier pulse is considered to be the principal new effect for IMPATT diodes in applications with neutron exposure specifications. In fact, enhanced field emission will probably dictate the feasibility of using these high power high efficiency diodes in microwave systems with neutron hardening requirements. Experimental work and further analysis are needed to determine quantitative limits.

In MESFET's (metal-semiconductor field effect transistors), or Schottky-gate FET's, an anomalous reduction in transconductance has been reported.<sup>(11)</sup> The reduction in transconductance in Schottky-gate FET's occurred at an order of magnitude lower neutron fluence than "comparable" junction gate devices (with  $10^{17}/\text{cm}^3$  channel doping, a 10% reduction was measured at  $5 \times 10^{14} \text{ n/cm}^2$  and  $5 \times 10^{15} \text{ n/cm}^2$  in MESFET's and JFET's, respectively). In addition, the junction gate devices degraded at a fluence in agreement with calculations using carrier removal and mobility information on GaAs.<sup>(48)</sup>

The transconductance degradation in MESFET's could be a result of enhanced field emission from the Schottky gate with the gate metal being the source of electrons and electron emission from the defect being the rate limiting process (as described in Section 4.4). Due to the complicated carrier flow (hot electrons, two dimensional effects, etc.) in MESFET's, the correlation between the basic Schottky junction effects with neutron irradiation reported in Section 4 and MESFET irradiation effects is not readily apparent. A thorough program is needed so that this anomalous degradation is resolved before GaAs MESFET's are utilized in microwave systems with neutron exposure specifications.

In addition, the enhanced reverse leakage of the Schottky gate will tend to reduce the input impedance of the MESFET and the modified surface state density and/or enhanced field emission could effect the device noise performance. The input impedance reduction is expected to be tolerable as long as the barrier height reduction is comparable with other barrier metalization as reported herein with gold. (The continuing program with Al/n GaAs Schottky junctions will provide useful data as aluminum gates are often used in MESFET technology.) The possible effect on device noise is conjecture at this time, but should be evaluated in any program exploring MESFET radiation tolerance.

The noise degradation should also be explored in other GaAs devices using Schottky junctions such as mixers and parametric devices. Although microwave mixers have been evaluated under neutron exposure,<sup>(49)</sup> silicon Schottky barriers were used. The effects observed in this program with Au/n GaAs are expected to be different in silicon. This early data on silicon, while useful as a guide, should not be used as an indication of GaAs Schottky junction devices.

## 6.2 Transient Ionizing Radiation Implications in IMPATT's

From the data and discussion presented in Section 5.2, it is apparent that the anomolous aftereffects in Schottky junction GaAs IMPATT diodes<sup>(34)</sup> is not entirely caused by the Schottky junction. Bias circuit considerations appear to have been a principal cause of the aftereffect instabilities, although the reason that the diffused junction GaAs IMPATT's did not exhibit these instabilities is unresolved. Transient

ionizing radiation testing with controlled bias circuit impedance is necessary to verify the hypothesis described in Section 5.2. Naturally, the GaAs Schottky IMPATT's must be oscillating in a microwave circuit during the radiation testing.

It is possible that the GaAs Schottky IMPATT's may be suitable for transient ionizing radiation environments, although bias circuit constraints will be more stringent than in a non-radiation environment. Further work is needed to verify the hypothesis and quantize the bias circuit constraints.

AD-A034 425

RENSELAER POLYTECHNIC INST TROY N Y DEPT OF ELECTRI--ETC F/G 9/1  
INTERFACE STATES IN SCHOTTKY BARRIER DIODES.(U)

AUG 76 J M BORREGO, R J GUTMANN  
SCIENTIFIC-1

F19628-74-C-0102  
NL

UNCLASSIFIED

RADC-TR-76-266

2 OF 2

AD  
A034425



END  
DATE  
FILMED  
2-77

## 7.0 SUMMARY AND CONCLUSIONS

The following summarizes the accomplishments of this program on Au/nGaAs Schottky barrier diodes:

1. High quality guarded diodes were fabricated from bulk and epitaxial material having n factors of 1.03 and saturation current densities of  $10^{-8}$  amps/cm<sup>2</sup>, comparable to the best reported in the literature.
2. Automated I-V and 1MHz C-V facilities were developed to accurately evaluate junction characteristics from 77°K to 360°K.
3. The reverse current was found to be a sensitive parameter to neutron irradiation, increasing by one to two orders of magnitude at neutron fluences where carrier compensation was 10% and n factor increase was small ( $\sim 0.05$ ). This current increase has been shown not to be thermal generation current with a constant minority carrier lifetime.
4. The experimental results before and after neutron irradiation indicated that the interface density model of Levine<sup>(1,2)</sup> has a small range of validity when carrier concentration, temperature, electric field and neutron fluence are varied.
5. The surface state density is reasonably approximated by a sharp peak of between  $3 \times 10^{13}$  and  $10^{14}$  cm<sup>-2</sup> eV<sup>-1</sup> near the zero bias Fermi level and a lower constant level (about  $10^{13}$  cm<sup>-2</sup> eV<sup>-1</sup>) elsewhere in agreement with Crowell and Roberts.<sup>(26)</sup>
6. Below room temperature and/or at higher electric field intensity, enhanced field emission currents rather than thermionic current

dominate I-V characteristics.

7. Neutron irradiation at the fluences employed does not affect transient ionizing radiation characteristics of the Schottky barrier diodes. The response is similar to that reported previously for pn junction diodes.
8. Comparable transient ionizing radiation data on Schottky barrier GaAs IMPATT diodes indicate that aftereffects<sup>(34)</sup> observed in these devices are not exclusively a junction effect. Analytical work indicates that device-circuit interactions are a likely cause.

REFERENCES

1. J. D. Levine, "Schottky Barrier Anomalies and Interface States", *Journal of Applied Physics*, 42, 3991-3999 (1971).
2. J. D. Levine, "Power Law Reverse Current-Voltage Characteristics in Schottky Barriers", *Solid State Electronics*, 17, 1083-1086 (1974).
3. A. Y. Yu and E. H. Snow, "Radiation Effects on Silicon Schottky Barriers", *IEEE Trans. on Nuclear Science*, 16, 220-226 (1969).
4. L. W. Aukerman, "Low Energy Proton Irradiation on Silicon Surface Barrier Detectors", *IEEE Trans. on Nuclear Science*, 17, 245-249 (1970).
5. D. A. Neamen and W. W. Grannemann, "Fast Neutron Effects on GaAsP Schottky Barrier Diodes and Hall Effect Devices", *IEEE Trans. on Nuclear Science*, 19, 215-219 (1972).
6. R. J. Chaffin, Microwave Semiconductor Devices: Fundamentals and Radiation Effects, Wiley, Ch. 6 (1973).
7. J. M. Borrego, R. J. Gutmann, P. E. Cottrell, and S. K. Gandhi, "Aftereffects in IMPATT Oscillators with Transient Ionizing Radiation", *Proc. of the IEEE*, 61, 675-676 (1973).
8. J. M. Borrego, R. J. Gutmann, P. E. Cottrell, and S. K. Gandhi, "Transient Ionizing Radiation Effects on IMPATT Oscillators", *IEEE Trans. on Nuclear Science*, NS-19 328-334 (1972).
9. P. E. Cottrell, J. M. Borrego, and R. J. Gutmann, "IMPATT Diodes with Enhanced Leakage Current", *Solid State Electronics*, 18, 1-12 (1975).
10. Conversation with R. Dolan and W. Shedd, AFCRL.
11. C. A. Liechti and R. L. Tillman, "Design and Performance of Microwave Amplifiers with GaAs Schottky Gate Field-Effect Transistors", *IEEE Trans. on Microwave Theory and Techniques*, MTT-22, 510-517 (1974). See pg. 516.
12. J. P. Mitchell and D. K. Wilson, "Surface Effects of Radiation on Semiconductor Devices", *Bell System Technical Journal*, 46, 1-80 (1967). See pp. 39-40.
13. L. Cheng and J. W. Corbett, "Defect Creation in Electronic Materials", *Proc. of the IEEE*, 62, 1208-1214 (1974).

REFERENCES (Continued)

14. G. H. Marcus and H. P. Bruemmer, "Radiation Damage in GaAs Gunn Diodes", IEEE Trans. on Nuclear Science, NS-17, 230-232 (1970).
15. R. Hall and J. H. Leck, "Avalanche Breakdown of Gallium Arsenid p-n Junctions", Int. J. of Electronics, 25, 529-537 (1968).
16. B. L. Smith, "GaAs Schottky Diodes with Linear Log I/V Behavior Over Eight Decades of Current", Electronic Letters, 4, No. 16, 332-333 (1968).
17. C. A. Mead and W. G. Spitzer, "Fermi Level Position at Metal-Semiconductor Interfaces", Phys. Rev., 134, 713-716 (1964).
18. C. R. Crowell, "The Richardson Constant for Thermionic Emission in Schottky Barrier Diodes", S. S. Elec., 8, 395-399 (1965).
19. C. Herring and M. H. Nichols, "Evaluation of Thermionic Data", Rev. Mod. Phys., 21, 185-270 (1949).
20. O. Madelung, Physics of III-V Compounds, J. Wiley and Sons, New York (1964).
21. F. Larin, Radiation Effects in Semiconductor Devices, J. Wiley and Sons, New York, (1968).
22. C. T. Sah, R. N. Noyce and W. Shockley, "Carrier Generation and Recombination in P-N Junctions and P-N Junction Characteristics", Proc. IRE, 45, 1228-1242 (1957).
23. E. H. Rhoderick, "Comments on the Conduction Mechanism in Schottky Diodes", J. Phys. D. Appl. Phys., 5, 1920-1929 (1972).
24. C. T. Sah and V. G. K. Reddi, "Frequency Dependence of the Reverse-Biased Capacitance of Gold-Doped Silicon P<sup>+</sup>N Step Junctions", IEEE Trans. on Elec. Devices, ED-11, 345-349 (1964).
25. J. A. Grimshaw, "Defect Studies on Electron Irradiated GaAs by Electrical Measurements", Proc. of the 1972 Conf. on Radiation Damage and Defects in Semiconductors, pp. 355-363, The Institute of Physics, London (1973).
26. C. R. Crowell and G. I. Roberts, "Surface State and Interface Effects on the Capacitance-Voltage Relationship in Schottky Barriers", J. of Appl. Phys., 40, 3726-3730 (1969).
27. H. K. Henisch, Rectifying Semiconductor Contacts, Clarendon Press, Oxford (1957).

REFERENCES (Continued)

28. F. A. Padovani, "Thermionic Emission in Au-n GaAs Schottky Barriers", *Solid State Elec.*, 11, 193-200 (1968).
29. F. A. Padovani in *Semiconductor and Semimetals*, Vol. 7A, Academic Press, New York (1971).
30. G. H. Parker and C. A. Mead, "The Effect of Trapping States on Tunneling in Metal-Semiconductor Junctions", *Appl. Phys. Lett.*, 14, 21-23 (1969).
31. R. M. Hill, "Poole-Frenkel Conduction in Amorphous Solids", *Phil. Mag.*, 23, 59-86 (1971).
32. W. Franz in *Handbook of Physics*, Vol. 17, Springer-Verlag (1956).
33. F. Hasegawa and A. Majerfeld, "Electron and Hole Traps in Epitaxial n- and p-GaAs", Conf. on Preparation and Properties of Electronic Materials, Princeton University, New Jersey, August 25-27, 1975.
34. S. K. Ghandhi, J. M. Borrego, R. J. Gutmann and P. E. Cottrell, "Effects of Transient Ionizing Radiation on X-Band IMPATT's", Scientific Report No. 1, AFCRL-TR-73-0111, Ch. 6.
35. W. Shedd, B. Buchanan and R. Dolan, "Transient Radiation Effects in Silicon Diodes Near and In Avalanche Breakdown", *IEEE Trans. on Nuclear Science*, NS-18, 304-309 (1971).
36. J. M. Borrego, R. J. Gutmann and J. Narain, "Transient Ionizing Radiation Effects on BARITT Diode Oscillators", IEEE Conference on Nuclear and Space Radiation Effects, Arcata, California, July 1975.
37. C. A. Brackett, "The Elimination of Tuning-Induced Burnout and Bias-Circuit Oscillations in IMPATT Oscillators", *Bell System Technical Journal*, 52, 271-306 (1973).
38. T. Misawa, "Saturation Current and Large-Signal Operation of a Read Diode", *Solid State Electronics*, 13, 1363-1368 (1970).
39. B. B. Van Iperen, "Efficiency Limitation by Transverse Instability in Silicon IMPATT Diodes", *Proc. of the IEEE*, 62, 284-285 (1974).
40. R. J. Chaffin, *Microwave Semiconductor Devices: Fundamentals and Radiation Effects*, Wiley, Ch. 8 (1973).
41. R. J. Gutmann, J. B. Borrego, and S. K. Ghandhi, "Radiation Effects in Transit-Time Microwave Diodes", *Proc. of the IEEE*, 62, 1256-1264 (1974).

REFERENCES (Continued)

42. G. Salmer, J. Prebetich, A. Farragre, and B. Kramer, "Theoretical and Experimental Study of GaAs IMPATT Oscillator Efficiency", J. Appl. Phys., 44, 314-324 (1973).
43. C. Kinn, R. Steels and R. Bierig, "High-Power High-Efficiency Operation of Read Type IMPATT Diode Oscillators", Electronic Letters, 9, 173-174 (1973).
44. M. Chive, E. Constant, M. Lefebvre, and J. Pribetich, "Effects of Tunneling on High-Efficiency IMPATT Avalanche Diodes", Proc. of the IEEE, 63, 824-826 (1975).
45. E. P. ErNisse and R. J. Chaffin, "Carrier Trapping and Recombination in Avalanche Diodes", IEEE Trans. on Electron Devices, ED-17, 520-526 (1970).
46. R. J. Chaffin, "The Effect of Neutron Radiation on an IMPATT Diode", IEEE Trans. on Microwave Theory and Techniques, MTT-17, 119-120 (1969).
47. P. E. Cottrell, J. M. Borrego, R. J. Gutmann, "IMPATT Diodes with Enhanced Leakage Current", Solid State Electronics, 18, 1-12 (1975).
48. A. F. Behle and R. Zuleeg, "Fast Neutron Tolerance of GaAs JFET's Operating in Hot Electron Range", IEEE Trans. on Electron Devices, ED-19, 993-995 (1972).
49. R. J. Chaffin, Microwave Semiconductor Devices: Fundamentals and Radiation Effects, Wiley, Ch. 6 (1973).

TRW SYSTEMS GROUP  
ATTN AARON H NAREVSKY R1-2144

ONE SPACE PARK  
REDONDO BEACH, CA 90278

LABEL 000000000AJ03LB 0007623701762

LABEL 000000000AJ03LB 0007623701762

DIRECTOR  
DEFENSE ADVANCED RSCH PROD AGENCY  
ATTN STU LTC ROBERT P SULLIVAN  
ARCHITECT BUILDING  
ARLINGTON, VA. 22209

DEFENSE COMMUNICATION ENGINEER CENTER  
ATTN CODE R320 C W BERGMAN  
1860 WIEHLE AVENUE  
RESTON, VA 22090

WESTINGHOUSE ELECTRIC CORPORATION  
ATTN HENRY P KALAPACA M S 3525  
DEFENSE AND ELECTRONIC SYSTEMS CTR  
P.O. BOX 1693  
FRIENDSHIP INTERNATIONAL AIRPORT  
BALTIMORE, MD 21203

WESTINGHOUSE ELECTRIC CORPORATION  
ATTN WILLIAM E NEWELL  
RESEARCH AND DEVELOPMENT CENTER  
1310 BEULAH ROAD, CHURCHILL BOROUGH  
PITTSBURGH, PA 15235

IRT CORPORATION  
ATTN R L HERTZ  
P.O. BOX 81087  
SAN DIEGO, CA 92138

IRT CORPORATION  
ATTN LEO D COTTER  
P.O. BOX 81087  
SAN DIEGO, CA 92138

IRT CORPORATION  
ATTN RALPH H STAHL

P.O. BOX 81087  
SAN DIEGO, CA 92138

IRT CORPORATION  
ATTN JAMES A NABER  
P.O. BOX 81087  
SAN DIEGO, CA 92138

JOHNS HOPKINS UNIVERSITY  
ATTN PETER E PARTRIDGE  
APPLIED PHYSICS LABORATORY  
JOHNS HOPKINS ROAD  
LAUREL MD 20810

KAMAN SCIENCE CORPORATION  
ATTN DONALD H BRYCE  
P.O. BOX 7463  
COLORADO SPRINGS, CO 80933

UNITED TECHNOLOGIES CORPORATION  
ATTN RAYMOND G GIGUERE  
HAMILTON STANDARD DIVISION  
BRADLEY INTERNATIONAL AIRPORT  
WINDSOR LUCAS, CT 06069

CHARLES STARK DRAPER LABORATORY INC  
ATTN RICHARD G HALTMAIER  
68 ALBANY STREET  
CAMBRIDGE, MA 02139

CHARLES STARK DRAPER LABORATORY INC  
ATTN KENNETH FERTIG  
68 ALBANY STREET  
CAMBRIDGE, MA 02139

CHARLES STARK DRAPER LABORATORY INC  
ATTN PAUL R KELLY  
68 ALBANY STREET  
CAMBRIDGE, MA 02139

CINCINNATI ELECTRONICS CORPORATION  
ATTN C R STUMP  
2630 GLENDALE - MILFORD ROAD  
CINCINNATI, OH 45241

CINCINNATI ELECTRONICS CORPORATION  
ATTN LOIS HAMMOND  
2630 GLENDALE - MILFORD ROAD  
CINCINNATI, OH 45241

COMPUTER SCIENCES CORPORATION  
 ATTN RICHARD H DICKHAUT  
 201 LA VETA DRIVE N.E.  
 ALBUQUERQUE, NM 87108

CUTLER-HAMMER, INC.  
 ATTN CENTRAL TECH FILES ANNE ANTHONY  
 AIL DIVISION  
 COMAC ROAD  
 DEER PARK, NY 11729

DIKEOOD CORPORATION, THE  
 ATTN L WAYNE DAVIS  
 1009 BRADBURY DRIVE, S.E.  
 UNIVERSITY RESEARCH PARK  
 ALBUQUERQUE, NM 87106

E-SYSTEMS INC.  
 ATTN LIBRARY 8-50100  
 GREENVILLE DIVISION  
 P.O. BOX 1056  
 GREENVILLE, TX 75401

EFFECTS TECHNOLOGY, INC.  
 ATTN EDWARD JOHN STEELE  
 5383 HOLLISTER AVENUE  
 SANTA BARBARA, CA 93105

ELECTRONICS TECHNOLOGY LABORATORY  
 ATTN R CURRY (UNCL ONLY)  
 ENGINEERING EXPERIMENT STATION  
 GEORGIA INSTITUTE OF TECHNOLOGY  
 ATLANTA, GA 30332

EXP AND MATH PHYSICS CONSULTANTS  
 ATTN THOMAS M JORDAN  
 P.O. BOX 66331  
 LOS ANGELES, CA 90066

FAIRCHILD CAMERA AND INSTRUMENT CORP  
 ATTN SEC DEPT FOR 2-233 DAVID K MYERS  
 464 ELLIS STREET  
 MOUNTAIN VIEW, CA 94040

FAIRCHILD INDUSTRIES, INC.  
 ATTN MGR COUFIG DATA AND STANDARDS  
 SHERMAN FAIRCHILD TECHNOLOGY CENTER  
 20301 CENTURY BOULEVARD  
 GERMANTOWN, MO 20767

SANDIA LABORATORIES  
 ATTN DOC CON FOR ORG 2110 A HOOD  
 P.O. BOX 5800  
 ALBUQUERQUE, NM 87115

SANDIA LABORATORIES  
 ATTN DOC CON FOR ORG 1933 FN COPPAGE  
 P.O. BOX 5300  
 ALBUQUERQUE, NM 87115

SANDIA LABORATORIES  
 ATTN DOC CON FOR JACK V WALKER 5220  
 P.O. BOX 5800  
 ALBUQUERQUE, NM 87115

SANDIA LABORATORIES  
 ATTN DIV 5231 JAMES H RENKEN  
 P.O. BOX 5800  
 ALBUQUERQUE, NM 87115

SANDIA LABORATORIES  
 ATTN DOC CON FOR 3141 SANDIA RPT COL  
 P.O. BOX 5800  
 ALBUQUERQUE, NM 87115

U S ENERGY RSCH AND DEV ADMIN  
 ATTN DOCUMENT CONTROL FOR WSSR  
 ALBUQUERQUE OPERATIONS OFFICE  
 P.O. BOX 5400  
 ALBUQUERQUE, NM 87115

CENTRAL INTELLIGENCE AGENCY  
 ATTN ALICE A PADGETT  
 ATTN: RD/S1 RM 5G48 HQ BLDG  
 WASHINGTON, DC 20505

UNIVERSITY OF CALIFORNIA  
 LAWRENCE LIVERMORE LABORATORY  
 ATTN DONALD J MEEKER L-545 (CLASS L -153)  
 P.O. BOX 808  
 LIVERMORE CA 94550

UNIVERSITY OF CALIFORNIA  
 LAWRENCE LIVERMORE LABORATORY  
 ATTN HANS KRUGER L-96 (CLASS L-94)  
 P.O. BOX 808  
 LIVERMORE CA 94550

UNIVERSITY OF CALIFORNIA  
LAWRENCE LIVERMORE LABORATORY  
ATTN FREDERICK R KOVAR L-31 (CLASS L -91)  
P.O. BOX 808  
LIVERMORE CA 94550

LOS ALAMOS SCIENTIFIC LABORATORY  
ATTN DOC CON FOR MARVIN M HOFFMAN  
P.O. BOX 1663  
LOS ALAMOS, NM 87545

LOS ALAMOS SCIENTIFIC LABORATORY  
ATTN DOC CON FOR J ARTHUR FREED  
P.O. BOX 1663  
LOS ALAMOS, NM 87545

LOS ALAMOS SCIENTIFIC LABORATORY  
ATTN DOC CON FOR BRUCE W NOEL  
P.O. BOX 1663  
LOS ALAMOS, NM 87545

SANDIA LABORATORIES  
ATTN DOC CON FOR THEODORE A DELLIN  
LIVERMORE LABORATORY  
P.O. BOX 969  
LIVERMORE, CA 94550

SAMSO/DY  
ATTN DYS MAJ LARRY A DARDA  
POST OFFICE BOX 92960  
WORLDWAY POSTAL CENTER  
LOS ANGELES, CA 90009  
(TECHNOLOGY)

SAMSO/DY  
ATTN DYS CAPT WAYNE SCHOBEL  
POST OFFICE BOX 92960  
WORLDWAY POSTAL CENTER  
LOS ANGELES, CA 90009  
(TECHNOLOGY)

SAMSO/IN  
ATTN IND I J JUDY  
POST OFFICE BOX 92960  
WORLDWAY POSTAL CENTER  
LOS ANGELES, CA 90009  
(INTELLIGENCE)

SAMSO/MN  
ATTN MNNG CAOT DAVID J STROBEL  
NORTON AFB, CA 92409  
(MINUTEMAN)

SAMSO/RS  
ATTN RSSE LTC KENNETH L GILBERT  
POST OFFICE BOX 92960  
WORLDWAY POSTAL CENTER  
LOS ANGELES, CA 90009  
(REENTRY SYSTEMS)

SAMSO/RS  
ATTN RSE  
POST OFFICE BOX 92960  
WORLDWAY POSTAL CENTER  
LOS ANGELES, CA 90009  
(REENTRY SYSTEMS)

SAMSO/SZ  
ATTN SZJ CAPT JOHN H SALCH  
POST OFFICE BOX 92960  
WORLDWAY POSTAL CENTER  
LOS ANGELES, CA 90009  
(SPACE DEFENSE SYSTEMS)

SAMSO/YD  
ATTN YDD MAJ MARION F SCHNEIDER  
POST OFFICE BOX 92960  
WORLDWAY POSTAL CENTER  
LOS ANGELES, CA 90009  
(DEF METEOROLOGICAL SAT SYS)

COMMANDER IN CHIEF  
STRATEGIC AIR COMMAND  
ATTN NPI-STINFO LIBRARY  
OFFUTT AFB, NB 68113

COMMANDER IN CHIEF  
STRATEGIC AIR COMMAND  
ATTN PFS MAJ BRIAN G STEPHAN  
OFFUTT AFB, NB 68113

UNIVERSITY OF CALIFORNIA  
LAWRENCE LIVERMORE LABORATORY  
ATTN JOSEPH F KELLER JR L-125  
P.O. BOX 808  
LIVERMORE CA 94550

UNIVERSITY OF CALIFORNIA  
LAWRENCE LIVERMORE LABORATORY  
ATTN LAWRENCE CLFLAND L-156  
P.O. BOX 808  
LIVERMORE CA 94550

UNIVERSITY OF CALIFORNIA  
LAWRENCE LIVERMORE LABORATORY  
ATTN RONALD L OTT L-531  
P.O. BOX 808  
LIVERMORE CA 94550

UNIVERSITY OF CALIFORNIA  
LAWRENCE LIVERMORE LABORATORY  
ATTN TECH INFO DEPT L-3  
P.O. BOX 808  
LIVERMORE CA 94550

DIRECTOR  
STRATEGIC SYSTEMS PROJECT OFFICE  
ATTN NSP-27331 PHIL SPECTOR  
NAVY DEPARTMENT  
WASHINGTON, DC 20376

DIRECTOR  
STRATEGIC SYSTEMS PROJECT OFFICE  
ATTN NSP-2342 RICHARD L COLEMAN  
NAVY DEPARTMENT  
WASHINGTON, DC 20376

AF GEOPHYSICS LABORATORY, AFSC  
ATTN LGO-STOP 30 FREEMAN SHEPERD  
HANSOM AFB, MA 01731

AF GEOPHYSICS LABORATORY, AFSC  
ATTN EMERY CORMIER  
HANSOM AFB, MA 01731

AF GEOPHYSICS LABORATORY, AFSC  
ATTN LQR EDWARD A BURKE  
HANSOM AFB, MA 01731

AF INSTITUTE OF TECHNOLOGY, AU  
ATTN ENP CHARLES J BRIDGMAN  
WRIGHT-PATTERSON AFB, OH 45433

AF MATERIALS LABORATORY, AFSC  
ATTN LTE  
WRIGHT-PATTERSON AFB, OH 45433

AF WEAPONS LABORATORY, AFSC  
ATTN ELA  
KIRTLAND AFB, NM 87117

AF WEAPONS LABORATORY AFSC  
ATTN SAT  
KIRTLAND AFB, NM 87117

AF WEAPONS LABORATORY, AFSC  
ATTN SAB  
KIRTLAND AFB, NM 87117

AFTAC  
ATTN TAE  
PATRICK AFB, FL 32925

HEADQUARTERS  
ELECTRONIC SYSTEMS DIVISION, (AFSC)  
ATTN YSEV LTC DAVIS C SPARKS  
L. G. HANSCOM FIELD  
REDFORD, MA 01730

COMMANDER  
FOREIGN TECHNOLOGY DIVISION, AFSC  
ATTN ETET APT RICHARD C HUSEMANN  
WRIGHT-PATTERSON AFB, OH 45433

COMMANDER  
ROME AIR DEVELOPMENT CENTER, AFSC  
ATTN RBRAC I L KRULAC  
GRIFFISS AFB, NY 13440

AERONUTRONIC FORD CORPORATION  
ATTN EDWARD R HAHN MS-x22  
WESTERN DEVELOPMENT LABORATORIES DIV.  
3939 FABIAN WAY  
PALO ALTO, CA 94303

AERONUTRONIC FORD CORPORATION  
ATTN DONALD R MCMORRO, MS G3)  
WESTERN DEVELOPMENT LABORATORIES DIV  
3939 FABIAN WAY  
PALO ALTO, CA 94303

AEROSPACE CORPORATION  
ATTN WILLIAM W WILLIS  
P.O. BOX 92957  
LOS ANGELES, CA 90009

AEROSPACE CORPORATION  
ATTN MELVIN BERNSTEIN  
P.O. BOX 92957  
LOS ANGELES, CA 90009

AEROSPACE CORPORATION  
ATTN IRVING M GARFUNKEL  
P.O. BOX 92957  
LOS ANGELES, CA 90009

AEROSPACE CORPORATION  
ATTN JULIAN REINHEIMER  
P.O. BOX 92957  
LOS ANGELES, CA 90009

AEROSPACE CORPORATION  
ATTN L W AUKERMAN  
P.O. BOX 92957  
LOS ANGELES, CA 90009

COMMANDER  
NAVAL SURFACE WEAPONS CENTER  
ATTN WILLIAM H HOLT  
DAHLGREN LABORATORY  
DAHLGREN, VA 22448

COMMANDER  
NAVAL WEAPONS CENTER  
ATTN CODE 533 TECH LIB  
CHINA LAKE, CA 93555

COMMANDING OFFICER  
NAVAL WEAPONS EVALUATION FACILITY  
ATTN CODE ATG MR STANLEY  
KIRTLAND AIR FORCE BASE  
ALBUQUERQUE, NM 87117

COMMANDING OFFICER  
NAVAL WEAPONS SUPPORT CENTER  
ATTN CODE 70242 JOSEPH A MUNARIN  
CRANE, IN 47522

COMMANDING OFFICER  
NAVAL WEAPONS SUPPORT CENTER  
ATTN CODE 7024 JAMES RAMSEY  
CRANE, IN 47522

COMMANDING OFFICER  
NUCLEAR WEAPONS TNG CENTER PACIFIC  
ATTN CODE 50  
NAVAL AIR STATION, NORTH ISLAND  
SAN DIEGO, CA 92135

DIRECTOR  
STRATEGIC SYSTEMS PROJECT OFFICE  
ATTN SP 2701 JOHN W PITSENBERGER  
NAVY DEPARTMENT  
WASHINGTON, DC 20376

DEPARTMENT OF COMMERCE  
ATTN APPL RAD DIV ROBERT C PLACIOUS  
NATIONAL BUREAU OF STANDARDS  
WASHINGTON, DC 20234

DEPARTMENT OF COMMERCE  
ATTN JUDSON C FRENCH  
NATIONAL BUREAU OF STANDARDS  
WASHINGTON, DC 20234

AEROJET ELECTRO-SYSTEMS CO DIV  
ATTN THOMAS D HANSCOME  
AEROJET GENERAL CORPORATION  
P.O. BOX 296  
AZUSA, CA 91702

AERONUTRONIC FORD CORPORATION  
ATTN E R PONCELET JR  
AEROSPACE AND COMMUNICATIONS OPS  
AERONUTRONIC DIVISION  
FORD AND JAMBOREE ROADS  
NEWPORT BEACH, CA 92663

AERONUTRONIC FORD CORPORATION  
ATTN KEN C ATTINGER  
AEROSPACE AND COMMUNICATIONS OPS  
AERONUTRONIC DIVISION  
FORD AND JAMBOREE ROADS  
NEWPORT BEACH, CA 92663

AERONUTRONIC FORD CORPORATION  
ATTN TECH INFO SECTION  
AEROSPACE AND COMMUNICATIONS OPS  
AERONUTRONIC DIVISION  
FORD AND JAMBOREE ROADS  
NEWPORT BEACH, CA 92663

AERONUTRONIC FORD CORPORATION  
ATTN SAMUEL R CRAWFORD MS 531  
WESTERN DEVELOPMENT LABORATORIES DIV  
3939 FABIAN WAY  
PALO ALTO, CA 94303

CHIEF OF NAVAL RESEARCH  
ATTN CODE 421 DORAN W PADGETT  
NAVY DEPARTMENT  
ARLINGTON, VA 22217

COMMANDER  
NAVAL ELECTRONIC SYSTEMS COMMAND  
ATTN ELEX 05323 CLEVELAND F WATKINS  
NAVAL ELECTRONIC SYSTEMS CMD HQS  
WASHINGTON, DC 20360

COMMANDER  
ATTN CODE 5032 CHARLES W NEILL  
NAVAL ELECTRONIC SYSTEMS CMD HQS  
WASHINGTON, DC 20360

COMMANDER  
NAVAL ELECTRONIC SYSTEMS COMMAND  
ATTN CODE 504510  
NAVAL ELECTRONIC SYSTEMS CMD HQS  
WASHINGTON, DC 20360

COMMANDER  
NAVAL ELECTRONIC SYSTEMS COMMAND  
ATTN PME 117-21  
NAVAL ELECTRONIC SYSTEMS CMD HQS  
WASHINGTON, DC 20360

COMMANDING OFFICER  
NAVAL INTELLIGENCE SUPPORT CTR  
ATTN P ALEXANDER  
4301 SUITLAND ROAD BLDG. 5  
WASHINGTON, DC 20390

COMMANDING OFFICER  
NAVAL INTELLIGENCE SUPPORT CTR  
ATTN NISC-45  
4301 SUITLAND ROAD BLDG. 5  
WASHINGTON, DC 20390

COMMANDER  
US ARMY MOBILITY EQUIP R AND D CTR  
ATTN STSFB-MW JOHN W BOND JR  
FORT BELVOIR, VA 22060

CHIEF  
U S ARMY NUC AND CHEMICAL SURETY GP  
ATTN MOSG-ND MAJ SIDNEY W WINSLOW  
BLDG. 2073 , NORTH AREA  
FT. BELVOIR, VA 22060

COMMANDER  
US ARMY NUCLEAR AGENCY  
ATTN ATCN- LTC LEONARD A SLUGA  
FORT BLISS, TX 79916

COMMANDER  
U S ARMY TEST AND EVALUATION COMD  
ATTN DRSTE-EL RICHARD I KOLCHIN  
ABERDEEN PROVING GROUND, MD 21005

COMMANDER  
U S ARMY TESTA AND EVALUATION COMD  
ATTN DRSTE-NB RUSSELL R GALASSO  
ABERDEEN PROVING GROUND, MD 21005

COMMANDER  
WHITE SANDS MISSILE RANGE  
ATTN STENS-TE-NT MARVIN P SQUIRES  
WHITE SANDS MISSILE RANGE, NM 88002

CHIEF OF NAVAL RESEARCH  
ATTN CODE 427  
NAVY DEPARTMENT  
ARLINGTON, VA 22217

COMMANDER  
ATTN DPCDE-O LAWRENCE FLYNN  
5001 EISENHOWER AVENUE  
ALEXANDRIA, VA 22333

COMMANDER  
U S ARMY MISSILE COMMAND  
ATTN DRSMI-RGO VIC RUNE(UNCL ONLY)  
REDSTONE ARSENAL, AL 35809

COMMANDER  
U S ARMY MISSILE COMMAND  
ATTN DRCPM-MDTI CPT JOE A SIMS  
REDSTONE ARSENAL, AL 35809

COMMANDER  
U S ARMY MISSILE COMMAND  
ATTN DRCPM-LCEX HOWARD H HENRIKSEN  
REDSTONE ARSENAL, AL 35809

COMMANDER  
U S ARMY MISSILE COMMAND  
ATTN DRSMI-RGP HUGH GREEN  
REDSTONE ARSENAL, AL 35809

COMMANDER  
U S ARMY MISSILE COMMAND  
ATTN DRSMI-RRR FAISON P GIBSON  
REDSTONE ARSENAL, AL 35809

COMMANDER  
U S ARMY MISSILE COMMAND  
ATTN DRCPM PE-EA WALLACE D WAGNER  
REDSTONE ARSENAL, AL 35809

COMMANDER  
U S ARMY ELECTRONICS COMMAND  
ATTN DRSEL-CT-HD. ABRAHAM F COHEN  
FORT MONMOUTH, NJ 07703

COMMANDER  
U S ARMY ELECTRONICS COMMAND  
ATTN DRSEL-GG-TED W R WERK (NO CNDWI)  
FORT MONMOUTH, NJ 07703

COMMANDER  
U S ARMY ELECTRONICS COMMAND  
ATTN DRSEL-TL-EN ROBERT LUX  
FORT MONMOUTH, NJ 07703

COMMANDER  
U S ARMY ELECTRONICS COMMAND  
ATTN DRSEL-TL-ND GERHART GAULE  
FORT MONMOUTH, NJ 07703

COMMANDER  
U S ARMY ELECTRONICS COMMAND  
ATTN DRSEL-TL-ND S KRONENBEY  
FORT MONMOUTH, NJ 07703

COMMANDER  
U S ARMY ELECTRONICS COMMAND  
ATTN DRSEL-PL-ENV HANS A BOMKE  
FORT MONMOUTH, NJ 07703

COMMANDER-IN-CHIEF  
U S ARMY EUROPE AND SEVENTH ARMY  
ATTN ODCSE-E AEAGE-PI  
APO NEW YORK 09403

DIRECTOR  
U S ARMY BALLISTIC RESEARCH LABS  
ATTN DRXBR-X JUL US J HESZAROS  
ABERDEEN PROVING GROUND, MD 21005

DIRECTOR  
US ARMY BALLISTIC RESEARCH LABS  
ATTN DRXBR-VL ROBERT L HARRISON  
ABERDEEN PROVING GROUND, MD 21005

DIRECTOR  
U S ARMY BALLISTIC RESEARCH LABS  
ATTN DRXBR-AM W R VANANTWERP  
ABERDEEN PROVING GROUND, MD 21005

DIRECTOR  
U S ARMY BALLISTIC RESEARCH LABS  
ATTN DRARD-RVL DAVID L RIGOTTI  
ABERDEEN PROVING GROUND, MD 21005

CHIEF  
U S ARMY COMMUNICATIONS SYS AGENCY  
ATTN SCCM-AU-SV LIBRARY  
FORT MONMOUTH, NJ 07703

COMMANDER  
U S ARMY ELECTRONICS COMMAND  
ATTN DRSEL-TL-EN E ROTH  
FORT MONMOUTH, NJ 07703

COMMANDER  
U S ARMY ELECTRONICS COMMAND  
ATTN DRSEL-TL-IR EDWIN T HUNTER  
FORT MONMOUTH, NJ 07703

COMMANDER  
PICATINNY ARSENAL  
ATTN SMUPA-TN BURTON V FRANKS  
DOVER, NJ 07801

COMMANDER  
PICATINNY ARSENAL  
ATTN SARPA-ND-C-E AMINA NORDIO  
DOVER, NJ 07801

COMMANDER  
PICATINNY ARSENAL  
ATTN SARPA-ND-N  
DOVER, NJ 07801

COMMANDER  
REDSTONE SCIENTIFIC INFORMATION CTR  
ATTN CHIEF, DOCUMENTS  
U.S. ARMY MISSILE COMMAND  
REDSTONE ARSENAL, AL 35809

SECRETARY OF THE ARMY  
ATTN DOUSA OR DANIEL WILLARD  
WASHINGTON, DC 20310

COMMANDER  
TRANSANA  
ATTN ATAA-EAC FRANCIS N INANS  
WHITE SANDS MISSILE RANGE, NM 88002

DIRECTOR  
U S ARMY BALLISTIC RESEARCH LABS  
ATTN DRXBR-VL JOHN W KINCH  
ABERDEEN PROVING GROUND, MD 21005

COMMANDER  
HARRY DIAMOND LABORATORIES  
ATTN DRXDO-TT TECH LTR  
2800 POWDER MILL ROAD  
ADELPHI, MD 20783

COMMANDING OFFICER  
NIGHT DIVISION LABORATORY  
ATTN CAPT ALLAN S PARKER  
U S ARMY ELECTRONICS COMMAND  
FORT BELVOIR, VA 22060

COMMANDER  
PICATINNY ARSENAL  
ATTN SMUPA-FR-S-P  
DOVER, NJ 07801

COMMANDER  
PICATINNY ARSENAL  
ATTN SARPA-FO-E LOUIS AVRAMI  
DOVER, NJ 07801

COMMANDER  
PICATINNY ARSENAL  
ATTN SMUPA-ND-W  
DOVER, NJ 07801

COMMANDER  
PICATINNY ARSENAL  
ATTN SMUPA-ND-N-E  
DOVER, NJ 07801

COMMANDER  
PICATINNY ARSENAL  
ATTN SMUPA-ND-D-R EDWARD J ARBER  
DOVER, NJ 07801

COMMANDER  
HARRY DIAMOND LABORATORIES  
ATTN DRXDU-RCC JOHN A ROSADO  
2800 POWDER MILL ROAD  
ADELPHI, MD 20783

COMMANDER  
HARRY DIAMOND LABORATORIES  
ATTN DRXDO-NP FRANCIS N WIMENITZ  
2300 POWDER MILL ROAD  
ADELPHI, MD 20783

COMMANDER  
HARRY DIAMOND LABORATORIES  
ATTN DRXDO-RB JOSEPH R HULETTA  
2800 POWDER MILL ROAD  
ADELPHI, MD 20783

COMMANDER  
HARRY DIAMOND LABORATORIES  
ATTN DRXDU-RCC JOHN E THOMPSON  
2800 POWDER MILL ROAD  
ADELPHI MD 20783

COMMANDER  
HARRY DIAMOND LABORATORIES  
ATTN DRXDO-EM R BOSTAK  
2800 POWDER MILL ROAD  
ADELPHI MD 20783

COMMANDER  
HARRY DIAMOND LABORATORIES  
ATTN DRXDO-RBH PAUL A CALDWELL  
2800 POWDER MILL ROAD  
ADELPHI MD 20783

COMMANDER  
HARRY DIAMOND LABORATORIES  
ATTN DRXDO-RB ROBERT E MCCOSKEY  
2800 POWDER MILL ROAD  
ADELPHI MD 20783

DIRECTOR  
NATIONAL SECURITY AGENCY  
ATTN TDL  
FT. GEORGE G. MEADE, MD 20755

PROJECT MANAGER  
ARMY TACTICAL DATA SYSTEMS  
ATTN DRCPN-TDS-SD  
U S ARMY ELECTRONICS COMMAND  
FORT MONMOUTH, NJ 07703

PROJECT MANAGER  
ARMY TACTICAL DATA SYSTEMS  
ATTN DWAIN H HUEE  
U S ARMY ELECTRONICS COMMAND  
FORT MONMOUTH, NJ 07703

COMMANDER  
RMD SYSTEM COMMAND  
ATTN BDMSC-TEN NOAH J HURST  
P.O BOX 1500  
HUNTSVILLE, AL 35807

101

COMMANDER  
FRANKFORD ARSENAL  
ATTN SARFA-PCD MARVIN ELNICK  
BRIDGE AND TACONY STREETS  
PHILADELPHIA, PA 19137

DIRECTOR  
DEFENSE NUCLEAR AGENCY  
ATTN RAEV  
WASHINGTON, DC 20305

COMMANDER  
HARRY DIAMOND LABORATORIES  
ATTN DRXDO-RC ROBERT B OSWALD JR  
2800 POWDER MILL ROAD  
ADELPHI MD 20783

DIRECTOR  
DEFENSE NUCLEAR AGENCY  
ATTN STVL  
WASHINGTON, DC 20305

COMMANDER  
HARRY DIAMOND LABORATORIES  
ATTN CRXDO-TR EDWARD E CONRAD  
2800 POWDER MILL ROAD  
ADELPHI MD 20783

COMMANDER  
FIELD COMMAND  
ATTN FCPR  
DEFENSE NUCLEAR AGENCY  
KIRTLAND AFB, NM 87115

DIRECTOR  
DEFENSE COMMUNICATIONS AGENCY  
ATTN CODE 930 MONTE I RUBGETT JR  
WASHINGTON, DC 20305

DIRECTOR  
INTERSERVICE NUCLEAR WEAPONS SCHOOL  
ATTN DOCUMENT CONTROL  
KIRTLAND AFB, NM 87115

DEFENSE DOCUMENTATION CENTER  
ATTN TC  
CAMERON STATION  
ALEXANDRIA, VA 22314

DIRECTOR  
JOINT STRAT TGT PLANNING STAFF JCS  
ATTN ULTW-2  
OFFUTT AFB  
OMAHA, NB 68113

DIRECTOR  
DEFENSE INTELLIGENCE AGENCY  
ATTN DS-4A2  
WASHINGTON, DC 20301

CHIEF  
LIVERMORE DIVISION FLD COMMAND DNA  
ATTN DOCUMENT CONTROL FOR L-395  
LAWRENCE LIVERMORE LABORATORY  
P.O. BOX 808  
LIVERMORE, CA 94550

DIRECTOR  
DEFENSE NUCLEAR AGENCY  
ATTN RATN  
WASHINGTON, DC 20305

CHIEF  
LIVERMORE DIVISION FLD COMMAND DNA  
ATTN FCPRL  
LAWRENCE LIVERMORE LABORATORY  
P.O. BOX 808  
LIVERMORE, CA 94550

DIRECTOR  
DEFENSE NUCLEAR AGENCY  
ATTN STTL TECH LIBRARY  
WASHINGTON, DC 20305

DIRECTOR  
NATIONAL SECURITY AGENCY  
ATTN ORLAND O VAN GUNTEN R-425  
FT. GEORGE G. MEADE, MD 20755

DIRECTOR  
DEFENSE NUCLEAR AGENCY  
ATTN DDST  
WASHINGTON, DC 20305

TRW SYSTEMS GROUP  
ATTN PAUL MOIMUD R1-1196  
ONE SPACE PARK  
REDONDO BEACH, CA 90278

102

TRW SYSTEMS GROUP  
ATTN LILLIAN D SINGLETAR R1-1070  
ONE SPACE PARK  
REDONDO BEACH, CA 90278

TRW SYSTEMS GROUP  
ATTN A M LIEBSCHUTZ R1-1162  
ONE SPACE PARK  
REDONDO BEACH, CA 90278

TRW SYSTEMS GROUP  
ATTN R D LOVELAND R1-1028  
ONE SPACE PARK  
REDONDO BEACH, CA 90278

TRW SYSTEMS GROUP  
ATTN TECH INFO CENTER R/S-1930  
ONE SPACE PARK  
REDONDO BEACH, CA 90278

TRW SYSTEMS GROUP  
ATTN RICHARD H KINGSLAND R1-2154  
ONE SPACE PARK  
REDONDO BEACH, CA 90278

TRW SYSTEMS GROUP  
ATTN WILLIAM H ROBINETTE JR  
ONE SPACE PARK  
REDONDO BEACH, CA 90278

TRW SYSTEMS GROUP  
ATTN H S JENSEN  
SAN BERNARDINO OPERATIONS  
P.O. BOX 1310  
SAN BERNARDINO, CA 92402

TRW SYSTEMS GROUP  
ATTN JERRY T LUBELL  
ONE SPACE PARK  
REDONDO BEACH, CA 90278

TRW SYSTEMS GROUP  
ATTN JOHN E DAHNKE  
SAN BERNARDINO OPERATIONS  
P.O. BOX 1310  
SAN BERNARDINO, CA 92402

DIRECTOR  
NAVAL RESEARCH LABORATORY  
ATTN CODE 6631 JAMES C RITTER  
WASHINGTON, DC 20375

TRW SYSTEMS GROUP  
ATTN EARL W ALLEN  
SAN BERNARDINO OPERATIONS  
P.O. BOX 1310  
SAN BERNARDINO, CA 92402

DIRECTOR  
NAVAL RESEARCH LABORATORY  
ATTN CODE 4004 EMANUAL L BRANCATO  
WASHINGTON, DC 20375

TEXAS TECH UNIVERSITY  
ATTN TRAVIS L SIMPSON  
P.O. BOX 5404 NORTH COLLEGE STATION  
LUBBOCK, TX 79417

DIRECTOR  
NAVAL RESEARCH LABORATORY  
ATTN CODE 7701 JACK D BROWN  
WASHINGTON, DC 20375

TRW SYSTEMS GROUP  
ATTN ALLAN ANDERMAN R1-1132  
ONE SPACE PARK  
REDONDO BEACH, CA 90278

DIRECTOR  
NAVAL RESEARCH LABORATORY  
ATTN CODE 5216 HAROLD L HUGHES  
WASHINGTON, DC 20375

TRW SYSTEMS GROUP  
ATTN A A WITTELES MS R1-1120  
ONE SPACE PARK  
REDONDO BEACH, CA 90278

DIRECTOR  
NAVAL RESEARCH LABORATORY  
ATTN CODE 6601 E WOLICKI  
WASHINGTON, DC 20375

DIRECTOR  
NAVAL RESEARCH LABORATORY  
ATTN CODE 5210 JOHN E DAVEY  
WASHINGTON, DC 20375

DIRECTOR  
 NAVAL RESEARCH LABORATORY  
 ATTN CODE 2627 DORIS R FOLEN  
 WASHINGTON, DC 20375

BOEING COMPANY, THE  
 ATTN DAVID L DYE M S 87-75  
 P.O. BOX 3707  
 SEATTLE, WA 98124

COMMANDER  
 NAVAL SEA SYSTEMS COMMAND  
 ATTN SEA-9931 SAMUEL A BARHAM  
 NAVY DEPARTMENT  
 WASHINGTON DC 20362

BOEING COMPANY, THE  
 ATTN HOWARD W WICKLEIN MS 17-11  
 P.O. BOX 3707  
 SEATTLE, WA 98124

COMMANDER  
 NAVAL SEA SYSTEMS COMMAND  
 ATTN SEA-9931 RILEY B LANE  
 NAVY DEPARTMENT  
 WASHINGTON DC 20362

BOEING COMPANY, THE  
 ATTN ROBERT S CALDWELL 2R-00  
 P.O. BOX 3707  
 SEATTLE, WA 98124

COMMANDER  
 NAVAL SHIP ENGINEERING CENTER  
 ATTN CODE 6174D2 EDWARD F DUFFY  
 CENTER BUILDING  
 HYATTSVILLE, MD 20782

BOOZ-ALLEN AND HAMILTON, INC.  
 ATTN RAYMOND J. CHRISNER  
 106 APPLE STREET  
 NEW SHREWSBURY NJ 07724

COMMANDER  
 NAVAL SURFACE WEAPONS CENTER  
 ATTN CODE WA501 NAVY NUC PRGMS OFF  
 WHITE OAK, SILVER SPRING, MD 20910

CALIFORNIA INSTITUTE OF TECHNOLOGY  
 ATTN A G STANLEY  
 JET PROPULSION LABORATORY  
 4800 OAK PARK GROVE  
 PASADENA, CA 91103

COMMANDER  
 NAVAL SURFACE WEAPONS CENTER  
 ATTN CODE 431 EDWIN B DEAN  
 WHITE OAK, SILVER SPRING, MD 20910

CALIFORNIA INSTITUTE OF TECHNOLOGY  
 ATTN J BRYDEN  
 JET PROPULSION LABORATORY  
 4800 OAK PARK GROVE  
 PASADENA, CA 91103

COMMANDER  
 NAVAL SURFACE WEAPONS CENTER  
 ATTN CODE WA50 JOHN H MALLOY  
 WHITE OAK, SILVER SPRING, MD 20910

AEROSPACE CORPORATION  
 ATTN LIBRARY  
 P.O. BOX 92957  
 LOS ANGELES, CA 90009

COMMANDER  
 NAVAL SURFACE WEAPONS CENTER  
 ATTN CODE WX21 TECH LIB  
 WHITE OAK, SILVER SPRING, MD 20910

ANALOG TECHNOLOGY CORPORATION  
 ATTN JOHN JOSEPH BAUM  
 3410 EAST FOOTHILL BOULEVARD  
 PASADENA, CA 91107

BOEING COMPANY, THE  
 ATTN AEROSPACE LIBRARY  
 P.O. BOX 3707  
 SEATTLE, WA 98124

AVCO RESEARCH AND SYSTEMS GROUP  
 ATTN RESEARCH LIB A830 RM 7201  
 201 LOWELL STREET  
 WILMINGTON, MA 01887

BDM CORPORATION, THE  
 ATTN T H NEIGHBORS  
 P O BOX 9274  
 ALBUQUERQUE, NM 87119

BENDIX CORPORATION, THE  
ATTN DOCUMENT CONTROL  
COMMUNICATION DIVISION  
EAST JOPPA ROAD - TOWSON  
BALTIMORE, MD 21204

BENDIX CORPORATION, THE  
ATTN MAX FRANK  
RESEARCH LABORATORIES DIVISION  
BENDIX CENTER  
SOUTHFIELD, MI 48076

BENDIX CORPORATION, THE  
ATTN MGR PRGM DEV DONALD J NIEHAUS  
RESEARCH LABORATORIES DIVISION  
BENDIX CENTER  
SOUTHFIELD, MI 48076

FLORIDA, UNIVERSITY OF  
ATTN D P KENNEDY  
231 AEROSPACE BLDG  
GAINESVILLE, FL 32611

FRANKLIN INSTITUTE, THE  
ATTN RAMIE H THOMPSON  
20TH STREET AND PARKWAY  
PHILADELPHIA, PA 19103

GARRETT CORPORATION  
ATTN ROBERT E WEIR DEPT 93-9  
P.O BOX 92248  
LOS ANGELES, CA 90009

GENERAL DYNAMICS CORP.  
ATTN D N COLEMAN  
ELECTRONICS DIV ORLANDO OPERATIONS  
P.O. BOX 2566  
ORLANDO, FL 32302

GENERAL ELECTRIC COMPANY  
ATTN JOHN L ANDREWS  
SPACE DIVISION  
VALLEY FORGE SPACE CENTER  
GODDARD BLVD KING OF PRUSSIA  
P.O. BOX 8555  
PHILADELPHIA PA 19101

GENERAL ELECTRIC COMPANY  
ATTN JOSEPH C PEDEN CCF8301  
SP CE DIVISION  
VALLEY FORGE SPACE CENTER  
GODDARD BLVD KING OF PRUSSIA  
P.O. BOX 8555, PHILADELPHIA PA 19101

GENERAL ELECTRIC COMPANY  
ATTN LARRY I CHASEN  
SPACE DIVISION  
VALLEY FORGE SPACE CENTER  
GODDARD BLVD KING OF PRUSSIA  
P.O. BOX 8555  
PHILADELPHIA PA 19101

GENERAL ELECTRIC COMPANY  
ATTN JAMES P SPRATT  
SPACE DIVISION  
VALLEY FORGE SPACE CENTER  
GODDARD BLVD KING OF PRUSSIA  
P.O. BOX 8555  
PHILADELPHIA PA 19101

GENERAL ELECTRIC COMPANY  
ATTN JOHN N PALCHEFSKY  
RE-ENTRY AND ENVIRONMENTAL SYSTEMS DIV  
P.O. BOX 7722  
3198 CHESTNUT STREET  
PHILADELPHIA, PA 19101

GENERAL ELECTRIC COMPANY  
ATTN ROBERT V BENEDICT  
RE-ENTRY AND ENVIRONMENTAL SYSTEMS DIV  
P.O. BOX 7722  
3198 CHESTNUT STREET  
PHILADELPHIA, PA 19101

GENERAL ELECTRIC COMPANY  
ATTN JOSEPH REIDL  
ORDNANCE SYSTEMS  
100 PLASTICS AVENUE  
PITTSFIELD, MA 01201

GENERAL ELECTRIC COMPANY  
ATTN DASIAC  
TEMP-CENTER FOR ADVANCED STUDIES  
816 STATE STREET (P.O. DRAWER QQ)  
SANTA BARBARA, CA 93102

GENERAL ELECTRIC COMPANY  
ATTN ROYDEN R RUTHERFORD  
TEMPO-CENTER FOR ADVANCED STUDIES  
816 STATE STREET (P.O. DRAWER QQ)  
SANTA BARBARA, CA 93102

GENERAL ELECTRIC COMPANY  
ATTN M ESPIG  
TEMPO-CENTER FOR ADVANCED STUDIES  
816 STATE STREET (P.O. DRAWER QQ)  
SANTA BARBARA, CA 93102

GENERAL ELECTRIC COMPANY  
TTN CSP 0-7 L H DEF  
P.O. BOX 1122  
SYRACUSE, NY 13201

GENERAL RESEARCH CORPORATION  
ATTN DAVID K OSIAS  
WASHINGTON OPERATIONS  
WESTGATE RESEARCH PARK  
7655 OLD SPRINGHOUSE ROAD, SUITE 700  
MCCLEAN, VA 22101

GENERAL ELECTRIC COMPANY  
ATTN JOHN A ELLERHORST E 2  
AIRCRAFT ENGINE GROUP  
EVENDALE PLANT  
CINCINNATI OH 45215

GRUMMAN AEROSPACE CORPORATION  
ATTN JERRY ROGERS DEPT 533  
SOUTH OYSTER BAY ROAD  
BETHPAGE, NY 11714

GENERAL ELECTRIC COMPANY  
ATTN W J PATTERSON DROP 233  
AEROSPACE ELECTRONICS SYSTEMS  
FRENCH ROAD  
UTICA, NY 13503

GTE SYLVANIA INC.  
ATTN LEONARD L BLAISDELL  
ELECTRONICS SYSTEMS GRP-EASTERN DIV  
77 A STREET  
NEEDHAM, MA 02194

GENERAL ELECTRIC COMPANY  
ATTN CHARLES U HEWISON DROP 624  
AEROSPACE ELECTRONICS SYSTEMS  
FRENCH ROAD  
UTICA, NY 13503

GTE SYLVANIA, INC.  
ATTN CHARLES A THORNHILL LIBRARIAN  
ELECTRONICS SYSTEMS GRP-EASTERN DIV  
77 A STREET  
NEEDHAM, MA 02194

GENERAL ELECTRIC COMPANY  
ATTN DAVID W PEPIN DROP 160  
P.O. BOX 5000  
BINGHAMTON, NY 13902

GTE SYLVANIA, INC.  
ATTN JAMES A WALDON  
ELECTRONICS SYSTEMS GRP-EASTERN DIV  
77 A STREET  
NEEDHAM, MA 02194

GENERAL ELECTRIC COMPANY-TFMPO  
ATTN WILLIAM ALFONTE  
ATTN: DASTAC  
C/O DEFENSE NUCLEAR AGENCY  
WASHINGTON, DC 20305

GTE SYLVANIA, INC.  
ATTN PAUL B FREDRICKSON  
189 B STREET  
NEEDHAM HEIGHTS, MA 02194

GENERAL RESEARCH CORPORATION  
ATTN ROBERT D HILL  
P.O. BOX 3587  
SANTA BARBARA, CA 93105

GTE SYLVANIA, INC.  
ATTN H AND V GROUP MARIO A NURPFORA  
189 B STREET  
NEEDHAM HEIGHTS, MA 02194

GTE SYLVANIA, INC.  
ATTN HERBERT A ULLMAN  
189 B STREET  
NEEDHAM HEIGHTS, MA 02194

HONEYWELL INCORPORATED  
ATTN RONALD R JOHNSON A 1622  
GOVERNMENT AND AERONAUTICAL  
PRODUCTS DIVISION  
2600 RIDGEWAY PARKWAY  
MINNEAPOLIS, MN 55413

GTE SYLVANIA, INC.  
ATTN CHARLES H RAMS OTTOM  
189 B STREET  
NEEDHAM HEIGHTS, MA 02194

HONEYWELL INCORPORATED  
ATTN R J KELL MS S2572  
GOVERNMENT AND AERONAUTICAL  
PRODUCTS DIVISION  
2600 RIDGEWAY PARKWAY  
MINNEAPOLIS, MN 55413

GULTON INDUSTRIES, INC.  
ATTN ENGNMAGNETICS DIV  
13041 CERISE AVENUE  
HAWTHORNE, CA 90250

HONEYWELL INCORPORATED  
ATTN HARRISON H NOBLE M S 725-5A  
AEROSPACE DIVISION  
13350 U.S. HIGHWAY 19  
ST. PETERSBURG, FL 33733

HARRIS CORPORATION  
ATTN T L CLARK M S 4040  
HARRIS SEMICONDUCTOR DIVISION  
P.O. BOX 883  
MELBOURNE, FL 32901

HONEYWELL INCORPORATED  
ATTN M S 725- STACEY H GRAFF  
AEROSPACE DIVISION  
13350 U. S. HIGHWAY 19  
ST. PETERSBURG, FL 33733

HARRIS CORPORATION  
ATTN CARF F DAVOS ,S ;7-220  
HARRIS SEMICONDUCTOR DIVISION  
P.O. BOX 883  
MELBOURNE, FL 32901

HONEYWELL INCORPORATED  
ATTN TECHNICAL LIBRARY  
RADIATION CENTER  
2 FORRES ROAD  
LEXINGTON, MA 02173

HARRIS CORPORATION  
ATTN WAUME E ABARE MS 16-111  
HARRIS SEMICONDUCTOR DIVISION  
P.O. BOX 883  
MELBOURNE, FL 32901

HUGHES AIRCRAFT COMPANY  
ATTN BILLY CAMPBELL M S 6-E-110  
CENTINELA AND TEALE  
CULVER CITY, CA 90230

HAZELTIME CORPORATION  
ATTN TECH INFO CTR M WAITE  
PULASKI ROAD  
GREEN LAWN, NY 11740

HUGHES AIRCRAFT COMPANY  
ATTN DAN BINDER MS 6-0147  
CENTINELA AND TEALE  
CULVER CITY, CA 90230

HUGHES AIRCRAFT COMPANY  
ATTN KENNETH R WALKER M S 0157  
CENTINELA AND TEALE  
CULVER CITY, CA 90230

KAMAN SCIENCES CORPORATION  
ATT ALBERT P BRIDGES  
P. O. BOX 7463  
COLORADO SPRINGS, CO 80933

HUGHES AIRCRAFT COMPANY  
ATTN-EDWARD C SMITH MS A620  
SPACE SYSTEMS DIVISION  
P.O. BOX 92919  
LOS ANGELES, CA 90009

KAMAN SCIENCES CORPORATION  
ATTN WALTER E WARE  
P.O. BOX 7463  
COLORADO SPRINGS, CO 80933

HUGHES AIRCRAFT COMPANY  
ATTN WILLIAM W SCOTT MS 1080  
SPACE SYSTEMS DIVISION  
P.O. BOX 92919  
LOS ANGELES, CA 90009

LITTON SYSTEMS, INC.  
ATTN JOHN P RETZLER  
GUIDANCE AND CONTROL SYSTEMS DIVISION  
5500 CANOGA AVENUE  
WOODLAND HILLS, CA 91364

IBM CORPORATION  
ATTN FRANK FRANKOWSKY  
ROUTE 170  
OWEGO, NY 13827

LITTON SYSTEMS, INC.  
ATTN VAL J ASHBY MS 67  
5500 CANOGA AVENUE  
WOODLAND HILLS, CA 91364

IBM CORPORATION  
ATTN HARRY MATHERS DEPT M41  
OWEGO, NY 13827

LOCKHEED MISSILES AND SPACE CO INC.  
P.O. BOX 504  
SUNNYVALE, CA 94088

ION PHYSICS CORPORATION  
ATTN ROBERT D EVANS  
SOUTH BEDFORD STREET  
BURLINGTON, MA 01803

LOCKHEED MISSILES AND SPACE CO INC  
ATTN GEORGE F HEATH D/81-14  
P.O. BOX 504  
SUNNYVALE, CA 94088

IRT CORPORATION  
ATTN MDC  
P.O. BOX 81087  
SAN DIEGO, CA 92138

LOCKHEED MISSILES AND SPACE CO INC  
ATTN EDWIN A SMITH DEPT R5-A5  
P.O. BOX 504  
SUNNYVALE, CA 94088

MARTIN MARIETTA AEROSPACE  
ATTN MONA C GRIFFITH LIB MP-30  
ORLANDO DIVISION  
P.O. BOX 5837  
ORLANDO, FL 32805

LOCKHEED MISSILES AND SPACE CO INC.  
ATTN I ROSSI DEPT 81-64  
P.O. BOX 504  
SUNNYVALE, CA 94088

MARTIN MARIETTA AEROSPACE  
ATTN WILLIAM W MRAS MP-413  
ORLANDO DIVISION  
P.O. BOX 5837  
ORLANDO, FL 32805

LOCKHEED MISSILES AND SPACE CO INC  
ATTN PHILIP J HART DEPT 81-14  
P.O. BOX 504  
SUNNYVALE, CA 94088

MARTIN MARIETTA AEROSPACE  
ATTN JACK M ASHFORD MP-537  
ORLANDO DIVISION  
ORLANDO, FL 32805

LOCKHEED MISSILES AND SPACE CO INC.  
ATTN BEN AMIN T KIMJURA DEPT 81-14  
P.O. BOX 504  
SUNNYVALE, CA 94088

MARTIN MARIETTA CORPORATION  
ATTN PAUL G WASE MAIL 8203  
DENVER DIVISION  
P.O. BOX 179  
DENVER, CO 80211

LOCKHEED MISSILES AND SPACE COMPANY  
ATTN TECH INFO CTR D/COLL  
3251 HANDOVER STREET  
PALO ALTO, CA 94304

MARTIN MARIETTA CORPORATION  
 ATTN RESEARCH 'IB 6617 JAY R MCKEE  
 DENVER DIVISION  
 P.O. BOX 179  
 DENVER, CO 80201

LTV AEROSPACE CORPORATION  
 ATTN TECHNICAL DATA CENTER  
 VOUGHT SYSTEMS DIVISION  
 P.O. BOX 6267  
 DALLAS, TX 75222

MARTIN MARIETTA CORPORATION  
 ATTN BEN T GRAHAM MS PO-454 8  
 DENVER DIVISION  
 P.O. BOX 179  
 DENVER, CO 80201

LTV AEROSPACE CORPORATION  
 ATTN TECHNICAL DATA CTR  
 P.O. BOX 5907  
 DALLAS, TX 75222

MARTIN MARIETTA CORPORATION  
 ATTN J E GOODWIN MAIL 0452 (UNCL ONLY)  
 DENVER DIVISION  
 P.O. BOX 179  
 DENVER, CO 80201

M.I.T. LINCOLN LABORATORY  
 ATTN LEONA LOUGHLIN LIBRARIAN A-082  
 P.O. BOX 73  
 LEXINGTON, MA 02173

MITRE CORPORATION, THE  
 ATTN LIBRARY  
 P.O. BOX 208  
 BEDFORD, MA 01730

MCDONNELL DOUGLAS CORPORATION  
 ATTN TECHNICAL LIBRARY  
 POST OFFICE BOX 516  
 ST. LOUIS, MISSOURI 63166

NATIONAL ACADEMY OF SCIENCES  
 ATTN R S SHANE NAT MATERIALS ADVSY  
 ATTN: NATIONAL MATERIALS ADVISORY BOA  
 2101 CONSTITUTION AVENUE  
 WASHINGTON, DC 20418

MCDONNELL DOUGLAS CORPORATION  
 ATTN TO ENDER  
 POST OFFICE BOX 516  
 ST. LOUIS, MISSOURI 63166

NEW MEXICO, UNIVERSITY OF  
 ATTN W W GRANNEMANN (UNCLASS ONLY)  
 DEPT. OF CAMPUS SECURITY AND POLICE  
 1321 ROMA N.E.  
 ALBUQUERQUE, NM 87106

MCDONNELL DOUGLAS CORPORATION  
 ATTN STANLEY SCHNEIDER  
 5301 BOLSA AVENUE  
 HUNTINGTON BEACH, CA 92647

NORTHROP CORPORATION  
 ATTN BOYCE T AHLPORT  
 ELECTRONIC DIVISION  
 1 RESEARCH PARK  
 PALOS VERDES PENINSULA, CA 90274

MCDONNELL DOUGLAS CORPORATION  
 ATTN TECHNICAL LIBRARY, C1-290/36-84  
 3855 LAKEWOOD BOULEVARD  
 LONG BEACH, CA 90846

NORTHROP CORPORATION  
 ATTN JOHN M REYNOLDS  
 ELECTRONIC DIVISION  
 1 RESEARCH PARK  
 PALOS VERDES PENINSULA, CA 90274

MISSION RESEARCH CORPORATION  
 ATTN WILLIAM C HART  
 735 STATE STREET  
 SANTA BARBARA, CA 93101

NORTHROP CORPORATION  
 ATTN VINCENT R DEMARTINO  
 ELECTRONIC DIVISION  
 1 RESEARCH PARK  
 PALOS VERDES PENINSULA, CA 90274

MISSION RESEARCH CORPORATION-SAN DIEGO  
 ATTN V A J VAN LINT  
 7650 CONVOY COURT  
 SAN DIEGO, CA 92111

NORTHROP CORPORATION  
 ATTN GEORGE H TOWNER  
 ELECTRONIC DIVISION  
 1 RESEARCH PARK  
 PALOS VERDES PENINSULA, CA 90274

MITRE CORPORATION, THE  
 ATTN M E FITZGERALD  
 P.O. BOX 208  
 BEDFORD, MA 01730

NORTHROP CORPORATION  
 ATTN ORLIE L CURTIS R  
 NORTHROP RESEARCH AND TECHNOLOGY CTR  
 3401 WEST BROADWAY  
 HAWTHORNE, CA 90250

R AND D ASSOCIATES  
 ATTN S CLAY ROGERS  
 P.O. BOX 9695  
 MARINA DEL REY CA 90291

NORTHROP CORPORATION  
 ATTN DAVID N POCUCK  
 NORTHROP RESEARCH AND TECHNOLOGY CTR  
 3401 WEST BROADWAY  
 HAWTHORNE, CA 90250

RAYTHEON COMPANY  
 ATTN GAUANAN H JOSHI RADAR SYS LAB  
 HARTWELL ROAD  
 BEDFORD, MA 01730

NORTHROP CORPORATION  
 ATTN JOSEPH D RUSSO  
 ELECTRONIC DIVISION  
 2301 WEST 120TH STREET  
 HAWTHORNE, CA 90250

RAYTHEON COMPANY  
 ATTN HAROLD L FLESCHER  
 528 BOSTON POST ROAD  
 SUDBURY, MA 01776

PALISADES INST FOR RSCH SERVICES INC  
 ATTN RECORDS SUPERVISOR  
 201 VARICK STREET  
 NEW YORK, NY 10014

RCA CORPORATION  
 ATTN GEORGE J BRUCKER  
 GOVERNMENT AND COMMERCIAL SYSTEMS  
 ASTRO ELECTRONICS DIVISION  
 P.O. BOX 800, LOCUST CORNER  
 PRINCETON, NJ 08540

PHYSICS INTERNATIONAL COMPANY  
 ATTN DOC CON FOR CHARLES H STALLINGS  
 2700 MERCED STREET  
 SAN LEANDRO, CA 94577

RCA CORPORATION  
 ATTN K H ZAININGER  
 DAVID SARNOFF RESEARCH CENTER  
 W. WINDSOR TWP  
 201 WASHINGTON ROAD, P.O. BOX 432  
 PRINCETON, NJ 08540

PHYSICS INTERNATIONAL COMPANY  
 ATTN DOC CON FOR JOHN H HUNTINGTON  
 2700 MERCED STREET  
 SAN LEANDRO, CA 94577

RCA CORPORATION  
 ATTN E VAN KEUREN 13-5-2  
 CAMDEN COMPLEX  
 FRONT AND COOPER STREETS  
 CAMDEN, NJ 08012

POWER PHYSICS CORPORATION  
ATTN MITCHELL BAKER  
542 INDUSTRIAL WAY WEST  
P.O. BOX 626  
EATONTOWN, NJ 07724

RENSSELAER POLYTECHNIC INSTITUTE  
ATTN RONALD J GUTMANN  
P.O. BOX 965  
TROY, NY 12181

ROCKWELL INTERNATIONAL CORPORATION  
ATTN DENNIS SUTHERLAND  
ELECTRONICS OPERATIONS  
COLLINS RADIO GROUP  
5225 C AVENUE NE  
CEDAR RAPIDS, IA 52406

RESEARCH TRIANGLE INSTITUTE  
ATTN ENG DIV MAYRANT SIMONS  
P.O. BOX 12194  
RESEARCH TRIANGLE PARK, NC 27709

ROCKWELL INTERNATIONAL CORPORATION  
ATTN MILDRED A BLAIR  
ELECTRONICS OPERATIONS  
COLLINS RADIO GROUP  
5225 C AVENUE NE  
CEDAR RAPIDS, IA 52406

ROCKWELL INTERNATIONAL CORPORATION  
ATTN GEORGE C MESSENGER F 861  
3370 MIRALOMA AVENUE  
ANAHEIM, CA 92803

SANDERS ASSOCIATES, INC.  
ATTN ME L ATTEL NCA 1-3236  
95 CANAL STREET  
NASHUA, NH 03060

ROCKWELL INTERNATIONAL CORPORATION  
ATTN JAMES E BELL HA10  
3370 MIRALOMA AVENUE  
ANAHEIM, CA 92803

SCIENCE APPLICATIONS, INC.  
ATTN LARRY SCOTT  
P.O. BOX 2351  
LA JOLLA, CA 92038

ROCKWELL INTERNATIONAL CORPORATION  
ATTN K F HULL  
3370 MIRALOMA AVENUE  
ANAHEIM, CA 92803

SCIENCE APPLICATIONS, INC.  
ATTN J ROBERT BEYSTER  
P.O. BOX 2351  
LA JOLLA, CA 92038

ROCKWELL INTERNATIONAL CORPORATION  
ATTN DONAL J STEVENS FA70  
3370 MIRALOMA AVENUE  
ANAHEIM, CA 92803

SCIENCE APPLICATIONS, INC.  
ATTN NOEL R BYRN  
HUNTSVILLE DIVISION  
2109 W. CLINTON AVENUE  
SUITE 700  
HUNTSVILLE, AL 35805

ROCKWELL INTERNATIONAL CORPORATION  
ATTN T B YATES  
5701 WEST IMPERIAL HIGHWAY  
LOS ANGELES, CA 90009

SCIENCE APPLICATIONS, INC.  
ATTN CHARLES STEVENS  
2680 HANOVER STREET  
PALO ALTO, CA 94303

ROCKWELL INTERNATIONAL CORPORATION  
ATTN ALAN A LANGENFELD  
ELECTRONICS OPERATIONS  
COLLINS RADIO GROUP  
5225 C AVENUE NE  
CEDAR RAPIDS, IA 52406

SIMULATION PHYSICS, INC.  
 ATTN ROGER G LITTLE  
 41 "8" STREET  
 BURLINGTON, MA 01803

STANFORD RESEARCH INSTITUTE  
 ATTN ROBERT A ARMISTEIN  
 333 RAVENSWOOD AVENUE  
 MENLO PARK, CA 94025

SINGER COMPANY (DATA SYSTEMS), THE  
 ATTN TECH INFO CENTER  
 150 TOTU A ROAD  
 WAYNE, NJ 07470

STANFORD RESEARCH INSTITUTE  
 ATTN PHILIP I DOLAN  
 333 RAVENSWOOD AVENUE  
 MENLO PARK, CA 94025

SINGER COMPANY, THE  
 ATTN IRWIN GOLDMAN ENG MANAGEMENT  
 1150 MC BRIDE AVENUE  
 LITTLE FALLS, NJ 07424

STANFORD RESEARCH INSTITUTE  
 ATTN MACPHERSON MORGAN  
 306 WYNN DRIVE, N. W.  
 HUNTSVILLE, AL 35805

SPERRY FLIGHT SYSTEMS DIVISION  
 ATTN D ANDREW SCHON  
 SPERRY RAND CORPORATION  
 P.O. BOX 21111  
 PHOENIX, AZ 85036

SUNDSTRAND CORPORATION  
 ATTN CURTIS B WHITE (NO CLASS)  
 4751 HARRISON AVENUE  
 ROCKFORD, IL 61101

SPERRY RAND CORPORATION  
 ATTN JAMES A INDA MS 41T25  
 UNIVA DIVISION  
 DEFENSE SYSTEMS DIVISION  
 P.O. BOX 3525 MAIL STATION 1931  
 ST. PAUL, MN 55101

SYSTRON-DONNER CORPORATION  
 ATTN HAROLD D MORRIS  
 1090 SAN MIGUEL ROAD  
 CONCORD, CA 94518

SPERRY RAND CORPORATION  
 ATTN CHARLES L CRAIGEN  
 SPERRY DIVISION  
 SPERRY GYROSCOPE DIVISION  
 SPERRY SYSTEMS MANAGEMENT DIVISION  
 MARCUS AVENUE  
 GREAT NEACK, NY 11020

SYSTRON-DONNER CORPORATION  
 ATTN GORDON R DEAN  
 1090 SAN MIGUEL ROAD  
 CONCORD, CA 94518

TEXAS INSTRUMENTS, INC.  
 ATTN DONALD J HANUS M S 72  
 P.O. BOX 5474  
 DALLAS, TX 75222

SPERRY RAND CORPORATION  
 ATTN PAUL MARAFFIND  
 SPERRY DIVISION  
 SPERRY GYROSCOPE DIVISION  
 SPERRY SYSTEMS MANAGEMENT DIVISION  
 MARCUS AVENUE  
 GREAT NECK, NY 11020